

FINAL REPORT

INTERDIFFUSION BEHAVIOR OF TUNGSTEN
OR RHENIUM AND GROUP V AND VI ELEMENTS
AND ALLOYS OF THE PERIODIC TABLE
PART IIA (APPENDICES)

by
F. G. Arcella

Prepared for
National Aeronautics and Space Administration
NASA Lewis Research Center
Cleveland, Ohio 44135
Contract NAS 3-13231



Astronuclear Laboratory
Westinghouse Electric Corporation



Vertical text on the right side of the page, possibly a library or archival stamp, including the words "RECEIVED" and "NASA STI FACILITY".

75-10209

1 Report No NASA CR-134526	2 Government Accession No	3 Recipient Category	
4 Title and Subtitle Interdiffusion Behavior of Tungsten or Rhenium and Group V and VI Elements and Alloys of the Periodic Table - Part II (Appendices)		5 Report Date September, 1974	6 Performing Organization Code
		8 Performing Organization Report No WANL-M-FR-74-005	10 Work Unit No
7 Author(s) F. G. Arcella	9 Performing Organization Name and Address Westinghouse Astronuclear Laboratory P. O. Box 10864 Pittsburgh, Pennsylvania 15236		11 Contract or Grant No NAS 3-13231
12 Sponsoring Agency Name and Address National Aeronautics and Space Administration Cleveland, Ohio 44135			13 Type of Report and Period Covered Final Report
		15 Supplementary Notes Project Manager, R. A. Lindberg, NASA Lewis Research Center, Cleveland, Ohio	
16 Abstract Arc cast W, CVD W, CVD Re, and powder metallurgy Re materials were hot isostatically pressure welded to ten different refractory metals and alloys (Cb, Cb-1Zr, Ta, Ta-10W, T-111, ASTAR-811C, W-25Re, Mo-50Re, W-30Re-20Mo, etc.) and thermally aged at 10^{-8} torr at 1200, 1500, 1630, 1800, and 2000°C for 100 to 2000 hours. Electron beam microprobe analysis was used to characterize the interdiffusion zone width of each couple system as a function of age time and temperature. Each system was least squares fitted to the equation: $\ln \left(\frac{\Delta X^2}{t} \right) = \frac{B}{T} + A$ where ΔX is net interdiffusion zone width, t is age time, and T is age temperature. Extrapolations of interdiffusion zone thicknesses to 10,000 hours were made. Classic interdiffusion analysis was performed for several of the systems by Boltzmann-Matano analysis. A method of inhibiting Kirkendall voids from forming during thermal ageing of dissimilar metal junctions was devised and experimentally demonstrated. An electron beam weld study of Cb-1Zr to Re and W-25Re demonstrated the limited acceptability of these welds. The report is presented in two parts. Part I contains the results and discussion of the experimental investigation. Part II contains detailed descriptions of experimental and analytical procedures utilized in conducting experimental program presented in Part I.			
17. Key Words (Suggested by Author(s)) Tungsten, Rhenium, Diffusion, Refractory Metal Interdiffusion, Chemical Interdiffusion, Autoclave Hot Isostatic Pressure Welding, Kirkendall Void Inhibition, Electron Beam Welding, Electron Beam Microprobe Analysis		18. Distribution Statement Unclassified, and unlimited.	
19. Security Classif. (of this report) Unclassified	20. Security Classif. (of this page) Unclassified	21. No. of Pages	22. Price*

* For sale by the National Technical Information Service, Springfield, Virginia 22151

FOREWORD

This final report describes work performed for the National Aeronautics and Space Administration under Contract NAS 3-13231 by the Westinghouse Astronuclear Laboratory. Mr. R. A. Lindberg of the Lewis Research Center was the NASA Program Manager.

The program was administered for the Westinghouse Astronuclear Laboratory by Mr. R. W. Buckman, Jr. Dr. F. G. Arcella was the principal investigator.

Assistance in several key task areas is appreciably acknowledged:

Autoclave HIP Welding: G. G. Lessman, D. R. Stoner and R. P. Spreccace

Metallographic Preparation: S. Laciak and R. Sabolcik

Microprobe Analysis: A. W. Danko and R. W. Conlin

Electron Beam Weld Study: L. G. Stemann

Program Consultation: R. W. Buckman, Jr., and R. A. Lindberg

This study was performed from July, 1970 to July, 1973.

Because of size limitations, the Appendices
are presented in two volumes.

Part IIA - Appendices A-G

Part IIB - Appendices H-K

APPENDICES

		<u>Page</u>
	Foreword	ii
	Summary	1
A	References	A-1
B	Diffusion Bibliography	B-1
C	Interdiffusion Predictive Model	C-1
D	HIP-Welding Operations	D-1
E	Hot Press Operation	E-1
F	Diffusion Couple Age/Identificator. Chart	F-1
G	Diffusion Analysis Methods	G-1
H	Hartley Computer Program	H-1
I	Lifshin Computer Program	I-1
J	Modification of the Colby MAGIC Program for Quantitative Electron Microprobe Analysis	J-1
K	Error Analysis	K-1

Part I of this report is NASA-CR-134490

I. SUMMARY

Dissimilar metal joints in thermionic power conversion systems can degrade through material interdiffusion. Such degradation effects occur (1) as cracks in brittle intermetallic phases which form in the juncture; (2) as Kirkendall voids which form in one side of the juncture; (3) or as an impurity which reduces the emittance efficiency of the diode. In order to resolve the time dependency of these effects, an experimental study was performed. Four diode emitter materials, (1) arc cast tungsten; (2) CVD tungsten; (3) powder metallurgy rhenium; and (4) CVD rhenium were autoclave hot isostatic pressure or hot press welded to each of the structural support alloys listed below:

Cb
Cb-1Zr
Ta
Ta-10W
T-111
ASTAR811C
Mo-50Re
W-30.9Re-20.1Mo
W-25Re
W or Re

The resulting bimetallic interdiffusion couples were vacuum aged for periods of 100, 1000, and 2000 hours at 1200, 1500, 1630, 1800, and 2000°C. Metallographic investigation as well as electron microprobe trace and spot count scans were employed to analyze the extent of interdiffusion as a function of age time and temperature. Computer programs were employed to correct the microprobe analysis data for fluorescence and adsorption and also to perform the Boltzmann-Mantano analysis of the interdiffusion concentration profiles. Engineering

relationships were established to predict the extent of interdiffusion for each system as a function of age temperature and age time. These relations are expressed for each couple system in the form:

$$\ln \left(\frac{\Delta X^2}{t} \right) = \frac{B}{T} + A \quad (1)$$

where ΔX is the net interdiffusion zone width (cm)

t is the age time at temperature (sec)

T is the age temperature ($^{\circ}$ K)

and A , B are constants.

Table 1 presents the parameters A and B for equation (1) for the interdiffusion systems studied.

High temperature solid state interdiffusion between two metallurgically joined metals of widely different melting points can also result in a coalescence of vacancies in the lower melting point material. The resulting pores form in a plane on one side of the juncture and can result in fracture in that plane, as well as through leakage of cesium plasma or containment gases. A method was devised to retard the formation of these Kirkendall voids, and a cursory investigation showed it to be quite successful.

Although all of the selected diffusion junctions survived the one age thermal cycle without fracture, several observations could be noted. Welded (hot isostatic pressure) interfaces with Re are not recommended for long term elevated temperature service due to brittle intermetallic phases and cracks which formed in the diffusion interface during short term thermal ageing. Nonplanar joints such as tubular (concentric cylinder) face joints with Re to Ta all cracked and fractured in the interdiffusion zone. Tungsten joined to columbium

Table 1. Parameters to Predict Net Interdiffusion Zone Width
As a Function of Age Time (t-seconds) and Temperature (T - °K)

$$\ln \left(\frac{\Delta X^2}{t} \right) = B \left(\frac{1}{T} \right) + A$$

(with 95% confidence limits)

System	A	B
W/Cb, Cb-1Zr	-3.8689 ± 0.2266	-37,390 ± 2810
Re/Cb, Cb-1Zr	-0.4899 ± 0.2266	-43,880 ± 3060
W/Ta, Ta-10W	-7.3385 ± 0.1891	-35,290 ± 2210
W/T-111, ASTAR	-3.3585 ± 0.1530	-44,720 ± 3760
Re/Ta, Ta-10W	-7,1024 ± 0.0980	-35,020 ± 1100
Re/T-111, ASTAR	-6.4489 ± 0.1374	-36,560 ± 1730
W/Mo-50Re	+0.1554 ± 0.1921	-45,140 ± 4500
Re/Mo-50Re	-8,4797 ± 0.1466	-30,140 ± 2940
W/W-30.9Re-20.1Mo	-7.2084 ± 0.1719	-34,750 ± 3890
Re/W-30.9Re-20.1Mo	-9.3027 ± 0.1440	-28,580 ± 3290
W/Re	-4.4641 ± 0.3317	-41,300 ± 7470
W/W-25Re	-2.1992 ± 0.4407	-47,100 ± 9930
Re/W-25Re	+2.4148 ± 0.5513	-53,990 ± 11,900

and tantalum alloys were not subject to joint cracking but were susceptible to considerable Kirkendall void formation. The most acceptable joints for long term high temperature service should be those of W to alloys such as T-111 or ASTAR-811C after being pretreated for Kirkendall void inhibition.

Studies were also conducted into the weldability of Re/Cb-1Zr and Cb-1Zr/W-25Re systems. EB weld parameters such as beam energy, width, traverse speed, sample geometry, etc. were evaluated.

Successful electron beam welds were produced between Cb-1Zr alloy and W-25Re or Re. These joints had braze characteristics in that the lower melting point Cb-1Zr was melted against the more refractory material, and little intermixing occurred. Due to the brittle nature of these welds and the limited extent of this study, employment of junctions of these materials cannot be recommended for specific application without more definitive characterization.

NOTE:

APPENDIX A - REFERENCES
are included within body of
NASA-CR-134490, Part I, Section XIII

APPENDIX B
DIFFUSION BIBLIOGRAPHY

By

F. G. Arcella

APPENDIX B. Diffusion Bibliography

Section I presents a brief bibliography of diffusion references pertinent to this study. Included are general diffusion studies, references to particular material systems, the handling of refractory systems, and background material. Attention was particularly directed toward refractory metal interdiffusion (chemical diffusion) studies.

Section II presents a brief bibliography of diffusion bonding references.

NASA (Computer) literature searches in several topical areas are referenced. These surveys were very useful in gathering information and references pertinent to this study. For instance, in one NASA survey for diffusion references, 80 percent of the references cited were pertinent to this study.

Section I. Diffusion References

1. Adda, Y., et al., "Application de la Thermodynamique des Processus Irreversibles a la Diffusion a L'etate Solide," Thermodynamics, Vol. II, IAEA, Vienna, 1966, p. 255.
Calculation of location of Kirkendall voids.
2. Alleau, T., et al., "Post Mortem Examinations of Thermionic Emitters," IEEE Thermionic Conversion Specialist Conference, Palo Alto, Calif., 1967, p. 312.
Interdiffusion zone widths for W/Mo and Mo/Re couples at 1900°K.
3. Andelin, R. L., Knight, J. D., and Kahn, M., "Diffusion of W and Re Tracers in W," Trans. Met. Soc. of AIME, Vol. 233, January, 1965, p. 19.
Arrhenius equation for diffusivity of Re* into W for 2660°C to 3230°C.
4. Anon., "Studies of Thermionic Materials for Space Power Applications," GA-5665 (NASA-CR-54322), Annual Report for Spetember, 1963 through August, 1964. September, 1964, pp. 240 - 247.
Interdiffusion in Ta/W, Cb/W, Mo/W systems.
Also in GA-9495 and STAR Abstract N71-14140.
5. Askil, J., "A Bibliography on Tracer Diffusion in Metals,"
"Part I. Self-Diffusion in Pure Metals," ORNL-3795, 1965.
"Part II. Impurity Diffusion in Pure Metals," ORNL-3795 II, 1965.
"Part III. Self and Impurity Diffusion in Alloys," ORNL-3795 III, 1967.
"Supplement II to Parts I, II, III," ORNL-3795, 1967.
General diffusion references, mostly tracer work.
6. Baluffi, R. W., "The Determination of Diffusion Coefficients in Chemical Diffusion," Acta Met., Vol. 8, December, 1960, p. 871.
7. Barnes, R. S. and Mazey, D. J., "The Effect of Pressure Upon Void Formation in Diffusion Couples," Acta Met., Vol. 6, January, 1958.
8. Barrer, R. M., Diffusion in and Through Solids, Cambridge University Press, 1941.

9. Bokshtein, S. Z., et al., "Volume and Boundary Diffusion of Tungsten in Molybdenum," WPAFB, FTD-HT-23-887-67, November, 1967.
10. Boltzmann, L., Ann. Phys. (Leipzig), Vol. 53, 1894, p. 959.
11. Butz, R., Erley, W. and Wagner, H., "Diffusion Problems with W Coated Mo Emitters," 1970 Thermionic Conversion Specialists Conference (Proceedings of IEEE), October, 1970, Miami, Florida, p. 101.
Interdiffusion data for W/Mo system at 1900, 2250°C.
12. Bückle, H., "Emploi des Mesures de Microdurete a L'etude de la Diffusion Inter-metallique," Symposium on Solid State Diffusion, N. Holland Publ. Co., July, 1958, p. 21.
Interdiffusion analysis by microhardness indent traverses.
13. Castleman, L. S., "An Analytical Approach to the Diffusion Bonding Problem," Nucl. Sci. and Engr., Vol. 4, 1958, pp. 209 - 216.
14. Chandler, W. T. and Walter, R. J., "Hydrogen Effects in Refractory Metals," Refractory Metal Alloys, Metallurgy and Technology, Editors I. Machlin, R. T. Begley, and E. Weisent, Plenum Press, 1968, p. 197.
15. Crank, J., Mathematics of Diffusion, Oxford-Clarendon Press, 1956.
16. Darken, L. S., AIME Trans., Vol. 175, 1948, p. 184.
17. DeHoff, R. T., Anusavice, J. K., and Wan, C. C., "Diffusion Composition Path Patterns in Ternary Systems," University of Florida, ONR Contract No. N-00014-68-A, 0173-0011, Metallurgy Branch NR 031-697, undated. (Received on February 15, 1972).
18. Diffusion in Body-Centered Cubic Materials, Editors J. A. Wheeler, Jr. and F. R. Winslow, ASM Publication, 1965.
19. Diffusion Data, Published by the Diffusion Information Center, Bay Village, Ohio. Volumes 1 - 5,

An annotated bibliography of diffusion references categorized by type of diffusion, solvents, diffusion analysis, etc.

20. Dickinson, J. M. and Richardson, L. S., "Constitution of Re-W Alloys," Trans. ASM, Vol. 51, p. 758, April 18, 1958.
21. Eckel, J. F., "Diffusion Across Dissimilar Metal Joints," Journal of American Welding Society, Welding Res. Suppl. 170-S, April, 1964.
22. Fitterer, G. R., "Entropy, Lattice Parameters, and High Temperature Phenomena of Metals," ASM Trans. Quarterly, Vol. 60, March, 1950, p. 15.
23. Gertsriken, S. P. and Dekhyar, I. Ya., Solid State Diffusion in Metals and Alloys, AEC-TR-6313, April, 1964.
24. Girifalco, L. A., "Diffusion in Solids at High Pressures," Metallurgy at High Pressures and Temperatures, Vol. 22, Gordon Breach Publ., 1963, p. 260.
25. Guy, A. G., Blake, R. G. and Oikawa, H., "Predicting the Course of Homogenization in Multi-Component Alloys," AIME TMS Trans., Vol. 239, June, 1967, p.771.
26. Guy, A. G., Leroy, V. and Lindemer, T. B., "Diffusion Calculations in Three-Component Solid Solutions," ASM Trans., Vol. 59, No. 3, Sep., 1966, pp. 517 - 534.
27. Guy, A. G. and Leroy, V., "Diffusion en Systeme Ternaire Application on Systeme Co-Ni-Cr," Journes Internationales des Applications due Cobalt, Bruxellus, 1964.
28. Guy, A. G. and DeHoff, R. T., "The Study of Multi-Phase Diffusion in Three Component Metallic Systems," AFML-TR-68-360, WPAFB, January, 1969.
29. Hartley, C. S. and Hubbard, K., "A Computer Program for the Matano Analysis of Binary Diffusion Data," ASD-TRD-62-858, November, 1962.
Modified for CDC 6600 Fortran IV and used in this study.
30. Hartley, C. S., Steedly, J. E. and Parsons, L. D., "Binary Intradiffusion in Body-Centered Cubic Transition Metal Systems," ML-TDR-64-316, 1964.
31. Hehemann, R. F. and Leber, S., "Chemical Diffusion in the Cb-W System," AIME Trans., Vol. 236, July, 1966, p. 1040.
W/Cb interdiffusion at 1700, 1900, 2100, 2300°C.

32. Hudson, R. G., Horner, M. H., and Yang, L., "Some Investigations of Refractory Metal Systems of Thermionic Interest," IEEE Thermionic Conversion Specialist Conf. (proceedings) NASA-CR-111593 (GA-9495), Carmel, Calif., October 21, 1969.
W/Ta, W/Mo, W/Cb interdiffusion at 2000, 2100, 2200°C.
Interdiffusion zone widths given.
33. Hudson, R. G. and Yang, L., "Diffusion and Electron Emission Properties of Duplex Refractory Metal Thermionic Emitters," Refractory Metals and Alloys IV, Research and Development II, AIME publ., October, 1965, p. 1253.
Interdiffusion zone widths for W/Re, W/Ir systems at 1600, 1800, 2000, 2100°C.
34. Ivanov, A. N., Krasilnikova, G. B. and Mitin, B. S., "Diffusion Parameters in the Mo-Ta and W-Ta Systems," Fiz. Metal. Metalloved., Vol. 12, No. 2, 1970, pp. 520 - 524.
35. Jost, W., Diffusion in Solids, Liquids, and Gases, Academic Press, Inc., 1952.
General diffusion reference.
36. Kirby, L. J. and Fullam, H. T., "Promethium Heat Source Compatibility Studies, Part II. Metal-Metal Compatibility at 1100°C," BNWL-398, May, 1967.
37. Larikov, L. N. et al., "Investigation of Rhenium and Molybdenum Diffusion in Tungsten and Tungsten Alloys," Tech. Trans. FTD-HT-27-768-68 (AD-686985).
Not chemical interdiffusion, but tracer diffusion into poly- and single crystal solvents.
38. Lesueur, R., "Mesure des Flux Partiels de Degazage du Molybdene et du Tungstene a 2000°K," Colloque sur la Metrologie et L'Analyse des Gas en Ultra-Vide, CONF-700418-1, CEA, Paris, April 22, 1970.
Vacuum outgassing rates for Mo and W.
39. Levesque, P., et al. "Constitution of Re-Cb Alloys," ASM Preprint No. 192, 42nd Annual ASM Conf., Philadelphia, October 17, 1960.
40. Lifshin, E. and Hannemann, R., "Electron Microbeam Probe Analysis. II, Automated Data Collection and Computer Analysis," GE-66-C-250, September, 1966.

41. Lindemer, T. B. and Guy, A. G., "Apparatus for Bonding and Diffusing Metal Specimens Under Pressure," *Welding Journal Res. Suppl.*, May, 1968.
42. Lindemer, T. B. and Guy, A. G., "Analysis of Ternary Diffusion Curves Using a Second Integration of the Fick Law," *AIME TMS Trans.*, Vol. 239, December, 1967, p. 1924.
43. Manning, J. R., "Diffusion in a Chemical Concentration Gradient," *Phys. Rev.*, Vol. 124, No. 2, October 15, 1961.
44. Manzione, A. V., et al., "Observations Concerning the Interdiffusion of Cb-1Zr Alloy with 316 Stainless Steel," PWAC, USAEC Contract AT(30-1)-2789.
45. Matano, C., *Z. Phys. Japan*, Vol. 8, 1933, p. 109.
46. Maurice, F., "Microprobe Use in Diffusion Studies," *J. Microsc.*, Vol. 9, No. 3, 1970, pp. 296 - 299.
47. M'Hirsi, A., "Influence de la Pression sur la Diffusion dan les Metaux," *Memoires Scientifiques Rev. Metallurg*, Vol. LXIV, No. 7/8, 1967.
Effects of pressure on diffusion in metals.
48. Anon., "Diffusion in Refractory Metals," ML-TDR-64-61, WPAFB AFML, March, 1964.
Interdiffusion in the W/Ir, W/Ru, W/Rh, W/Pt systems.
49. Ogren; J. R., Blumenthal; J. L., and Ham, R. C., "Radioisotope Propulsion Technology Program (POODLE). Final Report. Vol. III - Oxidation and Diffusion in Noble Metal Alloy Claddings," STL-517-0049, October, 1966.
50. Peterson, N. L., "Diffusion in Refractory Metals," WADD Tech. Report TR-60-793, March, 1961.
Generally C, O, H, etc. interstitial diffusion.
51. Pawell, R. E. and Lundy, T. S., "Tracer Diffusion in Tungsten," *Acta Met.*, Vol. 17, No. 8, 1969, pp. 979 - 988.
Tracer diffusion of Nb*, Ta*, and W* into W.

52. Passmore, E. M. et. al., "Investigation of Diffusion Barriers for Refractory Metals," ASD-TDR-62-432, WPAFB AFML, July, 1962.
- Also,
WADD Tech. Report TR-60-343, August, 1960.
53. Patterson, J. W., "An Analysis of Intrinsic Diffusion and Interdiffusion in Single Phase Binary Diffusion Couples," ERL-528, Amex Laboratory, Preprint Proj. 713-S, (AD-708633).
54. Phillips, W. M., "Welding and Aging of Bi-Metallic Refractory Metal Joints," IEEE Thermionic Conversion Specialist Conf., October, 1970, Miami, Florida.
- Observed that wide weld joints had lower incidence of Kirkendall voids after aging.
55. Prokushkin, D. A. and Vasileva, E. V., "Mutual Diffusion of Niobium and Metals of the IV A, V A, and VI A Groups," WPAFB FTD, Ab 685 - 007, Nov., 1968.
56. Rapperport, E. J. and Hartley, C. S., "A Review of Diffusion in Refractory Metal Systems," Refractory Metals and Alloys II, Vol. 17, J. Wiley and Sons, 1962, p. 191.
57. Roux, F. and Vignes, A., "Diffusion dan les Systèmes Ti-Cb, Zr-Cb, W-Cb," Revue de Physique Appliquée, Tome 5, Juin, 1970, p. 393.
58. Sabatier, J. P. and Vignes, A., "Etude de Phenomenes de Diffusion dan les Systeme Ternaire Fe-Ni-Co," Memoires Scientifiques Rev. Metallurg, Vol. LXIV, No. 3, 1967.
- Good microprobe work, concentration profiles.
59. Shewmon, P. G., Diffusion in Solids, McGraw-Hill Co., 1963.
- General diffusion reference.
60. Smigelskas, A. D. and Kirkendall, E. O., Metals Technol., 13, Tech. Publ. 2071, 1946.
- Original description of vacancy flux and coalescence into voids.
- Also,
AIME Trans., Vol. 171, 1947, p. 130.

61. Smithells, C. J., Ed., Metals Reference Book, 4th Ed., Vol. II, p. 637, 1967.
62. Someren, L. Van, "Metallurgical Observations on Thermionic Converters," IEEE Thermionic Conversion Specialist Conference, Palo Alto, Calif., 1967, p. 321.
Interdiffusion data for Re-Ta at 2000°K.
63. Steichen, J. M., "Interdiffusion Between Certain Vapor Deposited - Foil Refractory Metal Couples," BNWL-1071 (UC-25), June, 1969.
64. Tregubov, E. A., et al., "Diffusion of Ta in W," *Koklady*, Vol. 180, *Academiia Nauk, SSSR*, 1968, p. 423 (In Russian).
W-Ta interdiffusion at 2000°C for 48 hours.
65. Wagner, C., "The Evaluation of Data Obtained with Diffusion Couples of Binary Single-Phase and Multi-Phase Systems," *Acta. Met.*, Vol. 17, February, 1969, pp. 99 - 107.
66. Wahl, G. and Demny, J., "Behavior of CVD W Layers on Mo," IEEE Thermionic Specialist Conf., Miami, Florida, October, 1970.
Some considerations on concentration profile time dependency.
67. Walker, G. H. and Lewis, B. W., "Cu-Ni Diffusion: Electron Microprobe Study of Effects of Voids and Discontinuities," *AIME TMS Trans.*, Vol. 1, September, 1970, p. 2643.
68. Zelikman, A. N., et. al., "Diffusion of Re in W," NDC-548526 (Russian Translation).
D(Re -W) at 1400°C to 2000°C.
69. Ziebold, T. O. and Ogilvie, R. E., "Ternary Diffusion in Cu-Ag-Au Alloys," *AIME TMS Trans.*, Vol. 239, July, 1967, p. 942.

Additional Diffusion References In:

1. NASA Literature Search No. 11870
"Interdiffusion of Tungsten, Rhenium, Tantalum, Columbium, Molybdenum, Hafnium, and Zirconium," May 13, 1970
Several good references to refractory metal interdiffusion and analysis.
2. NASA Literature Search No. 16622
"Interdiffusion Between Tungsten or Rhenium and other Refractory Metals,"
October 13, 1971
Several good references to refractory metal interdiffusion.
3. NASA Literature Search No. 16627
"Evolution of Absorbed Hydrogen," October 12, 1971
Used for analysis of post autoclave hydrogen removal from diffusion couples.
4. NASA Literature Search No. 16621
"Solid State Diffusion Analysis," October 13, 1971
Several references in analytical techniques as well as additional material references.
5. NASA Literature Search No. 16627
"Evolution of Absorbed Hydrogen," October 12, 1971
6. Defense Documentation Center Search, Control No. 038178
"Solid State Diffusion," April 17, 1970

Section 2. Diffusion Bonding References *

1. Bannin, P., "A Study of the Literature of Diffusion Bonding," CRNL-TR-851, 1965.
2. Batista, R. I., et. al, "Elevated Temperature Diffusion Bonding of Tungsten to Tungsten Under Pressure," LA-2751, 1966.
3. Crane, C. H., et al., "Study of Dissimilar Metal Joining by Solid State Welding," NASA-CR-82460, 1965.
4. Cunningham, G. W. and Spretnak, J. W., "The Mechanisms of Pressure Bonding," BMI-1512, 1961.
5. D'Annessa, A. T., "The Solid-State Bonding of Refractory Metals," Welding Journal Supplement, 1964.
6. Dunning, J. S. and Metcalfe, A. G., "Basic Metallurgy of Diffusion Bonding," AD-460949, 1964.
7. Fugardi, J. and Zambraw, J. L., "Bonding of Various Metals and Alloys by Isostatic Pressing at Elevated Temperatures," SCNC-272, 1958.
8. Hickox, G. K., "Diffusion Bonding of Tungsten Alloys," WAL-TR-465.54/4, 1963.
9. Hodge, E. S., "Gas Pressure Bonding of Refractory Metals," Engineering Quarterly, Vol. 1, No. 4, 1961, pp. 3 - 20.
10. Metcalfe, A. G., et al., "Diffusion Bonding of Refractory Metals," Progress Report Nos. 1-6, 1962 - 1964.
11. Paprochi, S. J., et al., "Gas Pressure Bonding," DMIC -159, 1961.
12. Paprochi, S. J., et al., "The Bonding of Molybdenum - and Niobium - Clad Fuel Elements," BMI-1451, 1960.
13. Samsonov, G. V., "The Electron Theory of Diffusion Welding," Automat. Weld., Vol. 19, No. 10, 1966, pp. 30 - 35.
14. Torgenson, R. T., et al., "State-of-the-Art Survey of Dissimilar Metals Joining by Solid State Welding," NASA-CR-76933, 1965.

* Hot Isostatic Pressure (HIP) Welding

Additional Autoclave Welding References In:

1. NASA Literature Search No. 16628
"Autoclave Applications in Welding," October 12, 1971

APPENDIX C
INTERDIFFUSION PREDICTIVE MODEL

By
F. G. Arcella

APPENDIX C. Interdiffusion Predictive Model

Before the age time/temperature schedule for this program was fixed, an interdiffusion zone width predictive model was derived. This model was necessary in that underageing of the diffusion couples would have resulted in small interdiffusion zone widths that would have been difficult to analyze and would have resulted in very high errors. The interdiffusion zone widths (Δx -cm) after ageing for time (t -seconds) at temperature (T - $^{\circ}$ K) were predicted as

$$\ln \left(\frac{\Delta x^2}{t} \right) = 21.0 \left(\frac{T}{T_m} \right) - 37.5$$

where T_m is the lowest melting point of the W or Re to metal X binary couple.

I. INTRODUCTION

An extensive literature review, including a computer key word search, of experimental refractory metal interdiffusion data was made in order to:

1. Establish the degree and extent of prior work with respect to the work planned for this study, and to
2. Construct an engineering level, predictive model to determine the extent of interdiffusion as a function of age time, age temperature, and material combination.

Experimental interdiffusion investigations between thermionic emitter materials (primarily W, Re) and refractory metal structural support materials (primarily Cb, Ta, W-Re alloys) were studied. Chemical interdiffusion studies (infinite, binary couples) were reviewed rather than isotope tracer or similar semi-infinite boundary condition work.

The published interdiffusion information in the above selected primary materials areas was quite sparse, indicating a definite area for valuable contributions. From the scant experimental data that was available, an engineering level predictive model was derived. The model predicts the interdiffusion zone width (the linear extent between 2 percent and 98 percent of W or Re) of tungsten or rhenium to refractory metal alloys as a function of age time at temperature. Two model equations were derived:

$$\ln \left(\frac{\Delta x^2}{t} \right) = 25.6 \left(\frac{T}{T_m} \right) - 43.2 \quad (C-1)$$

for W or Re to Group VIII elements of the periodic table, and

$$\ln \left(\frac{\Delta x^2}{t} \right) = 21.0 \left(\frac{T}{T_m} \right) - 37.5 \quad (C-2)$$

for W or Re to Group V and VII elements of the periodic table. In these equations Δx is the interdiffusion zone width (2 percent to 98 percent W or Re) in cm, t is the age time (seconds) at constant temperature T ($^{\circ}\text{K}$), and T_m is the lowest melting point ($^{\circ}\text{K}$) of the diffusion couple binary material combination (i.e., an eutectic for instance). The interdiffusion zone width predictive model derived presented a good correlation with experimental values. Its derivation is described below.

II. MODEL DEVELOPMENT

Solid state mass transport has been studied for many years, and many references attest to the degree of sophistication of analyses of the phenomenon.^{(1,2)*} For the purposes of establishing an engineering level predictive model, only the simplest precepts need be forwarded.

The temperature dependence of diffusion coefficients has been historically described by the Arrhenius relation

$$D = D_0 e^{-Q/RT} \quad (C-3)$$

where

- D = Diffusion Coefficient
- D₀ = Constant
- Q = Activation Energy
- R = Gas Constant
- T = Age Temperature (°K)

Since the interdiffusion distance, Δx , has also been expressed by relating it to D,

$$\Delta x \propto \sqrt{Dt} \quad (C-4)$$

where t is age time, then it follows that one could relate interdiffusion zone width and age time to D and thus to temperature:

$$\frac{\Delta x^2}{t} \propto D_0 e^{-Q/RT} \quad (C-5)$$

The natural logarithm of each side of equation (C-5) results in (C-6):

$$\ln \left(\frac{\Delta x^2}{t} \right) = C - \frac{Q}{RT} \quad (C-6)$$

*References cited are located at the end of this section, Section C.

where C is a constant. A semilogarithm graph of $\Delta x^2/t$ versus the reciprocal of the age temperature will generally be a straight line, and will yield a "quasi" activation energy for interdiffusion zone width determination.

Experimental data for W-Re interdiffusion from Hudson and Yang⁽³⁾ are plotted in Figure C-1 to demonstrate the validity of equation (C-6). The interdiffusion zone width for W-Re systems can be predicted for any one age time-temperature combination by the use of Figure C-1 where Q, the "quasi" activation energy, is 42,000 cal./mole.

However, if one wishes to predict interdiffusion zone thicknesses in other W-refractory metal systems, Figure C-1 would be inadequate, as demonstrated in Figure C-2, where the interdiffusion characteristics of several systems are presented.⁽⁴⁾

A general, Larson-Miller type parametric relationship can be established to relate all W-refractory metal interdiffusion data to one "Family" line by first referring to Fitterer.⁽⁵⁾ Fitterer shows that all metals possess the same total entropy at one degree below their respective melting points (T_m-1), and at zero degrees Kelvin. Thus, on a fractional scale, every element would possess the same relative entropy content when at equal T/T_m ratios. The maximum entropy of an alloy system would occur at its lowest melting point - whether eutectic or solid solution system. Thus, using T/T_m , where T_m is the lowest melting point of the binary W-refractory metal alloy couple, it is possible to relate different couple combinations to equal entropy levels.

To relate the relative entropy level to $\Delta x^2/t$, the activation energy, Q, must be investigated. Consider for a lattice jump that⁽²⁾

$$D = \left[K \exp. \left(\frac{S}{R} \right) \right] \exp. \left(\frac{-H}{RT} \right) \quad (C-5)$$

where H is the energy required for a lattice jump, S is the entropy created by the jump, and the bracket term is the D_0 in (C-3)⁽²⁾:

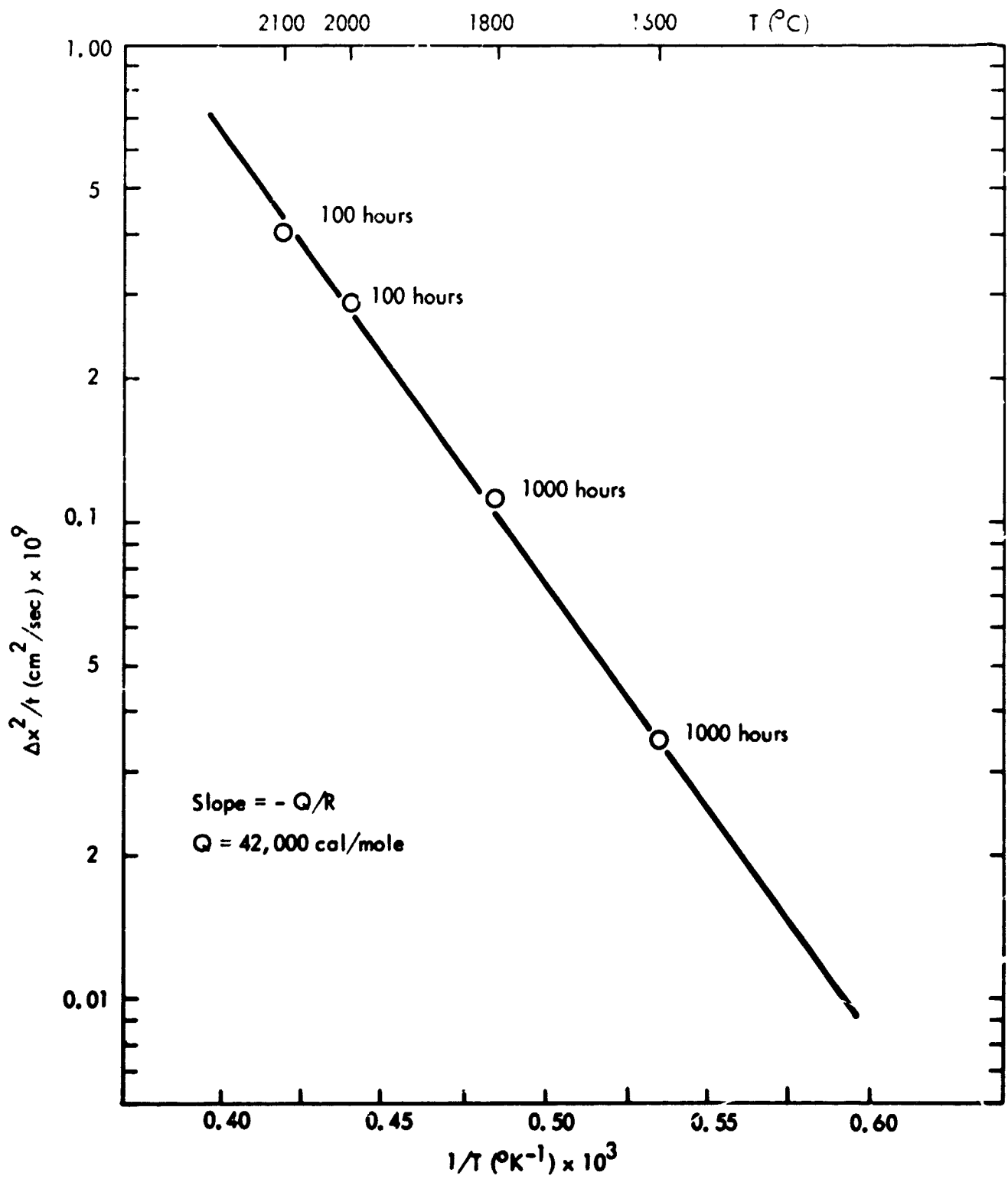


Figure C-1. Interdiffusion for W-Re System⁽³⁾, Independent of Time at Temperature. Can be used to Calculate Interdiffusion Zone Width (Δx) for any Age Time t at any Temperature T .

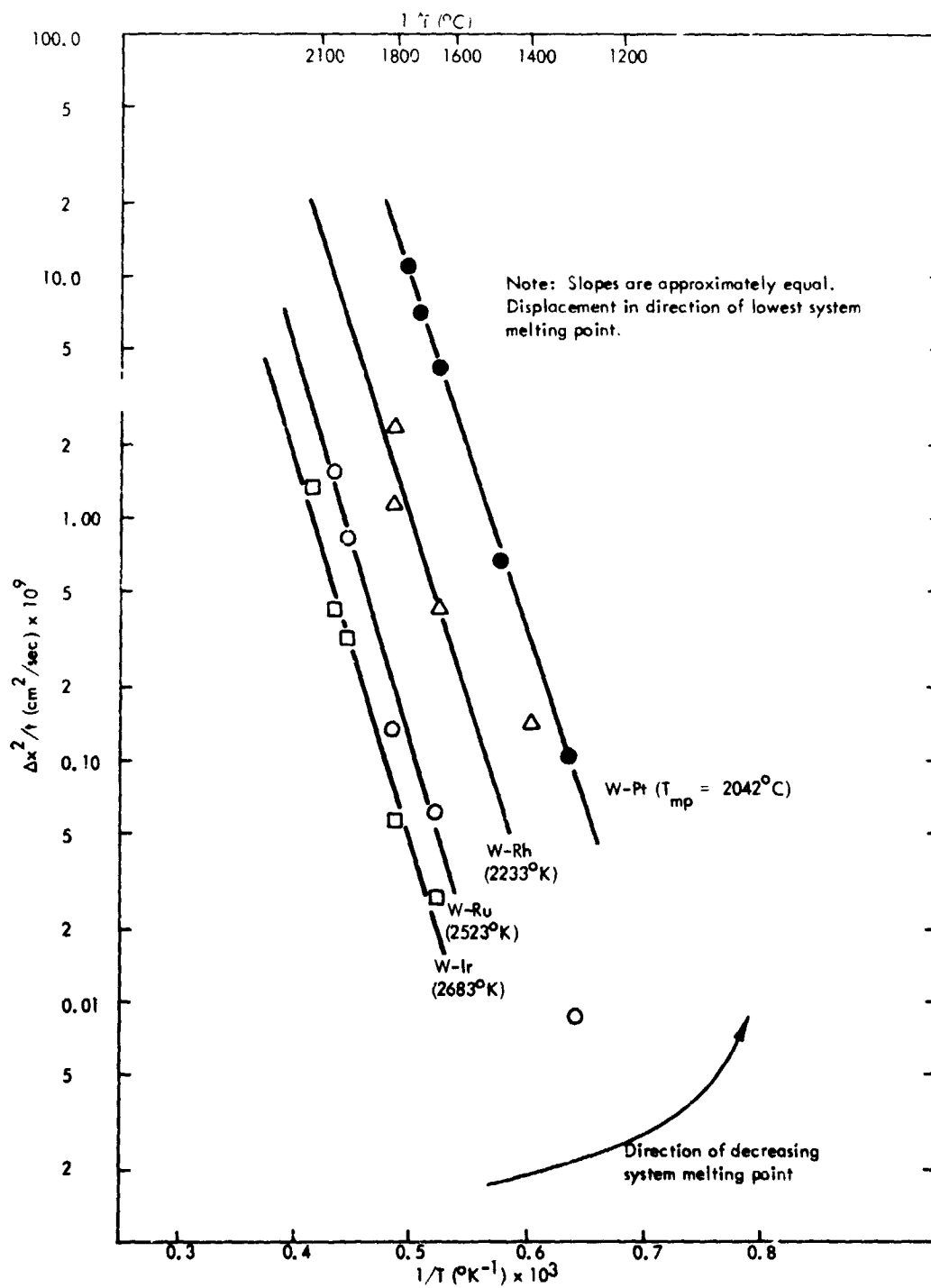


Figure C-2. Interdiffusion of W and Various Refractory Metals.⁽⁴⁾

Then,

$$\ln \left(\frac{\Delta x^2}{t} \right) = K - \frac{H}{RT} + \frac{S}{R} \quad (C-8)$$

By using Fitterer's relative entropy concept where

$$S \propto \frac{T}{T_m} \quad (C-9)$$

and since H will be approximately the same for all of the W/"X" systems studied as shown by the constant slopes of the W/"X" systems plotted in Figure C-2, then H/RT will approach a constant value, for the purposes of argument, for all of the W/"X" systems studied. Thus, for any W/"X" system of interest, the only variable will be T/T_m, where T is the temperature of interdiffusion, and T_m is the lowest system melting point, and equation (C-8) becomes

$$\ln \left(\frac{\Delta x^2}{t} \right) \propto \frac{T}{T_m} \quad (C-10)$$

The following systems and their melting points (lowest system melting point) are plotted in Figures C-2 and C-3.

<u>System</u>	<u>T_m</u>	<u>Ref.</u>
W/Ru	2523°	4
W/Ir	2683	4
W/Rh	2233	4
W/Pt	2042	4
W/Ir	2683	3

Note in Figure C-2 that the slopes, or activation energies are approximately the same for all of the systems. The displacement of the curves appears to be proportional to T/T_m - or, the relative entropy level of each system. Figure C-3 presents the same $\Delta x^2/t$ information that is in Figure C-2, except that it is plotted against T/T_m as expressed in equation (C-10).

The consistency of the line in Figure C-3 with the prediction of equation (C-10) reinforces the relative entropy level concept. Figure C-3 presents the extent of interdiffusion (zone width) for age time t and age temperature T for tungsten to Group VIII elements of the periodic table. Curve fitting to Figure C-3 resulted in the following function

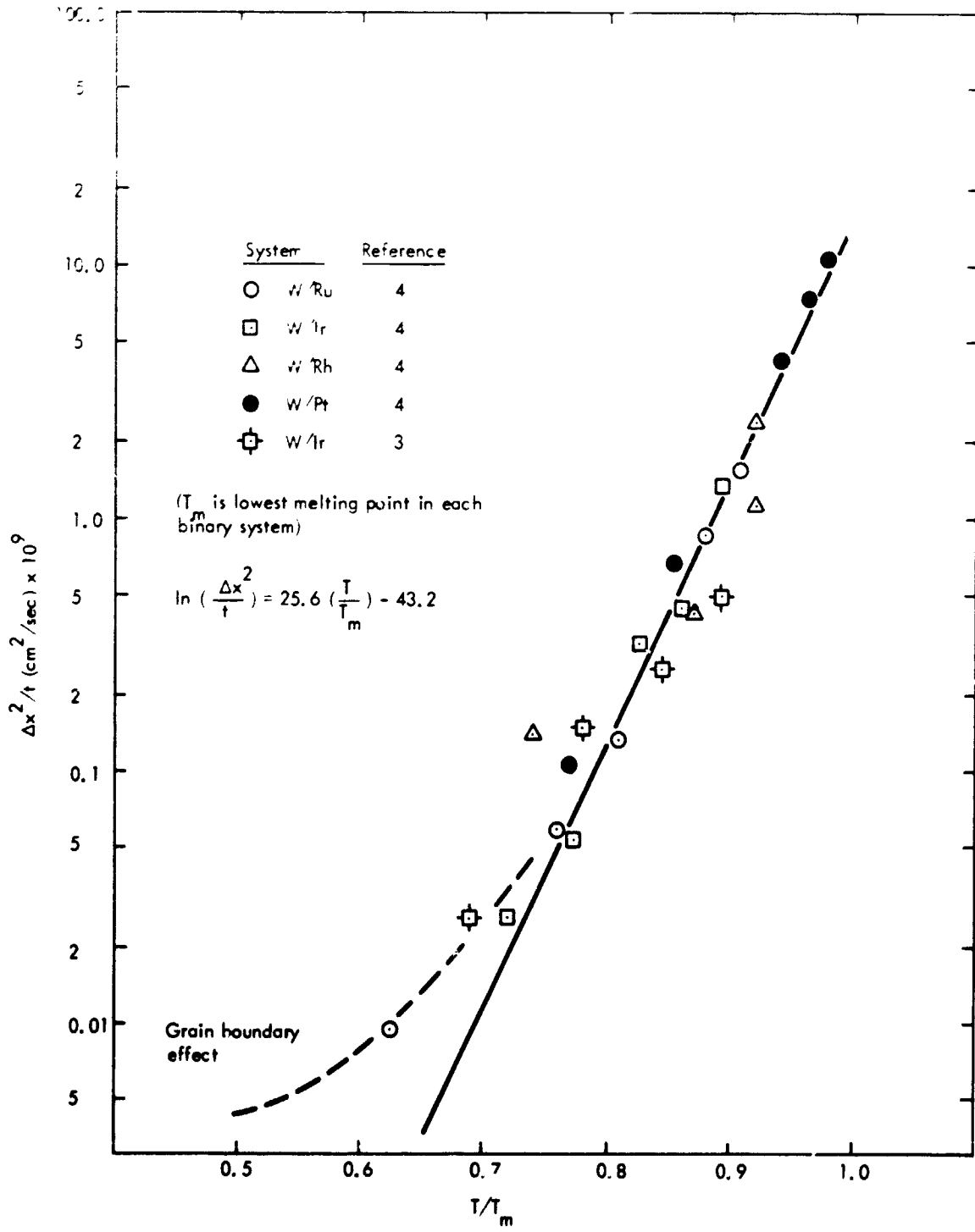


Figure C-3. Interdiffusion Zone Width (Δx) for Age Time t for W to Group VIII Elements of the Periodic Table.

$$\ln \left(\frac{\Delta x^2}{t} \right) = 25.6 \left(\frac{T}{T_m} \right) - 43.2 \quad (\text{C-11})$$

where Δx = Interdiffusion Zone Width (cm)
 t = Age Time (sec.)
 T = Age Temperature ($^{\circ}\text{K}$)
 T_m = Lowest System Melting Point ($^{\circ}\text{K}$)

III. PREDICTIVE MODEL FOR THIS STUDY

The model format was also applied to tungsten and rhenium literature data for interdiffusion with elements of Groups V and VII of the periodic table. The following systems and their melting point (lowest system melting point) ratios are presented in Figure C-4.

<u>System</u>	<u>T_{mp}</u>	<u>Ref.</u>
W/Cb	2743 ^o K	6,7
W/Re	3100	3
W/Ta	3269	7
Re/Ta	2963	WANL*

The zone width predictive model in Figure C-4 follows the equation

$$\ln \left(\frac{\Delta X^2}{t} \right) = 21.0 \left(\frac{T}{T_m} \right) - 37.5 \quad (C-12)$$

where Δx = Interdiffusion Zone Width (cm)
 t = Age Time (seconds)
 T = Age Temperature (^oK)
 T_m = Lowest Melting Point of Binary Combination (^oK)

Both Figures C-3 and C-4 demonstrate that a family relationship, commonality, can be established for W and Re interdiffusion between separate groups of the periodic table. Also, the T/T_m ratio places all data at the same relative fraction of the melting point - a position of common entropy levels. The effects of low temperature grain boundary diffusion can be seen by deviation from the linear relationship at temperatures below T/T_m = 0.6 in both figures.

Equation (C-12) and Figure C-4 were used to estimate tungsten and rhenium to Cb, Ta, Re, etc. interdiffusion zone widths for the proposed ageing conditions of this program. All inter-

* High temperature anneal of KVI couples. Preliminary program data.

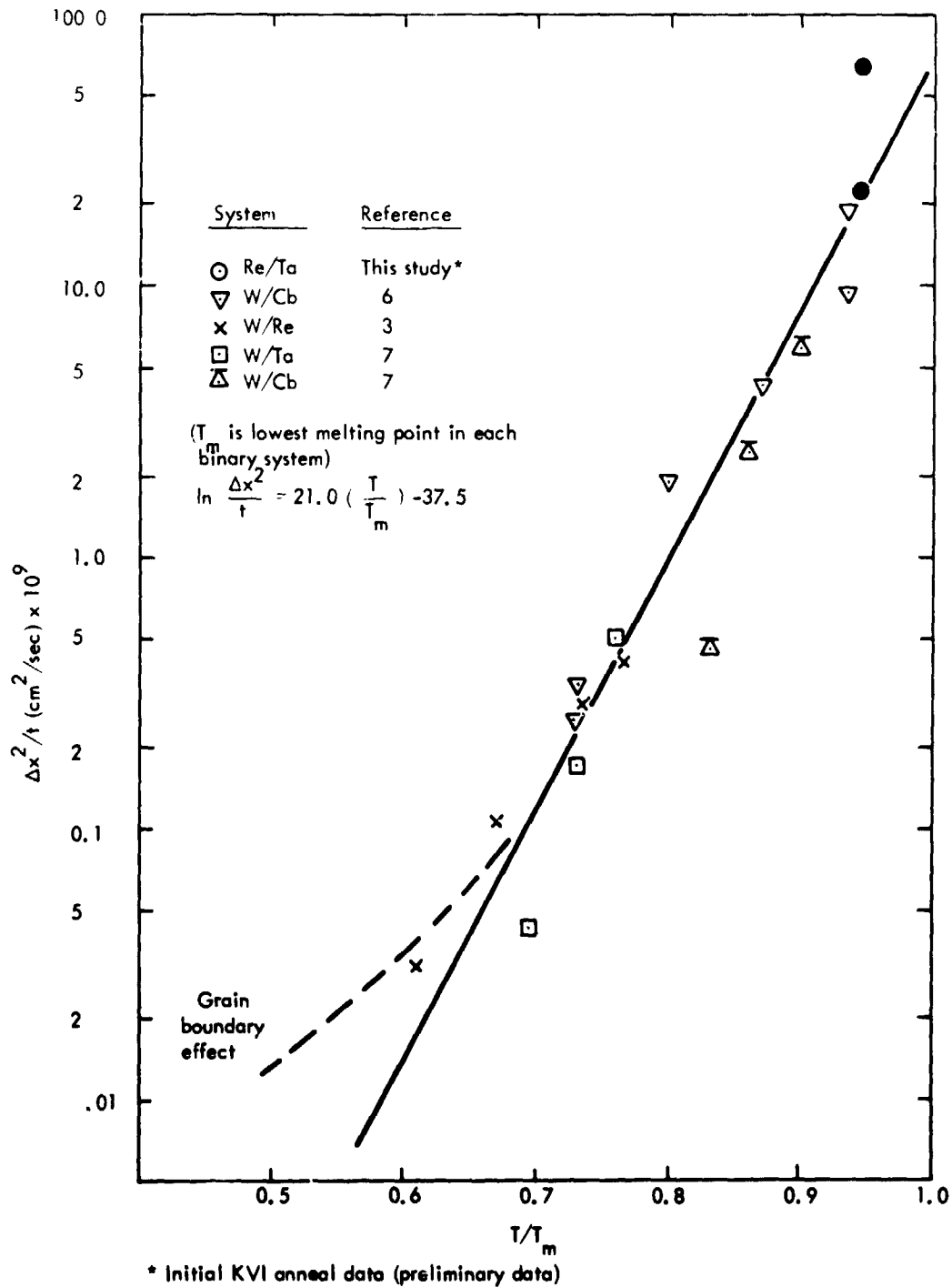


Figure C-4. Interdiffusion Zone Width (Δx) for Age Time t for W to Group V and VII Elements of the Periodic Table.

diffusion zone widths for the couples of this program were predicted to exceed 3.5×10^{-3} cm (i.e., 50μ at a 45° angle to the interface). This dimension was deemed acceptable for microprobe analysis.*

* Acceptable microprobe traverse being 25 spot count steps at 2μ step intervals.

IV. CONCLUSION

Two predictive interdiffusion zone width models were derived through relative entropy ratio concepts. For the interdiffusion of W with Group VIII elements of the periodic table, zone width relationships were established as:

$$\ln \left(\frac{\Delta x^2}{t} \right) = 25.6 \left(\frac{T}{T_m} \right) - 43.2 \quad (C-13)$$

For interdiffusion of W or Re with Group V and VI elements of the periodic table, zone widths followed the relation:

$$\ln \left(\frac{\Delta x^2}{t} \right) = 21.0 \left(\frac{T}{T_m} \right) - 37.5 \quad (C-14)$$

where Δx = Zone Width in cm
 t = Age Time (seconds)
 T = Age Temperature ($^{\circ}$ K)
 T_m = Lowest System Melting Point ($^{\circ}$ K)

Equation C-14 was employed early in the study to demonstrate that the age time/temperature conditions selected were adequate to achieve analyzable (microprobe) interdiffusion zones.

APPENDIX C: Interdiffusion Predictive Model References

1. Jost, W., Diffusion in Solids, Liquids, and Gases, Academic Press, Inc., 1952.
2. Shewmon, P. G., Diffusion in Solids, McGraw-Hill Co., 1963.
3. Hudson, R. G. and Yang, L., "Diffusion and Electron Emission Properties of Duplex Refractory Metal Thermionic Emitters," Refractory Metals and Alloys IV, Research and Development II, AIME publ., October, 1965, p. 1253.
4. Anon., "Diffusion in Refractory Metals," ML-TDR-64-61, WPAFB AFML, March, 1964.
5. Fitterer, G. R., "Entropy, Lattice Parameters, and High Temperature Phenomena of Metals," ASM Trans. Quarterly, Vol. 60, March, 1960, p. 15.
6. Hehemann, R. F. and Leber, S., "Chemical Diffusion in the Ch-W System," AIME Trans., Vol. 236, July, 1960, p. 1040.
7. Hudson, R. G., Horner, M. H., and Yang, L., "Some Investigations of Refractory Metal Systems of Thermionic Interest," IEEE Thermionic Conversion Specialist Conf., NASA-CR-111593 (Also GA-9495), Carmel, Calif., October 21, 1969.

APPENDIX D
HIP - WELDING OPERATIONS

By
D. R. Stoner

APPENDIX D. HIP - Welding Operations

- I. Summary
- II. HIP - Weld Parameters
 - A. Background - Model
 - B. Material Handling
- III. Parameter Evaluation Cycles
 - A. Autoclave Facility
 - B. Weld Parameter Resolution
 - C. Specimen Condition
- IV. HIP - Weld Cycles
 - A. Two Weld Cycles
 - B. Diffusion Couple Condition
 - C. Hydrogen and Interstitial Analysis
- V. Conclusions - Autoclave Operation

I. SUMMARY

This appendix reviews the autoclave HIP-welding operations which occurred during the course of this program. Operation and autoclave practice are reviewed, and special attention is given to hydrogen pickup in the sample materials, as well as oxidation prevention.

Table D-I shows that four autoclave cycles were made in this program, two to resolve HIP-weld parameters, and two to weld the program couples. Table D-II presents several conclusions concerning autoclave practice.

The following sections describe the autoclave facility; preparation, loading, and operating practices; the four HIP-weld cycles of this program; and contamination problems.

Table D-1. Diffusion Couple Evaluation - HIP-weld Cycles

<u>Cycle</u>	<u>Purpose</u>	<u>Results</u>
1	Evaluate HIP-weld T-P conditions for all-ys of program.	Molybdenum HIP-weld cans leaked due to oxygen hot tearing. Showed need to add getters (tantalum alloy chips) and baffles to furnace.
2	Evaluate HIP-weld T-P conditions for alloys of program.	Welding conditions of 193 MN/m^2 at 1440°C for 40 minutes yielded 95-100% welding of all alloys in the program. Ta chips and Ta foil baffles prevent oxygen hot tearing of molybdenum cans.
3	HIP-weld of all program diffusion couples at T-P conditions of cycle 2.	Problems in autoclave furnace control. 100% welding of Re/Cb, Re/Cb-1Zr, W/Cb, and W/Cb-1Zr. Other couples partially welded.
4.	HIP-weld of remainder of program couples.	Achieved 65% of desired program couple welds. Furnace melt-through precluded further cycles.

Table D-II. Pertinent Considerations Toward HIP-welding
Refractory Metal Structures

- Ta and Ta alloy and Ta chips effectively reduce the oxygen problem in the furnace zone.
- Ta and W foil baffles as well as Al_2O_3 powder packing eliminate the "Chimney effect" of flowing gases over the subject materials.
- Roughing pump-low temperature vacuum outgassing cycles are effective in removing absorbed oxygen.
- Molybdenum encapsulation of subject material welds is effective under these conditions and can be readily removed from W, Ta, Cb, etc. by preferential etching.
- Molybdenum encapsulation prevents oxygen, nitrogen, carbon contamination of welded structures -- but not hydrogen contamination.
- Effective welds are very geometry dependent -- small 1.25-cm by 1.25-cm diffusion couples HIP-welding more readily than 6.3-cm square plates of the same thickness for the same T-P conditions.
- Surface preparation for good HIP-welds only requires cleanliness.
- Small wire stress risers placed between the surfaces to be welded appear to enhance weldability of the structures.
- Control of the molybdenum wound autoclave furnace can best be achieved by responding to resistance rather than amperes, wattage, etc.
- Hydrogen contamination in HIP-weld materials could possibly be reduced by removing pressure before temperature (where interdiffusion is not a problem).

II. HIP-WELD PARAMETERS

A. Background - Model

Essentially only two requirements must be satisfied to produce a metallurgical bond between two metals by the process of diffusion welding. The first requirement is that intimate contact be achieved between the mating surfaces of the metals to be joined. The second requirement is that at least a minimum amount of diffusion occur at the dissimilar metal interface to accommodate the rather enormous atomic mismatch presented by different materials and lattice orientations. A significant effort was made to minimize the bonding related diffusion for this program since a small "zero" condition was required to accurately measure subsequent inter-diffusion zone growth.

Acting to prevent intimate contact are three "barriers": surface contamination, surface roughness and the resistance of the material(s) to plastic deformation. Surface contamination can be minimized but only rarely can it be entirely eliminated. Even the most sophisticated cleaning method is not likely to produce an absolutely clean surface since inherent oxide films, typically 20-50Å thick at room temperature, form almost immediately on clean surfaces. The importance of oxide films to bonding is reduced by employing bonding parameters which cause the material to flow. At these conditions, oxide films can be more easily disrupted and, for many of the materials in this program, the oxide will readily dissolve. Hence, very minor residual surface contamination was not expected to play a significant role in gas pressure bonding in this program.

As with residual surface contamination, surface roughness does not play a major role in diffusion welding at bonding conditions which exceed the material yield strength, since asperities are then readily deformed. In this respect the resistance of the material to plastic deformation is extremely important to diffusion welding since the effect of surface roughness and contamination are both minimized during bonding under conditions of plastic flow. In addition, plastic deformation in itself is vital to achieving intimate surface contact. (NOTE: the total deformation required is very small and does not alter the metallurgical structure).

Choice of the bonding parameters of pressure and temperature (bonding time is much less important) is clearly a critical factor in the development of a bonding process. Analysis⁴ of considerable bonding data has yielded the empirical relationship of Figure D-1. This curve establishes combinations of pressure and temperature likely to produce bonding. Data points represent the minimum conditions reported to bond a particular material either to itself or to another stronger material; however, in a few cases insufficient work was done to establish that the bonds produced were made at the minimum possible pressure-temperature combination. For this reason (and several others, including the assumption that optimal cleaning was indeed always provided) the curve was used to approximate those pressure-temperature combinations which generally produce bonding from those which do not. Notice that in Figure D-1 the abscissa is homologous temperature and the ordinate is the ratio of bonding pressure to ultimate tensile strength of the material at a temperature of 0.6 of its melting point. Strength at $0.6T_M$ was chosen since this is the range typical of successful bonding practice.

In this program initial bonding trials were conducted near 1300°C . However, it was found that the bonding temperature had to be increased to achieve complete bonding for some of the material combinations. This finding was supported by the data of D'Annessa for the solid-state bonding of tungsten-columbium couples at 928°C and 69 MN/m^2 (10,000 psi)⁽¹⁾. Using this data and an ultimate tensile strength at $0.6 T_M$ for columbium of 27.6 MN/m^2 (4,000 psi), the (♦) data point lying very near the curve in Figure D-1 was obtained. Since this curve represents minimum pressure and temperature conditions required for bonding, it was seen that successful bonding of tungsten-columbium couples at temperatures lower than 930°C could only be achieved at much greater pressures. (Note the slope of the curve in this temperature region.) It is the high temperature strength of the weaker component in the couple that is of importance to bond formation. Therefore, tungsten-columbium bonds require the least severe bonding conditions. Couples of materials having appreciable strength at temperatures significantly

* W. A. Bryant, WANL

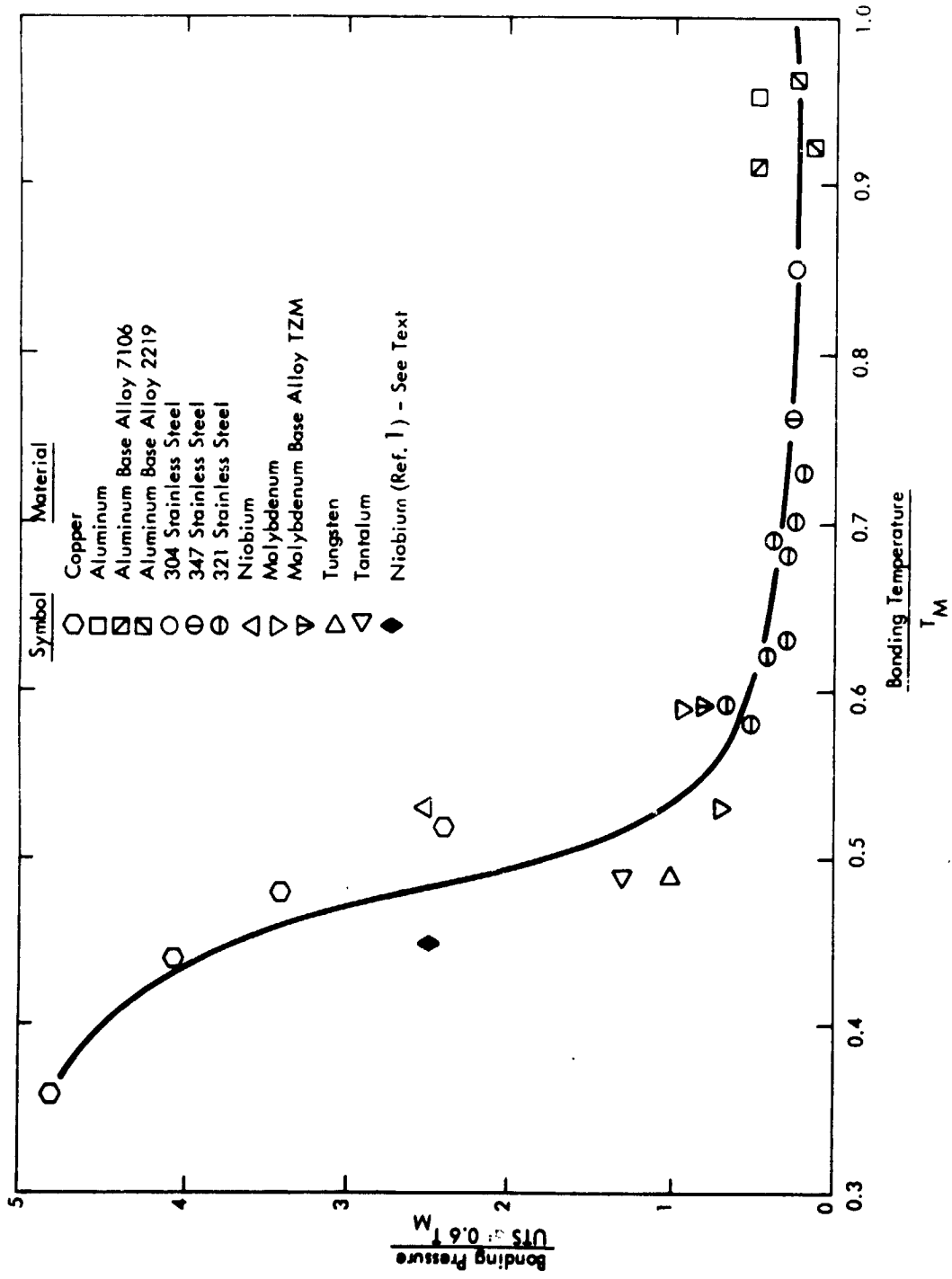


Figure D-1. Minimum Pressure-Temperature Combinations Required for the Diffusion Bonding of Metals and Alloys Using Little or No Deformation

higher than that required for columbium bonding must necessarily be subjected to more severe bonding conditions. For example, consider the worst case, the self-bonding of tungsten, a material of the highest melting point on the absolute temperature scale. Reference to Figure D-1 shows that a bonding pressure requirement of 345 MN/m^2 (50,000 psi), or approximately five times the ultimate tensile strength of tungsten at 0.6 of its absolute melting point, is required at this low temperature. Since the autoclave pressure limit is 206 MN/m^2 (30,000 psi), a bonding temperature of about 1460°C would be required to assure complete welding. Bonding temperatures for the remaining material combinations were expected to lie between 900 and 1460°C .

B. Material Handling

Since a large diversity of material combinations were to be autoclave welded for this study, two autoclave cycles were devoted to parameter evaluation tests to select the minimum temperature at which all couple combinations would weld 100 percent. In these trials 0.20 cm (0.080 inch) thick tungsten sheet 3.18 cm x 12.70 cm (1 - 1/4 inches x 5 inches) was coupled with 1.60 cm x 1.60 cm (5/8 inch x 5/8 inch) square coupons of refractory metals as illustrated in Figure D-2. Figure D-2 shows the tungsten sheet (half of each couple), the refractory metal pieces (other half of each couple), and the molybdenum envelope can which was electron beam weld sealed around the pieces to be autoclave welded. Reading across (Figure D-2), the couple materials are (1) Cb, (2) Cb-1Zr, (3) Ta, (4) Ta-10W, (5) T-111, second row, (6) W-25 Re, (7) ASTAR 811C, (8) W-20.1 Re-30.9 Mo, (9) Mo-50 Re, (10) Re, and the large piece, W.

The following section describes the parameter evaluation autoclave cycles.

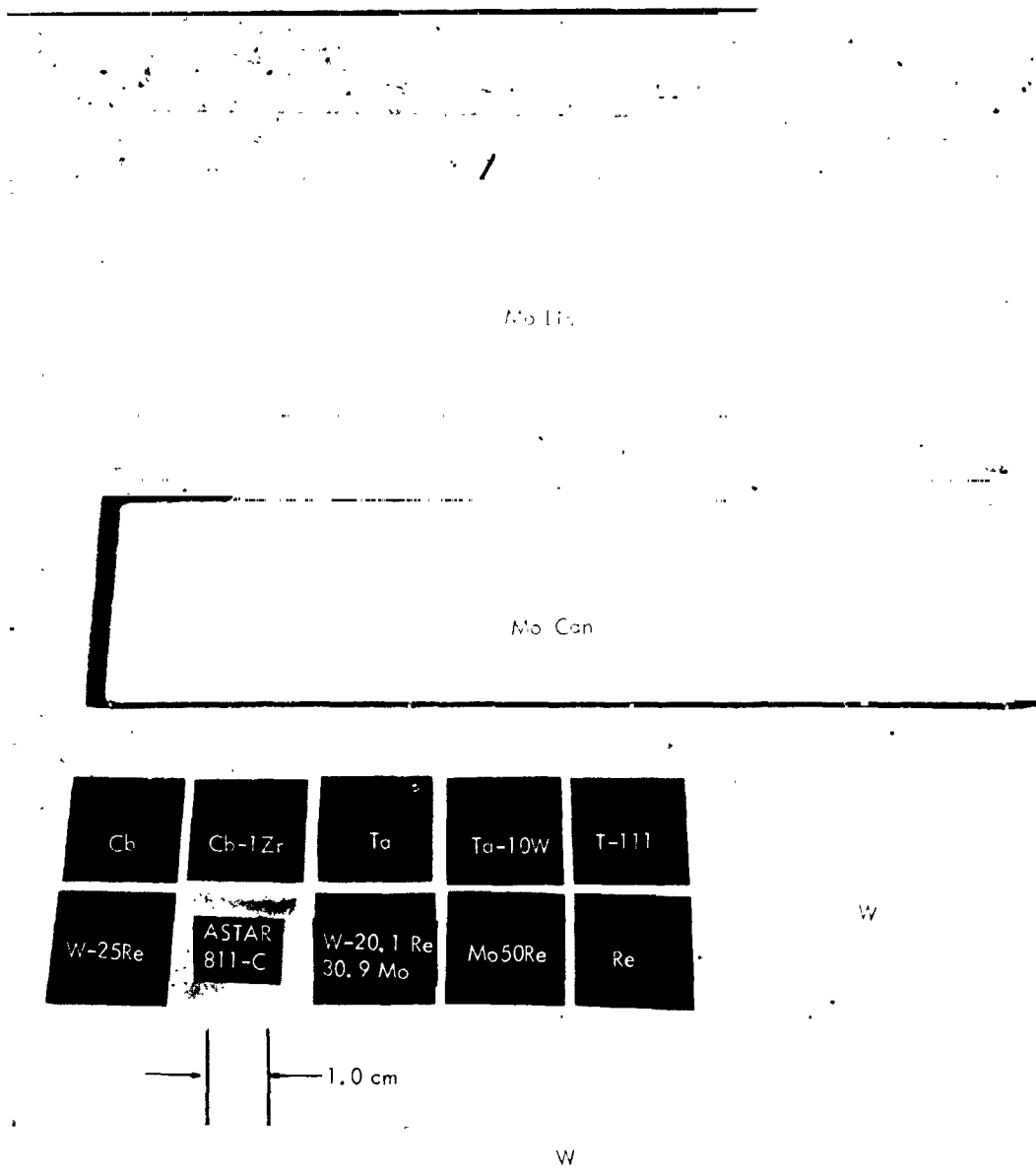


Figure D-2. Sample Diffusion Couple Materials with Molybdenum Can and Lid Prior to Autoclave Parameter Evaluation Cycle.

II. PARAMETER EVALUATION CYCLES

A. Autoclave Facility

The autoclave employed in the HIP-weld joining of the diffusion couples for this program is located at the Westinghouse Astronuclear Laboratory, Large, Pennsylvania. Its cold wall pressure vessel is 71 cm (28-inches) diameter by 346 cm (136-inches) long. Maximum specimen size is 15.2 cm (6 inches) diameter by 91 cm (36-inches) long. A molybdenum-wound five-zone resistance furnace provides uniform heating from 900 to 1500°C. Temperature distribution and monitoring can be accomplished with the aid of 16 thermocouple feed throughs into the pressure cavity. The pressure is supplied by helium gas which is reclaimed after each operation. A four-stage main compressor is used for pressures up to 117 MN/m² (17,000 psi), and a single-stage booster compressor allows compression up to 206 MN/m² (30,000 psi). Vessel closure is affected by a Gasche resilient thread closure. Almost any time-temperature pressure cycle configuration can be programmed for the facility.

B. Weld Parameter Resolution

A qualification run of the autoclave furnace was made with 2 sealed molybdenum containers of pressure bonding samples. In view of the specimen requirements, the target parameters were 1400°C and 193 MN/m² (28,000 psi) with the specimens at temperature for as short a time as possible. Special care was made prior to and during the initial furnace heating to remove as much of the furnace contamination as possible by initial evacuation and finally by a 1 atmosphere, low temperature (700°C) heating cycle followed by evacuation. The helium atmosphere impurity levels were measured before and after the run.

A maximum furnace temperature of 1480°C and a part temperature of 1330°C were obtained, but a delay in pressurizing to 193 MN/m² (28,000 psi) resulted in approximately a 4 hour dwell above 1250°C. Also, a marked cooling of the bottom furnace zones occurred at maximum pressure, presumably due to severe internal convection currents. It was decided to include refractory metal baffles to reduce the temperature instability in future runs. An examination

of the temperature distribution indicated a need to raise the specimens 30 cm above the geometric furnace centerline. Neither excessive furnace power demands or cooling water temperatures were encountered during the run. The maximum temperature was obtained at approximately one half of full power.

Furnace Loading - Two molybdenum clad, vacuum welded specimen packets were placed in the centerline of the furnace and buried in high purity tabular alumina as shown in Figure D-3. Work thermocouples 6 and 7 were sandwiched between the specimens and the remaining work thermocouple, No. 8, was placed in the furnace center at the Zone 1, 2 interface. Tabular alumina was filled to within 1.3 cm of the alumina furnace lid and fiberfrax was packed into the remaining gap.

Zirconia was packed into the area beneath the steel "hat", topped off with fiberfrax. Zirconia was packed above the steel hat to near the top of the vent tube and again covered with a layer of fiberfrax. The specimens were wired into a 0.157 cm (.062-inch) diameter molybdenum wire sling, reinforced with 0.051 cm (.020-inch) tantalum wire. All parts were handled with white gloves and the autoclave was maintained at 50°C prior to loading by circulating the cooling water with the heat exchanger inoperative.

Initial Bakeout - Low amperage settings were used to heat the furnace to 360°C, 200°C part temperature, during evacuation. Pressure increased to 700 μ at the vacuum pump and eventually dropped to 400 μ . Cooling water temperature was 36°C.

Low Temperature Heating - The autoclave was backfilled with $82.7 \times 10^3 \text{ N/m}^2$ (12 psi) helium. The initial heating rate was 100°C per hour to approximately 680°C furnace temperature, 650°C part temperature. At 650°C, the power was reduced and the chamber evacuated for 12 hours.

Initial Run - The chamber pressure fell to 125 μ following the 12 hour evacuation. Part temperature remained at 400°C. The chamber was backfilled to $82.4 \times 10^3 \text{ N/m}^2$ (12 psi) helium and heated to 730°C specimen temperature. The low pressure compressor was run to

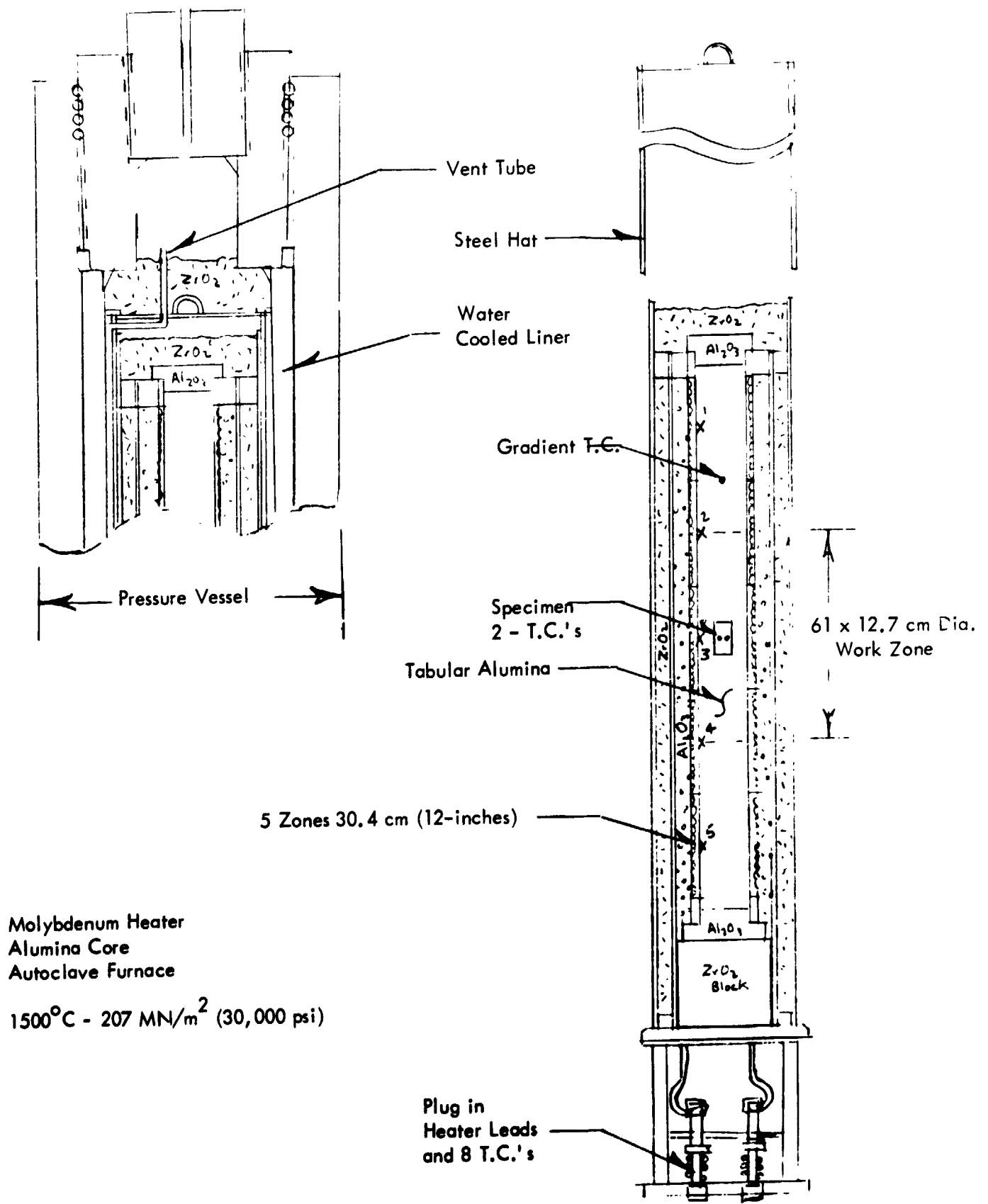


Figure D-3. High Temperature Autoclave Furnace

57.2 MN/m² (8,300 psi). After 1 hour at approximately 740°C specimen temperature, the compressor was stopped and the furnace power was increased. The temperature and power history is shown in Figure D-4. The heating rate exceeded 300°C per hour to a specimen temperature of 1060°C, at which point the compressor was again turned on. The compressor lagged considerably behind the heating rate and a specimen temperature of 1280°C (average) was reached at 93 MN/m² (13,500 psi) at 1400 hours as is shown in Figure D-5. The pumping continued until 1541 hours at 194 MN/m² (28,100 psi) and 1270°C specimen temperature. At 1430 hours a temperature instability ensued, apparently due to internal convection currents, and the specimen temperature dropped. From 1541 hours to 1719 hours an attempt was made to stabilize the furnace temperature. An average part temperature of 1315°C was reached with top center zone temperature of 1469°C at which point furnace temperature was reduced as shown in Figure D-4. The total furnace power requirement was 60 KW or approximately one half of the total available.

Cooling - The furnace was cooled by gradually reducing each zone power 5 amps every 5 to 10 minutes. At 2100 hours the furnace pressure was 134 MN/m² (19,500 psi) and the specimen temperature was 20°C.

Atmosphere Quality - The furnace helium atmosphere was pumped to storage to a chamber pressure of 13.8 MN/m² (2000 psi). A helium gas analysis including a mass spectrometer sample was obtained. A comparison of inlet and outlet gas is shown below:

	Helium In	Helium Out	
	Local Instruments ^(A)	Local Instruments ^(A)	Mass Spectrometry
Oxygen	3.5 ppm	132 ppm	200 ppm
Water	4.5 ppm	249 ppm	(not measured)
Nitrogen			900 ppm
Carbon Dioxide			100 ppm
Hydrogen			200 ppm
Organics			<100 ppm

(A) Lockwood & McLorie oxygen gage
CEC Dissociation Cell (H₂O)

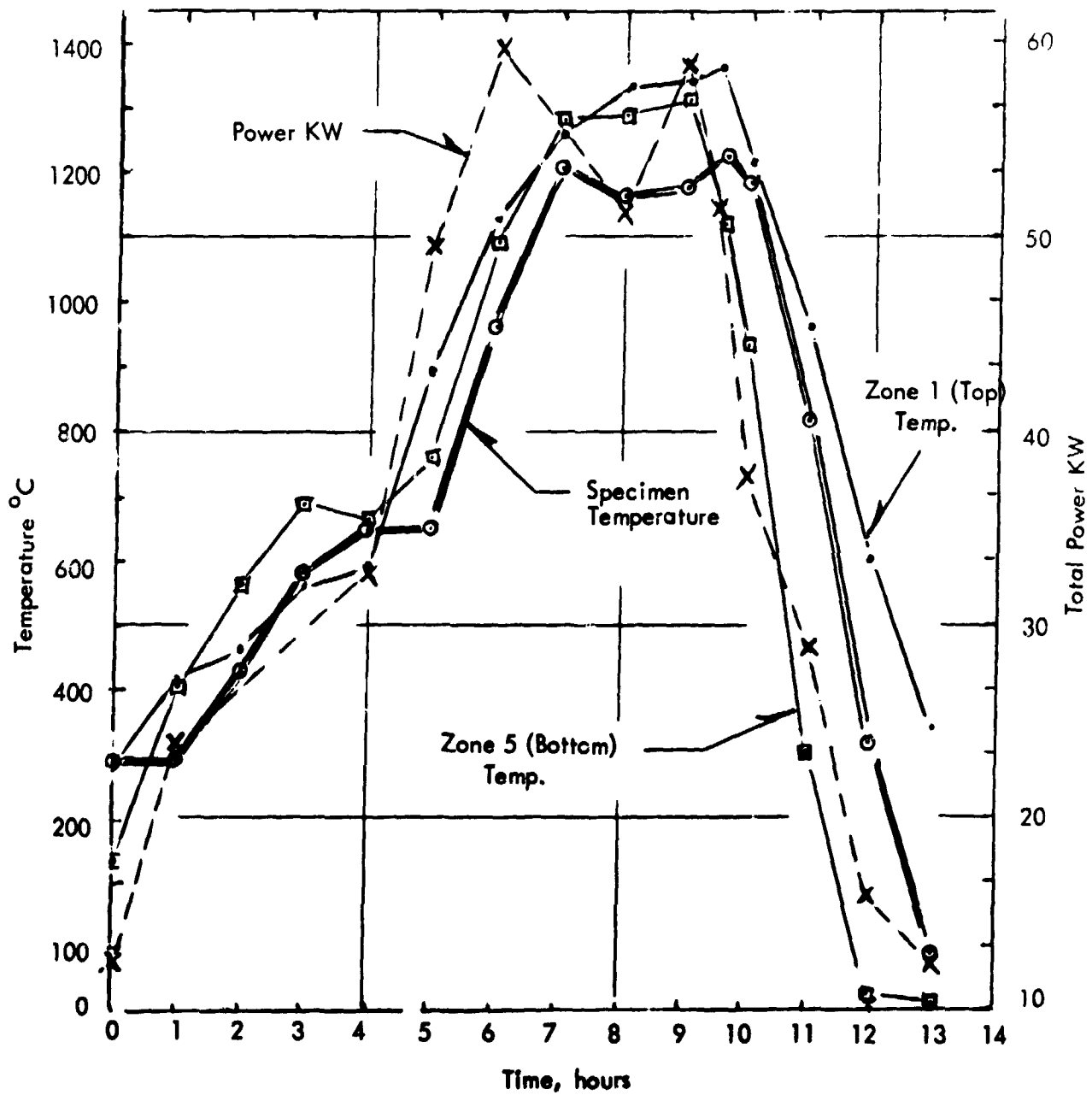


Figure D-4. Autoclave Temperature and Power During Initial Run

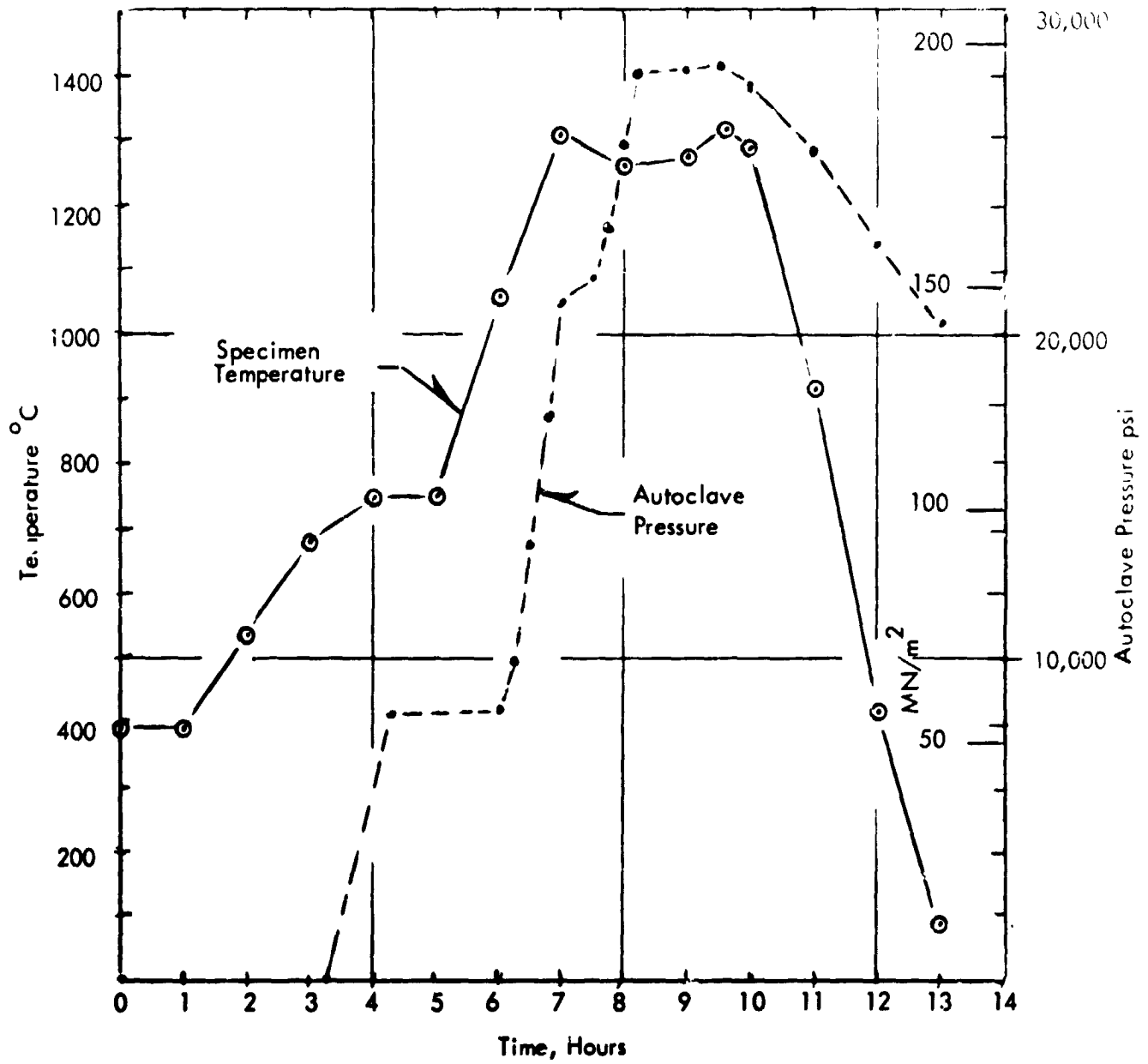


Figure D-5. Temperature - Pressure History of Specimen

The helium gas analysis showed the line filters and molecular sieve traps to be effective in removing impurities, including pump lubricating oil. It was expected that a subsequent run on the same furnace would produce less atmosphere contamination due to curing of cements, solvent removal, etc.

Specimen Condition - The molybdenum specimen and wire was bright and clean. The tantalum support wire, however, completely disintegrated and subsequent analysis indicated the remains to be Ta_2O_3 and TaC. Apparently the small partial pressure of hydrogen prevented the molybdenum from oxidizing. Post-cycle study of the molybdenum container cans found them to be leaking through small cracks adjacent to weld areas (lip weld). It was hypothesized that the oxygen environment of the autoclave gas was leading to hot tearing of the molybdenum. Tantalum alloy and zirconium chips to getter oxygen were prepared for the next cycle, as were foil baffles for the furnace to prevent gas circulation through a chimney effect. Metallographic examination of the diffusion couple junctions revealed little if any welding.

Work Thermocouple Fracture - All 3 Pt-6Rh, Pt-30Rh work thermocouples of 0.050 cm (.020-inch) diameter were fractured. Thermocouple No. 6 fractured during cooling at approximately 1240°C. An examination of the fractures showed a brittle intergranular fracture although the material is ductile at room temperature. Reducing atmosphere problems such as silicon or alkaline earth metal attack were suspected.

Temperature Control - As is shown in Figure D-6, the power input varied linearly with temperature as is typical of a conductive heat loss furnace. The 5 zone furnace was manually controlled using amperage settings on SCR power units. With the marked increase in molybdenum furnace element resistance with temperature, the power input varied even more than the I^2 relationship since resistance was also increasing with temperature. Figure D-7 compares the power input of zone 5 with amperage setting. Thus power input control was very sensitive and the lack of watt meter readings resulted in some hesitancy at the higher power levels to prevent overloading the windings and exceeding temperatures. It was recommended that watt meters be installed (ideally power input controllers) for future furnace runs to safeguard the furnace and specimens.

Table D-III summarizes the test cycle.

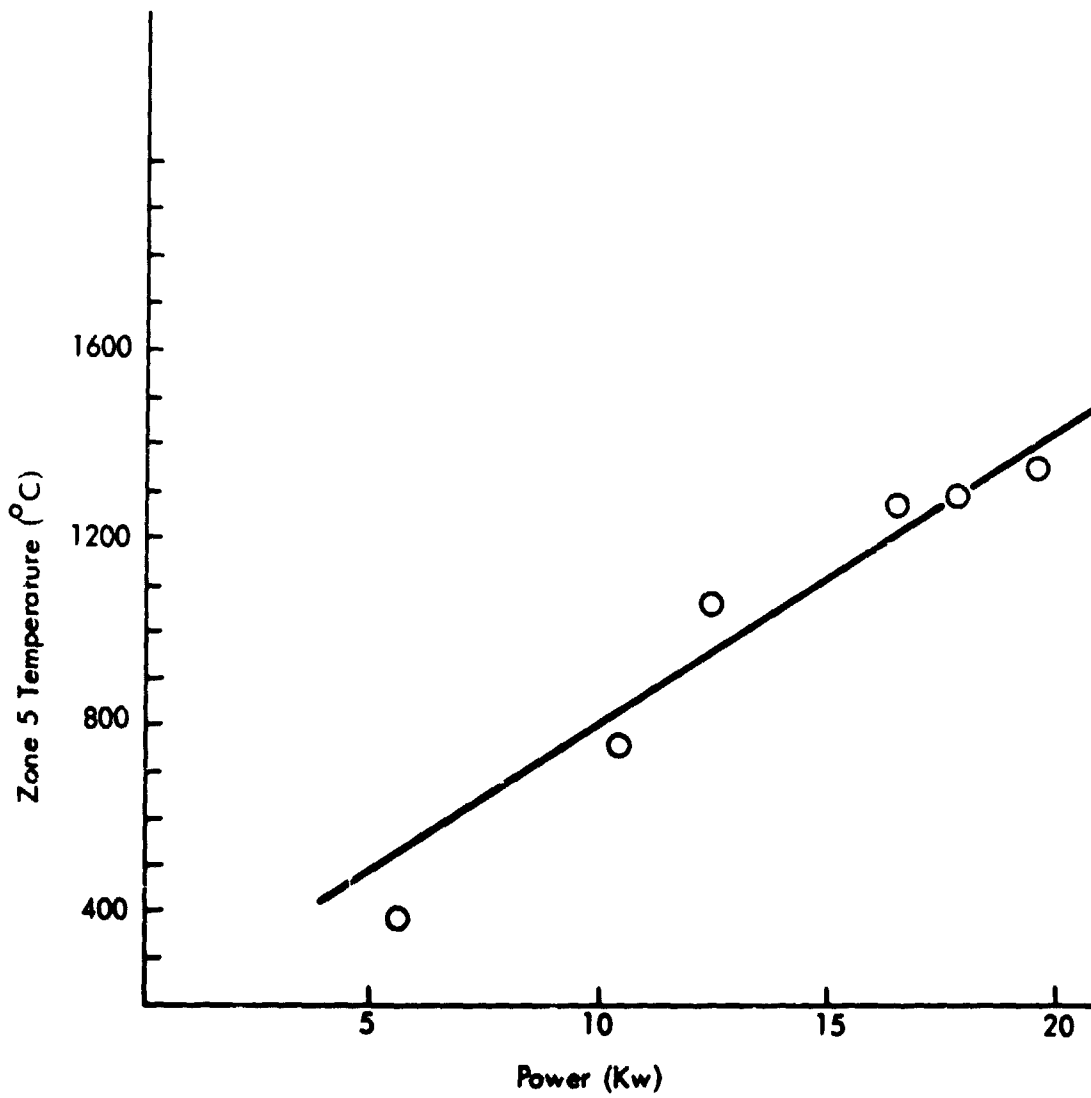


Figure D-6. Linear Variation of Temperature with Power in Furnace Zone 5

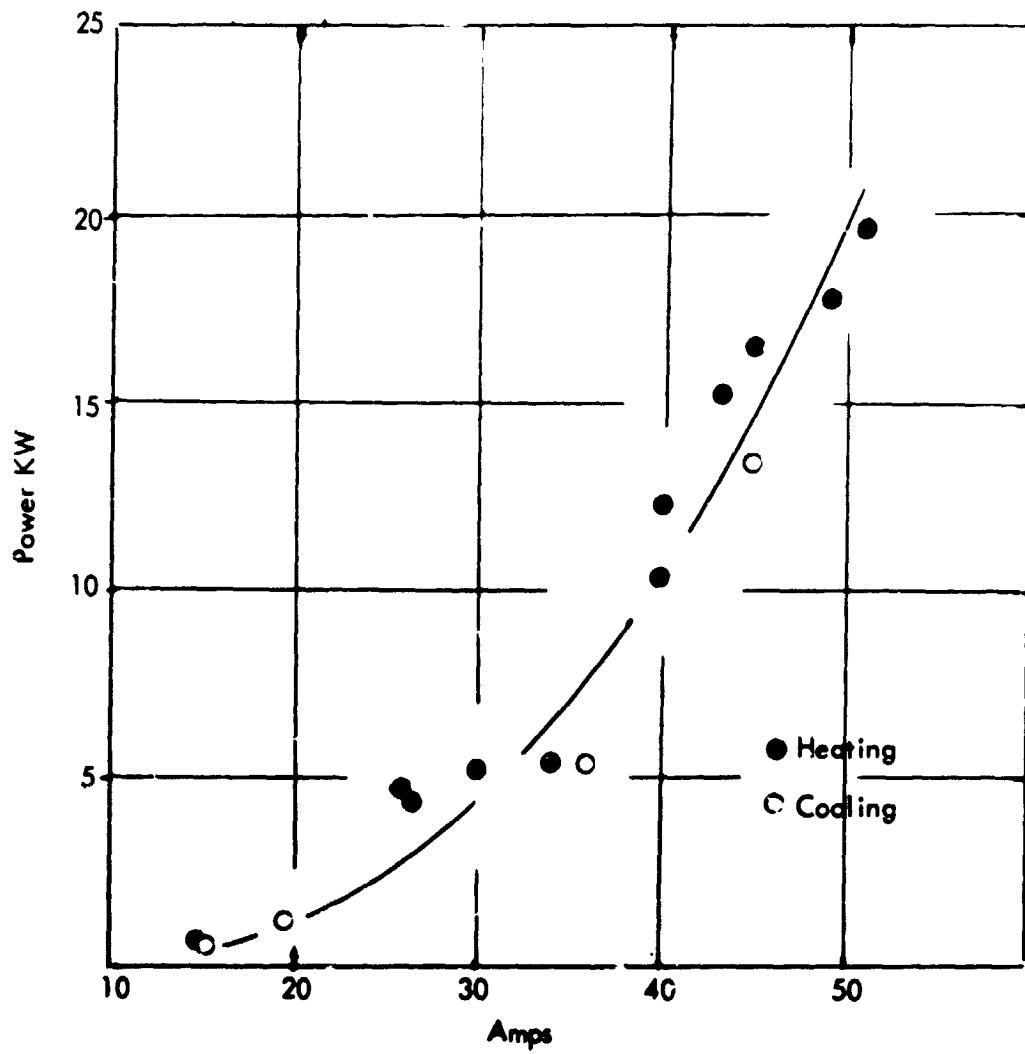


Figure D-7. Zone 5 Input Amps versus Power

Table D-III. Zone Power Input versus Part Temperature

Time	Power KW					Total KW	Part Temp. °C
	Furnace Zone Number						
	1	2	3	4	5		
732	1.02	.83	.44	.59	.88	3.76	398
833	1.86	1.88	3.50	3.88	5.44	16.56	398
1133	7.88	5.40	4.31	4.57	5.30	27.46	750
1233	8.25	9.17	9.85	9.95	10.40	47.62	752
1333	11.40	10.80	12.70	12.50	12.40	59.80	1060
1433	8.49	10.80	11.20	7.40			1304
1533	6.89	7.64	11.80	6.46	16.50	49.29	1272
1633	11.30	9.46	14.70	4.96	17.90	58.32	1286
1705	6.87	5.94	11.90	4.65	19.70	49.06	1332
1735	4.00	3.67	8.60	3.37	13.50	33.14	1282
1833	2.24	3.65	7.11	3.90	5.44	22.34	932
1935	--	1.48	3.18	1.20	1.34	7.20	418
2035	--	.73	1.14	.61	.78	3.26	90

A second test cycle of the high temperature autoclave furnace was made with 2 sealed molybdenum containers of HIP-weld specimens. Two problems of the initial run, temperature uniformity and atmosphere purity, were corrected. Rapid heating and cooling was obtained with a short (40 minute) soak time at temperature and the molybdenum containers survived the high pressures without rupturing. The moisture content of the post test helium was 11 ppm as compared to 250 ppm on the previous run. At the end of the soak time a maximum temperature differential of 6°C was observed between the center 3 zones. Difficulty was again experienced with the Pt-6 Pt-30 Rh work thermocouples with 2 of the 3 failing at 1300°C on the heating cycle and the remaining couple failing at 1030°C during cooling.

Furnace Loading - Two molybdenum clad, vacuum welded packets of diffusion couple materials were again prepared, but with short sections of molybdenum and tungsten wire used to fill the small void volumes inside the packets. This modification, which was made to reduce the extreme molybdenum container deformation into the void volume, was of questionable value since the total void volume, although considerably reduced, was made more tortuous in character.

The 0.635 cm (1/4-inch) thick specimen packets were placed into a 7.6 cm O.D. x 0.318 cm wall x 15.25 cm long (3-inch O.D. x 1/8-inch wall x 6-inch) molybdenum cylinder to provide protection from the autoclave convection atmosphere and to improve temperature uniformity. The packets were wrapped in tantalum foil with 2 of the 3 work thermocouples sandwiched between them. Several grams of T-111 machine chips were placed in the cylinder bottom as a getter and the excess cylinder volume was filled with less than 80 mesh alumina insulation. A tight fitting molybdenum lid was placed on top with a 0.318 cm (1/8-inch) hole for thermocouple penetration.

The 7.6 cm (3-inch) cylinder was placed 30.5 cm (12-inches) above the furnace centerline since the previous run had indicated an overall temperature gradient biased toward the top. Figure D-8 shows the specimen and work thermocouple Nos. 6, 7, and 8 placement.

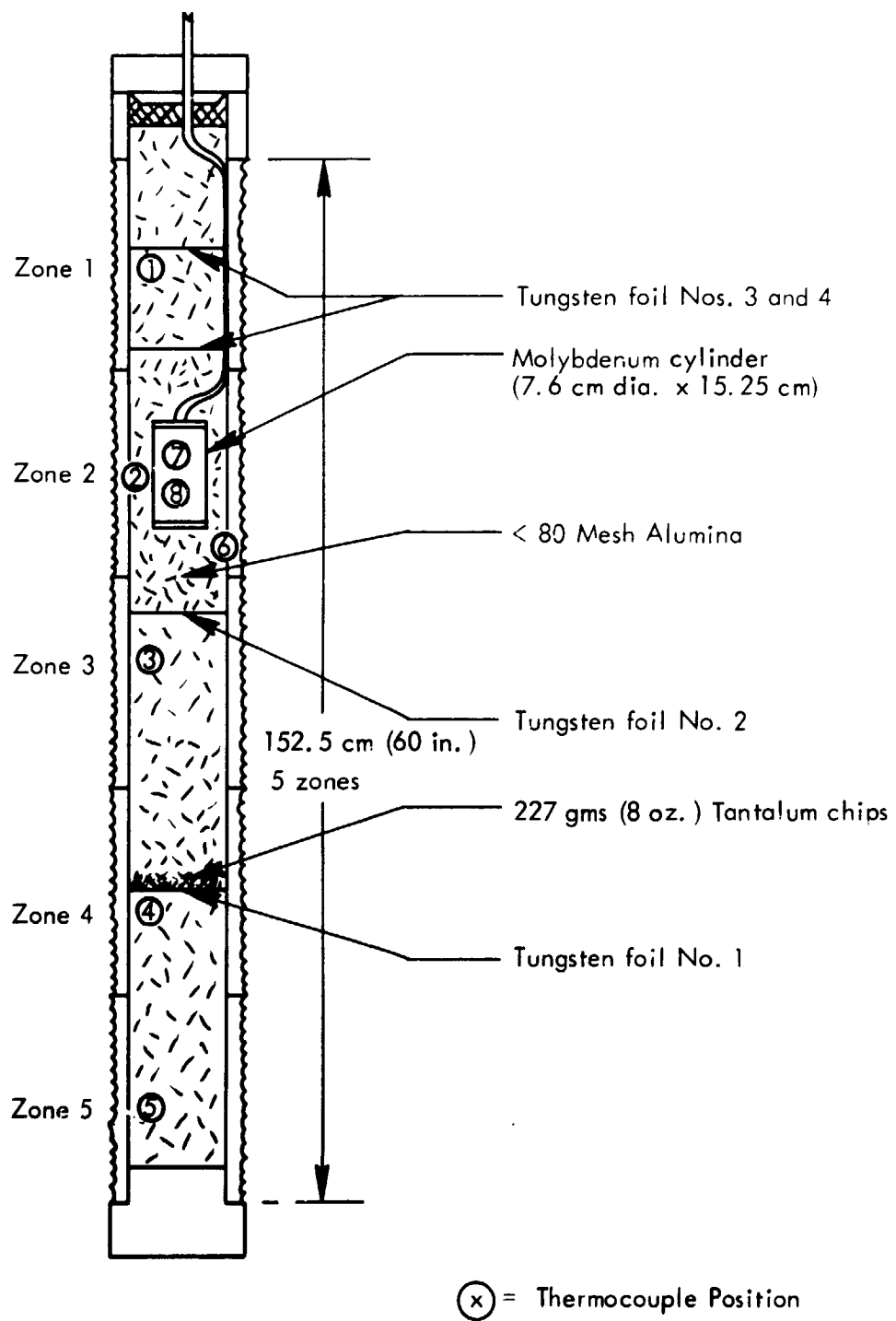


Figure D-8. Autoclave Furnace

The previous unstable furnace temperature distribution was assumed to be due to vertical convection currents of high pressure helium and four baffles of 0.0051 cm (.002-inch) tungsten foil were inserted as shown in Figure D-8. Two hundred grams of T-111 machine chips were placed above the first baffle to getter furnace atmosphere impurities. An estimate of the total quantity of getter required was calculated from an estimated total impurity level of 500 ppm oxygen equivalent from the initial run and assuming Ta_2O_5 was formed.

$$\begin{aligned}
 (5600 \text{ ft.}^3 \text{ helium}) (500 \text{ ppm}) &= 2.8 \text{ ft.}^3 \text{ oxygen (79.3 l)} \\
 (2.8 \text{ ft.}^3) (.089 \text{ lbs./ft.}^3) &= .25 \text{ lbs. oxygen (113 gms)} \\
 Ta_2O_5 \text{ requires } 360/80 &= 1.10 \text{ lbs. tantalum (500 gms)}
 \end{aligned}$$

Approximately 680 grams (1.5 lbs.) of T-111 chips were placed within the autoclave, including the lower baffle, the interior of the molybdenum cylinder and at the furnace top immediately beneath the steel hat. A post test evaluation of the chips showed a general embrittlement but not complete oxidation.

Furnace Run - A preliminary bakeout similar to the initial run was used including a low temperature (360°C) vacuum bakeout, a one atmosphere helium bakeout to 650°C followed by a twelve hour evacuation and a final rapid excursion to the HIP-welding temperature.

The HIP-welding cycle was begun with a part temperature of 425°C . A heating rate of 30°C per hour was maintained to 1400°C followed by a 10 minute hold and a cooling rate in excess of 300°C per hour. As shown in Table D-IV, excellent temperature uniformity was obtained at the maximum temperature. The temperature inertia of the furnace produced a higher than desired temperature for the specimen. A planned 10 minute hold time was not required since the specimen remained over 1400°C for 40 minutes (due to thermal inertia).

Manual amperage control of the 5 zone furnace was again used requiring constant monitoring by 3 operators.

The helium pumps were initiated at 750°C and pressurized to 193 MN/m^2 (28,000 psi) as shown in Figure D-9.

Table D-IV. HIP-Welding Run No. 2 Pressure and Temperature

Time	Pressure	Temperature (°C)							
		Zone 1	Zone 2	Zone 3	Zone 4	Zone 5	TC 6	TC 7	TC 8
6:45	15	390	452	365	285	255	430	427	420
7:00	15	440	510	400	320	300	460	446	440
7:30	15	602	650	500	452	466	572	552	550
8:00	15	718	758	634	617	644	679	662	659
8:30	2,840 ¹	779	819	770	767	755	782	779	766
9:00	8,300	920	930	876	895	822	860	847	835
9:30	13,790	1110	1085	1026	1033	954	993	980	969
10:00	18,650	1215	1229	1183	1201	1130	1127	1120	1106
10:30	23,200	1260	1309	1284	1313	1084	1234	1234	1219
11:00	28,100	1317	1324	1305	1356	1039	1300	---	---
11:30	28,100	1434	1433	1412	1446	1074	1363		
11:42	Reached 1400°C on T. C. No. 6, start 10 minute hold								
11:45	28,100	1463	1496	1477	1484	1089	1417		
11:52	28,160	1455	1502	1496	1500	1098	1441		
12:15	27,880	1326	1403	1356	1390	967	1427		
12:30	27,500	1259	1334	1252	1310	804	1375		
13:00	26,600	1151	1218	1095	1166	852	1262		
13:30	25,420	996	1054	923	950	370	1116		
13:45	24,910	929	976	852	831	300	(1034 Lost T.C.)		
14:00	---	823	859	746	673	205			

1. 8:14 compressor on

2. T.C.'s 7 and 8 failed at 10:48

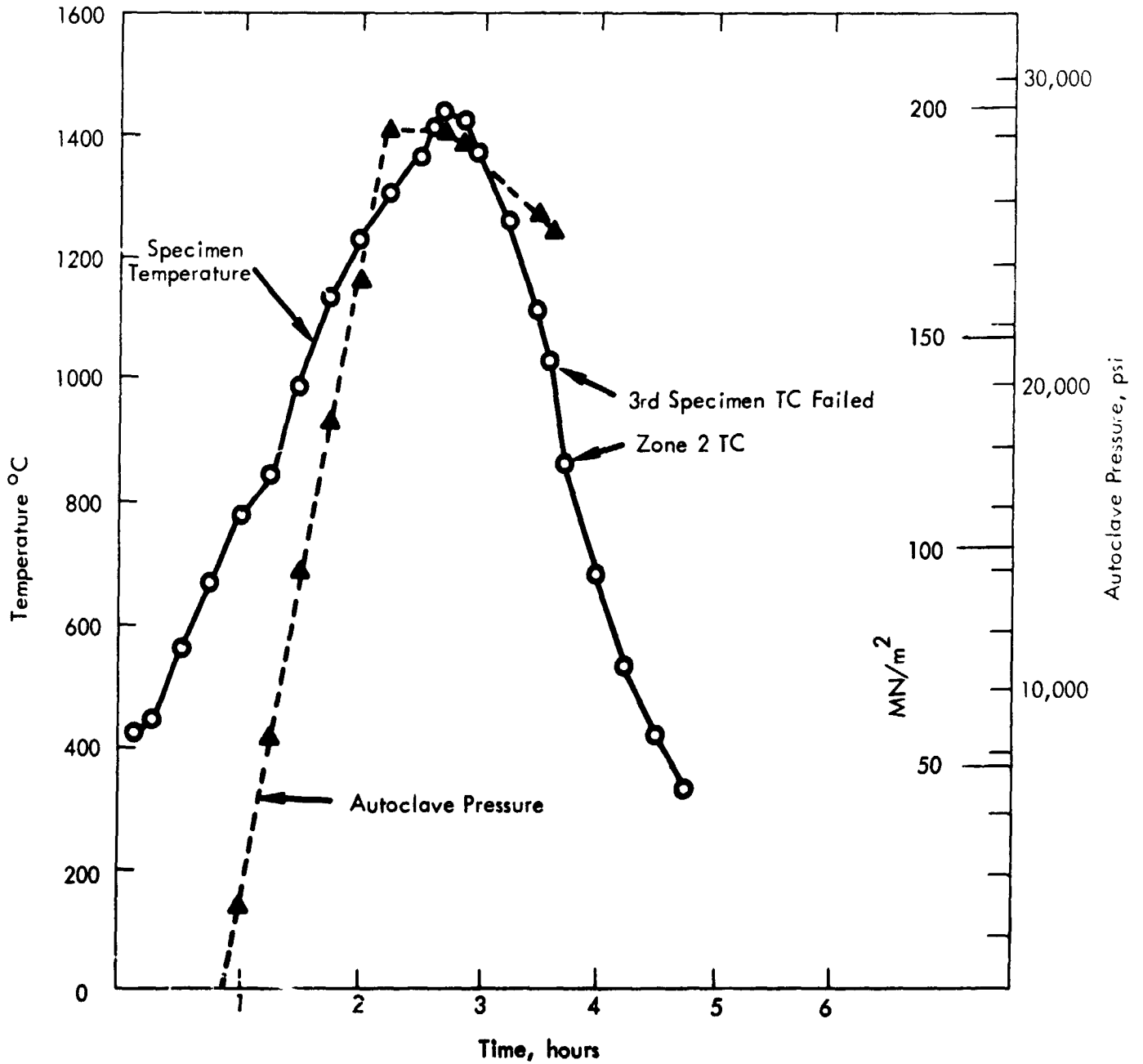


Figure D-9, Trial HIP Weld Run No. 2

Analysis - Post HIP-weld evaluation showed both specimen packets to be completely compressed with no fractures. The tantalum foil wrapping was embrittled and partially oxidized. The powdered alumina insulation was partially sintered and was removable in chunks. The sintered, solid condition of the insulation possibly contributed to a reduction in helium convection currents. The three work thermocouples were completely destroyed during disassembly, being immovable in the partly sintered alumina. It was decided to include molybdenum protection tubes in future cycles for the work thermocouples to prevent the thermal strain induced fracturing of the platinum couples.

C. Specimen Condition

Figure D-10 illustrates the HIP-weld test pieces prior to the second autoclave cycle. The tungsten was wrapped with small diameter .00508 cm (.002-inch) tungsten wire to serve as interdiffusion, original interface markers during the diffusion analyses. Figures D-11 and D-12 demonstrate the post HIP-weld cycle appearance of the molybdenum container can, and the deformation which occurred.

Post HIP-weld cycle helium leak checks (after a brief pressurization period) showed the molybdenum cans to be leak tight. Metallographic observation of the bimetal interfaces found good welding for all of the material combinations. These observations are presented in Table D-V. Figures D-13 through D-17 illustrate the interfaces involved and the wire markers. These figures are also presented to illustrate the deformation and penetration of the wire markers. While a quantitative relationship between wire deformation or penetration, and material strengths or hardness could not be resolved, the relative relationship between these parameters can be qualitatively viewed in the figures. Quantitative resolution of this effect could provide a better understanding of the HIP-welding process and indicate whether or not the small wires acted to enhance or retard the welding capability of the surfaces.

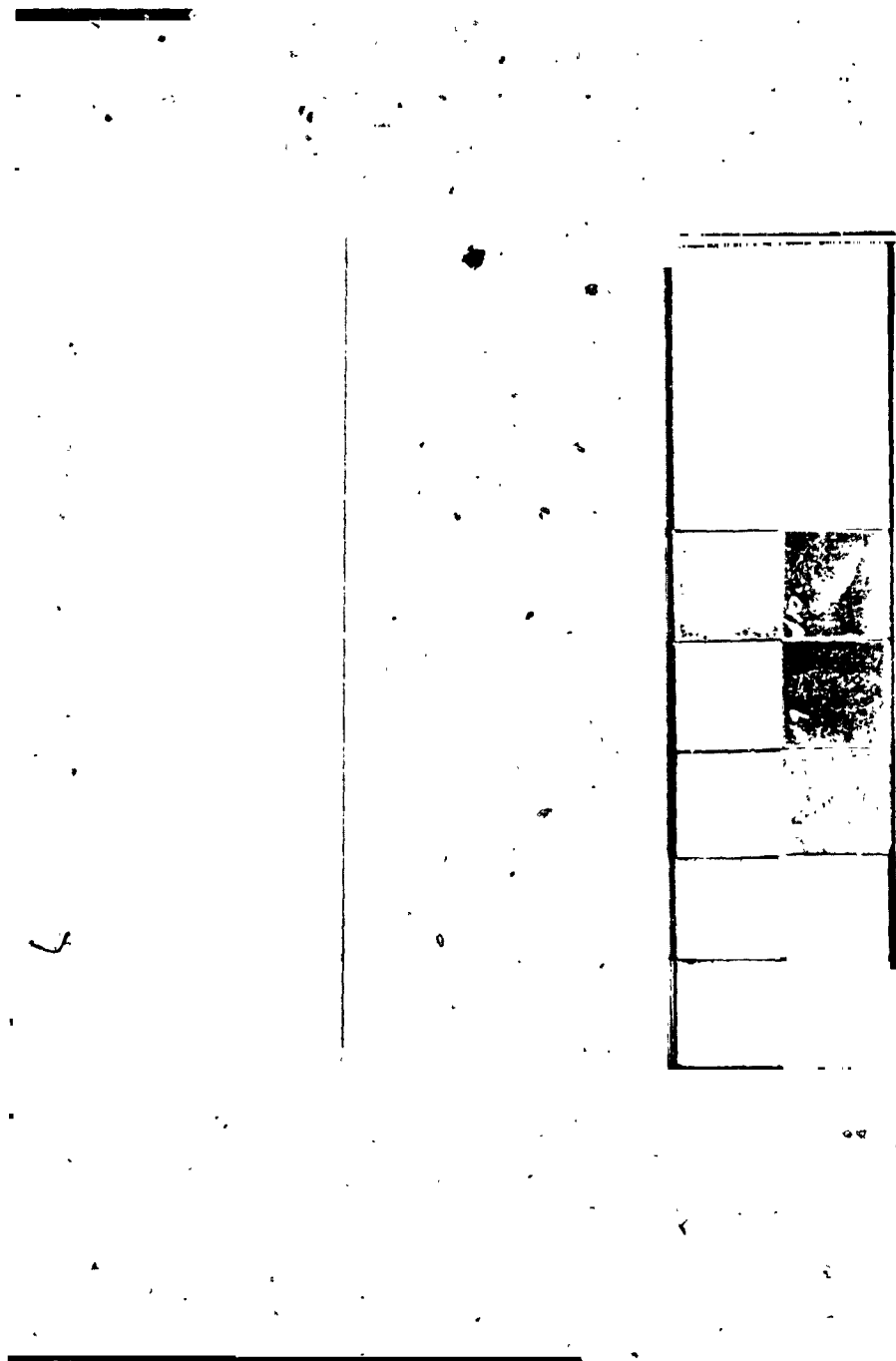


Figure D-10. Diffusion Couple Placement in Molybdenum Cans for Second Trial Pressure Welding Run. (Tungsten wrapped with 2 mil diameter tungsten wire)



Figure D-11. Post-Weld (1400°C for 40 minutes at 193 MN/m² (28,000 psi) Condition of Molybdenum Couple Container Cans

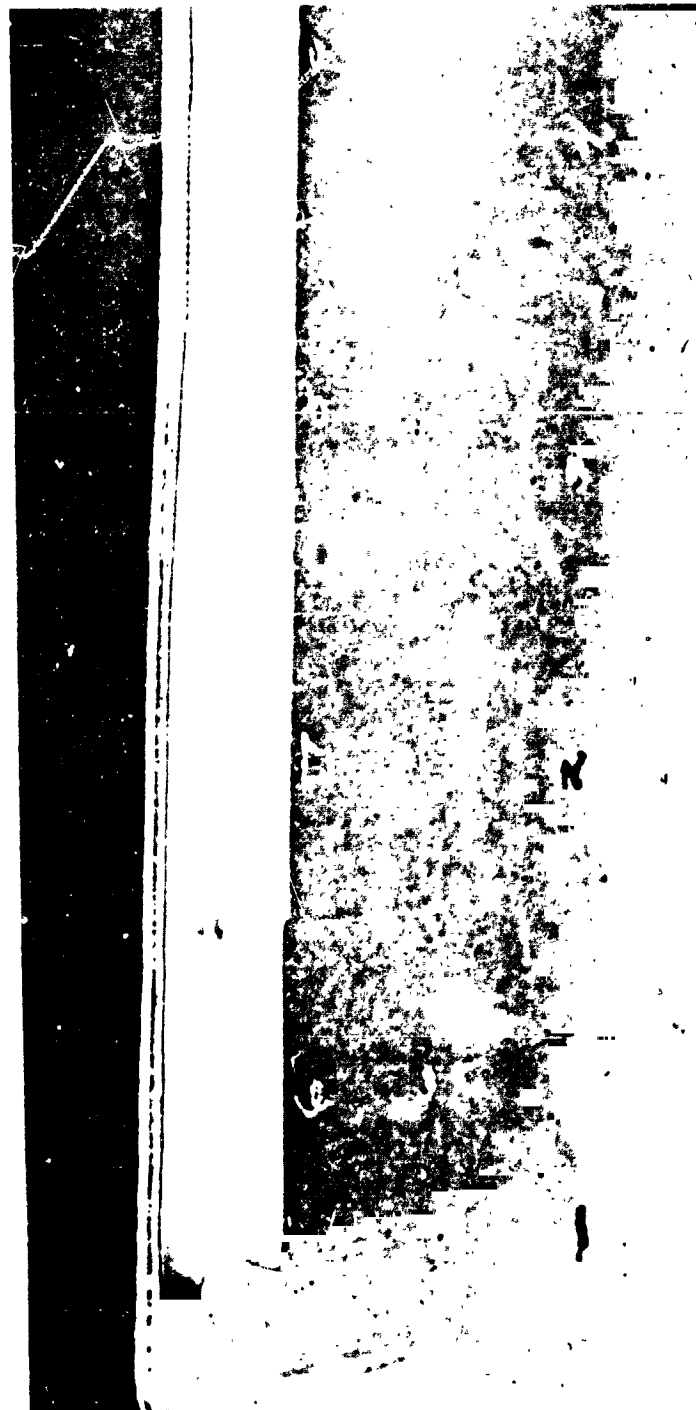


Figure D-12. Illustrating the Deformation of the Molybdenum Can
in the Hot Isostatic Pressure Weld Process

REPRODUCIBILITY OF THE
ORIGINAL PAGE IS POOR

Table D- V. Metallographic Observation of Weld Interfaces

W-Cb	100% welded ¹ , no voids along interface
W-Cb/1Zr	100% welded, no voids along interface
W-Ta	100% welded, no voids along interface
W-Ta/10W	95% welded, small voids along interface
W-T/111	95% welded, small voids along interface
W-W/25Re	75% welded ² , small voids along interface
W-ASTAR-811C	75% welded ² , small voids along interface
W-W/20.1Mo/30.9Re	95% welded, small voids along interface
W-Mo/50Re	95% welded, small voids along interface
W-Re	95% welded, small interdiffusion zone present (at 1000X)
W-W	100% welded, no interface discernible

All molybdenum surfaces (i.e., all couple interfaces with molybdenum) 100% welded.

¹ Subjective evaluation of relative surface area welded. Evaluation from visual scan of interface.

² Indicates 50% welded in one can, 95% in other can.



(a)

W

Interface

Cb

(b)

W

Interface

Cb-1Zr

Figure D-13. HIP Welds* - Columbium Series (400X - not etched)

*HIP - Hot isostatic pressure.

REPRODUCIBILITY OF THE
ORIGINAL PAGE IS POOR



(a)

W

Interface

Ta



(b)

W

Interface

Ta-10W

Figure D-14. HIP Welds - Tantalum Series (400X - not etched)



Figure D-15. HIP Welds - Tantalum Series (400X - not etched)

REPRODUCIBILITY OF THE
ORIGINAL PAGE IS POOR



(a) 1000X
Oblique light
W

Interface

Re



(b)

W

Interface

W-25Re

Figure D-16. HIP Welds - Rhenium Series (400X - not etched)



(c)

W

Interface

W-29Re-18Mo

(d) Oblique light

W

Interface

Mo-50Re

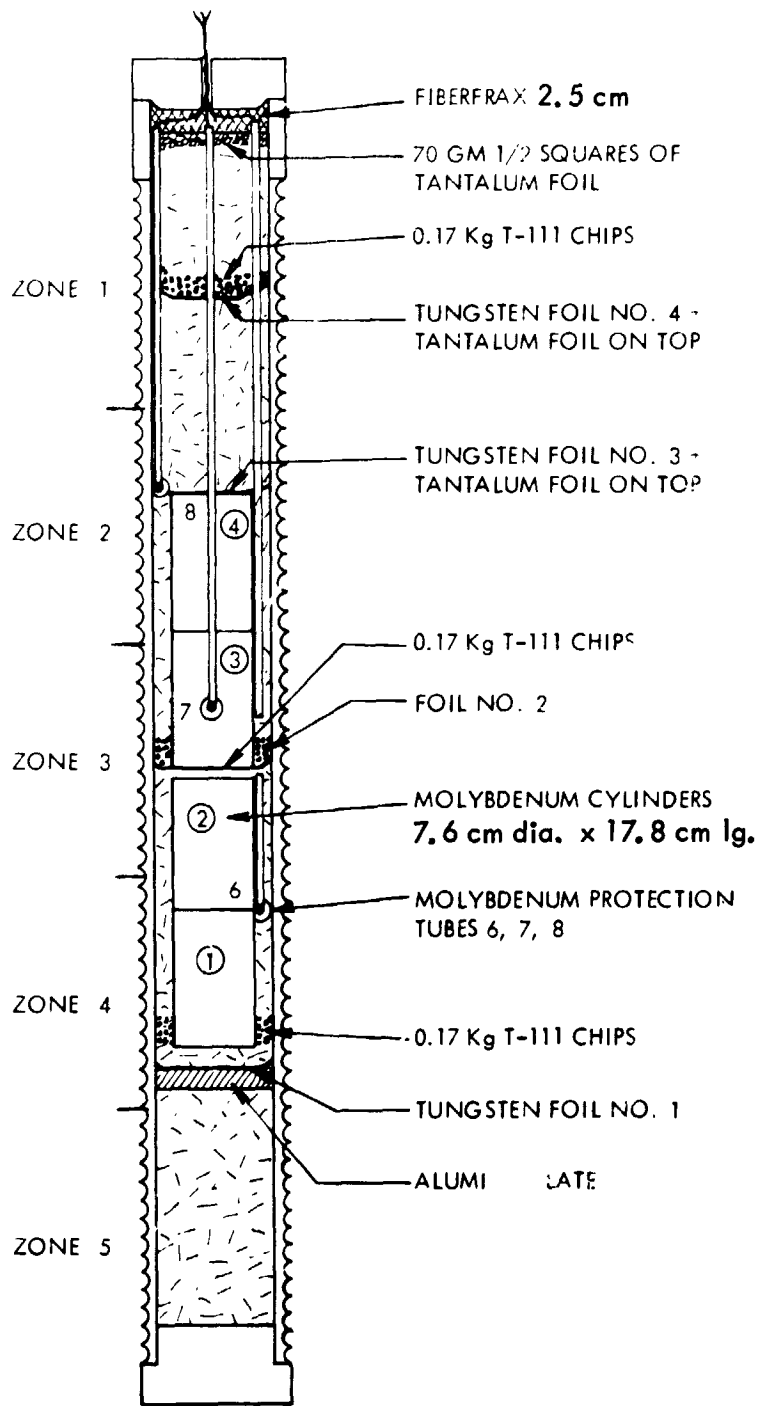
Figure D-17. HIP Welds - Rhenium Series (400X - not etched)

IV. HIP-WELD CYCLES

A. Two Weld Cycles

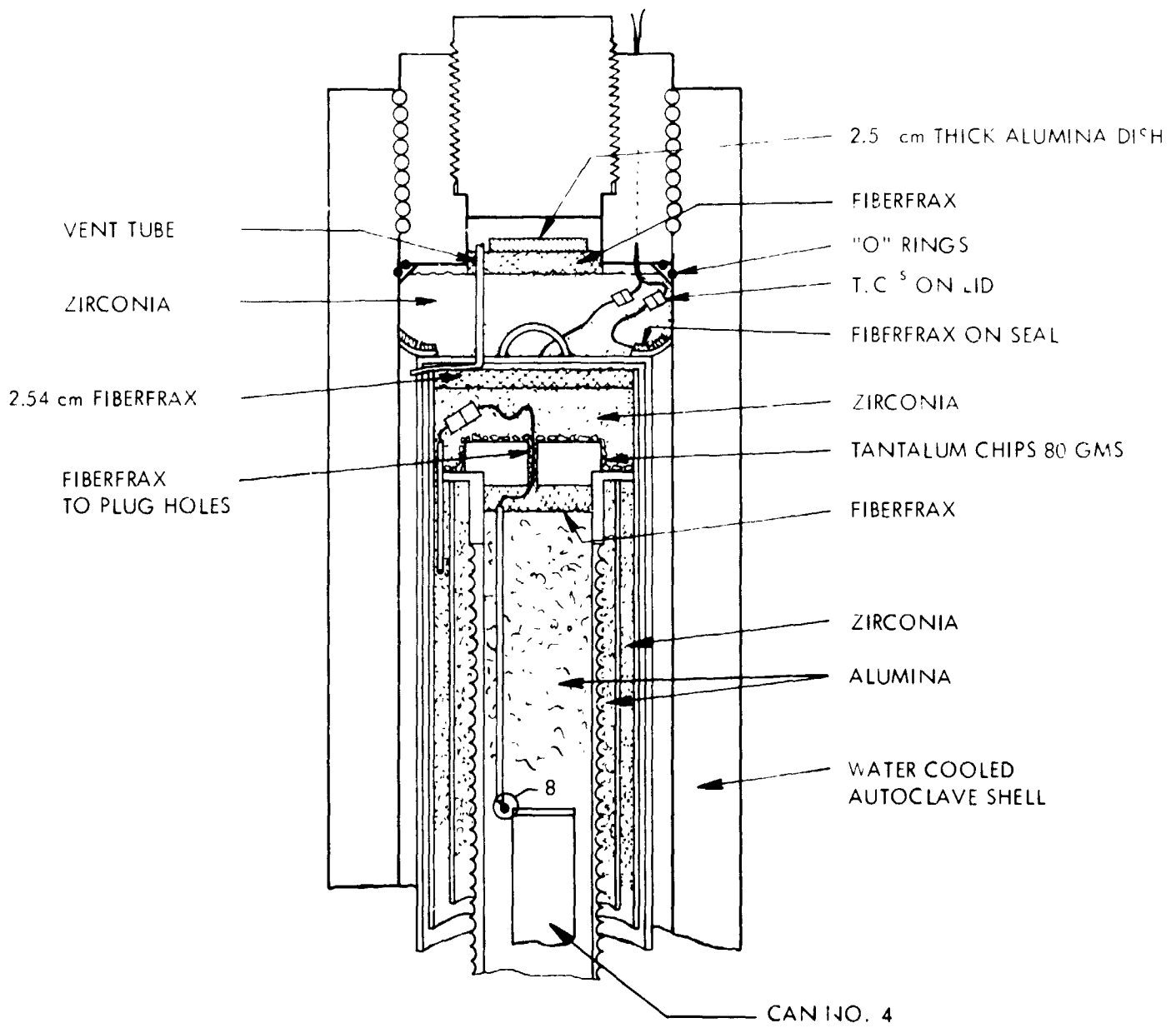
Because of the unpredictable furnace life (one cycle to 1500°C was guaranteed by the furnace vendor) all of the diffusion couples were loaded and run at the same time. Two previous runs had been made, the second of which was very successful with excellent temperature control in the center three furnace zones, 91.5 cm in length, and no problems with leaks in the molybdenum specimen packets. Borderline welding in the higher strength and melting point couples, W-Re, W-Mo-Re, indicated that slightly increased time or temperature over the 40 minutes at 1440°C would be beneficial. Twelve packets each were placed in four molybdenum buckets to accommodate a total furnace load of 48 packets. Figure D-18 shows the furnace load arrangement. Two layers of tantalum foil were used to line the molybdenum buckets to getter the impurities in the helium pressurizing gas. Tantalum alloy machine chips were used inside the foil layer as an additional gettering agent. Approximately 0.68 Kg of tantalum alloy chips were also placed at three locations within the granular alumina insulation as the furnace load was packed to provide additional gettering capacity. The furnace was sealed and insulated as shown in Figure D-19. An additional 0.15Kg of tantalum chips were placed at the furnace top and on the alumina furnace lid. Zirconia powder was poured to within 2.5 cm of the top of the steel "hat" and the remaining space was filled with "fiberfax." Zirconia powder was also poured over the hat to the mouth of the small plug. A thorough purging and evacuation cycle was performed as shown in Figure D-20. The furnace was initially evacuated with a 7.1 l/sec mechanical pump, backfilled to $6.9 \times 10^3 \text{ N/m}^2$ (1psig) helium, and heated to 200°C to outgas the furnace load. Following a 12 hour pumpdown the furnace was reheated to 350°C under $6.9 \times 10^3 \text{ N/m}^2$ helium and again evacuated for 12 hours. Typical pressures at the mechanical pump were 25 μ following the 12 hour evacuation.

To avoid excessive flexing of the autoclave "O" ring seals, the initial furnace bakeout at 200°C was done under vacuum and a single helium purge of $20.6 \times 10^3 \text{ N/m}^2$ (3 psig) was



613568-6B

Figure D-18. Furnace Loading for HIP RUN No. 3, April 13, 1971



613568-5B

Figure D-19. Details of Closure Insulation

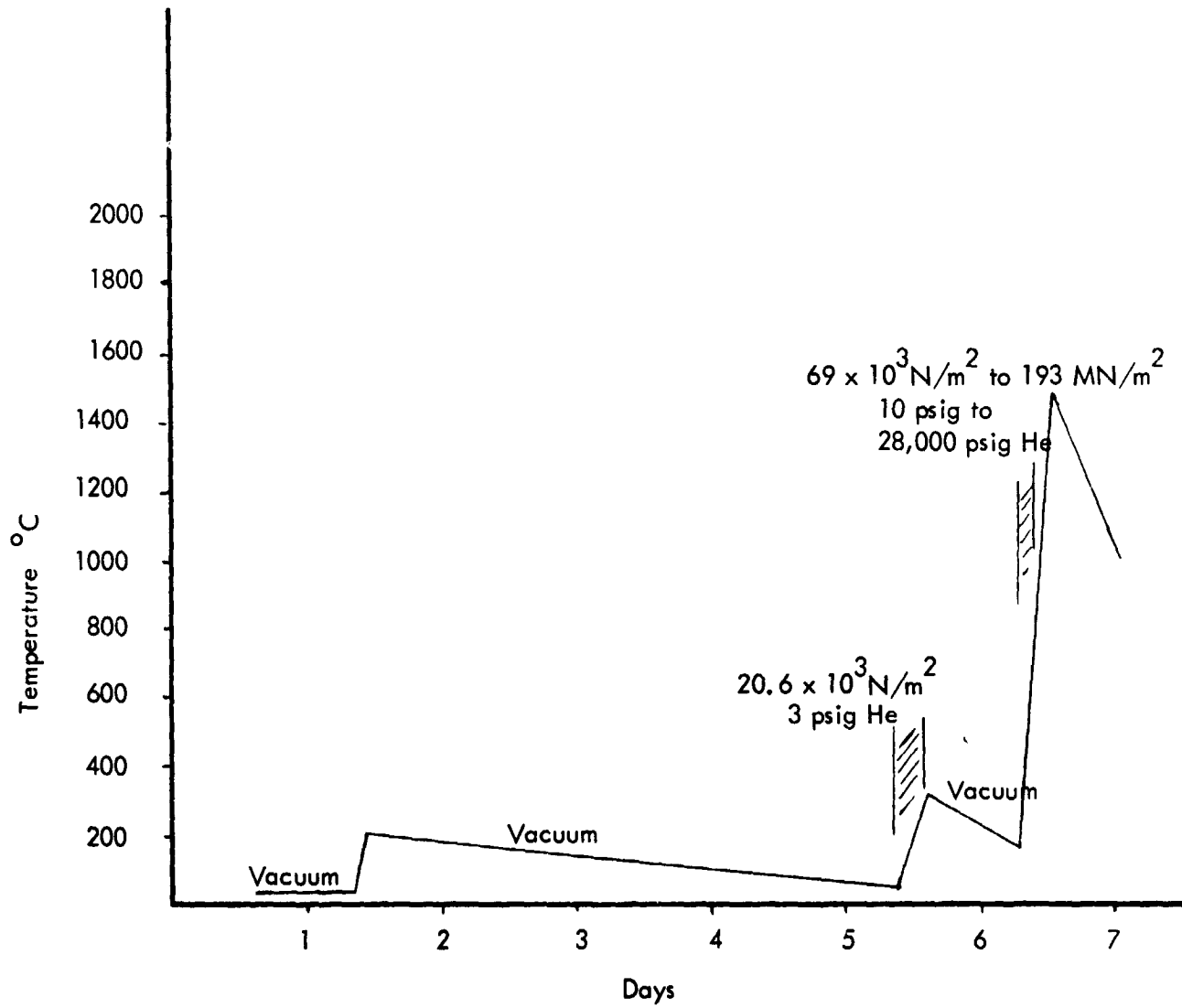
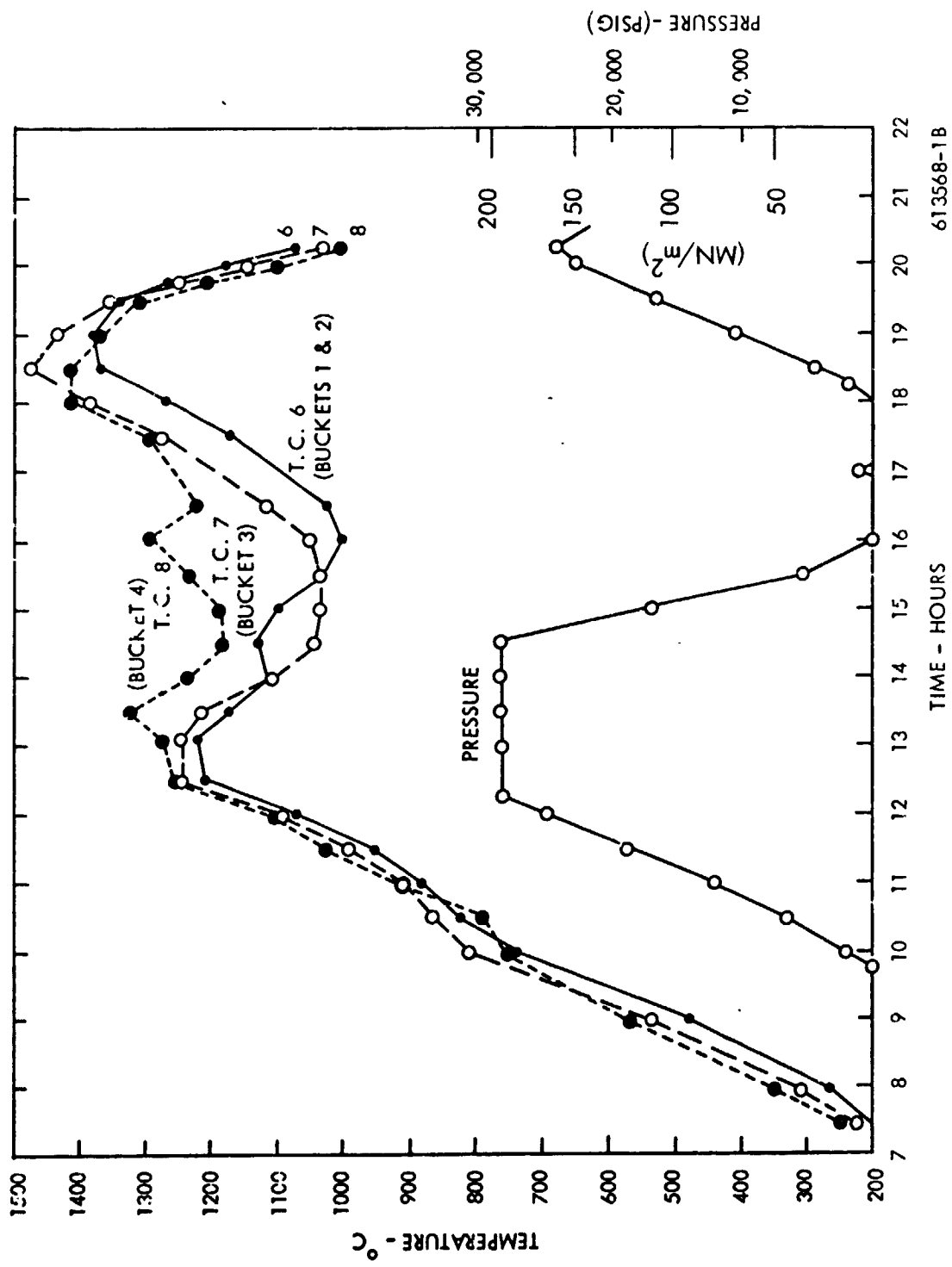


Figure D-20. Planned HIP-Weld Cycle No. 3

used during heating to 300°C. The initial 200°C and 300°C bakeouts were accomplished without difficulty and the autoclave was pressurized to $69 \times 10^3 \text{ N/m}^2$ (10 psig) helium and the 250°C heating rate to 1400°C was begun (Figure D-20). At a work temperature of 700°C, pressurizing to 193 MN/m^2 (28,000 psig) helium was begun at a rate to reach maximum pressure slightly before maximum temperature. No difficulties were encountered until full pressure and a work temperature of 1250°C were reached, at which point the SCR power supply for furnace zone 4 began to overload and blow fuses. No apparent furnace short circuits were observed and the entire power supply was replaced in 25 minutes with the other furnace zones at power to maintain as high a furnace temperature as possible. At the approximate time the replacement power supply was installed and zone 4 was brought back on line, a marked drop in resistance was observed in zones 3, 4, and 5. The resistance decrease prevented sufficient power from being developed to maintain furnace temperature at the maximum amperage available and the temperature of the lower zones gradually decreased. In an attempt to salvage the committed furnace run the 193 MN/m^2 (28,000 psig) helium was bled off to 1.38 MN/m^2 (200 psig) to decrease the heat loss and thus reach the required temperature of 1440°C. After a false start of pressurizing to 6.9 MN/m^2 (1000 psig), at which time the furnace temperature again decreased, the helium was bled back to $138 \times 10^3 \text{ N/m}^2$ (20 psig) and the work was heated to 1380°C at which point pressurizing was again started. During pressurizing, a maximum temperature of 1400°C in the work zones was obtained at 138 MN/m^2 (20,000 psig). At this point the temperature was gradually reduced while pressurizing was continued to 165 MN/m^2 (24,000 psig). Figure D-21 shows the temperature and pressure cycle obtained. Heating was not continued because of the danger of excessive diffusion zone growth during welding.

Figure D-22 shows the resistance versus temperature of a molybdenum furnace zone winding which behaves in a normal manner and closely follows the change in resistance with temperature reported for molybdenum, Figure D-23. Figure D-24 is a similar curve for furnace zone 3 which, like all the three lower furnace zones, showed a sharp drop in resistance at high



613568-1B

Figure D-21. HIP-Welding - CYCLE NO. 3 - Temperature and Pressure Versus Time

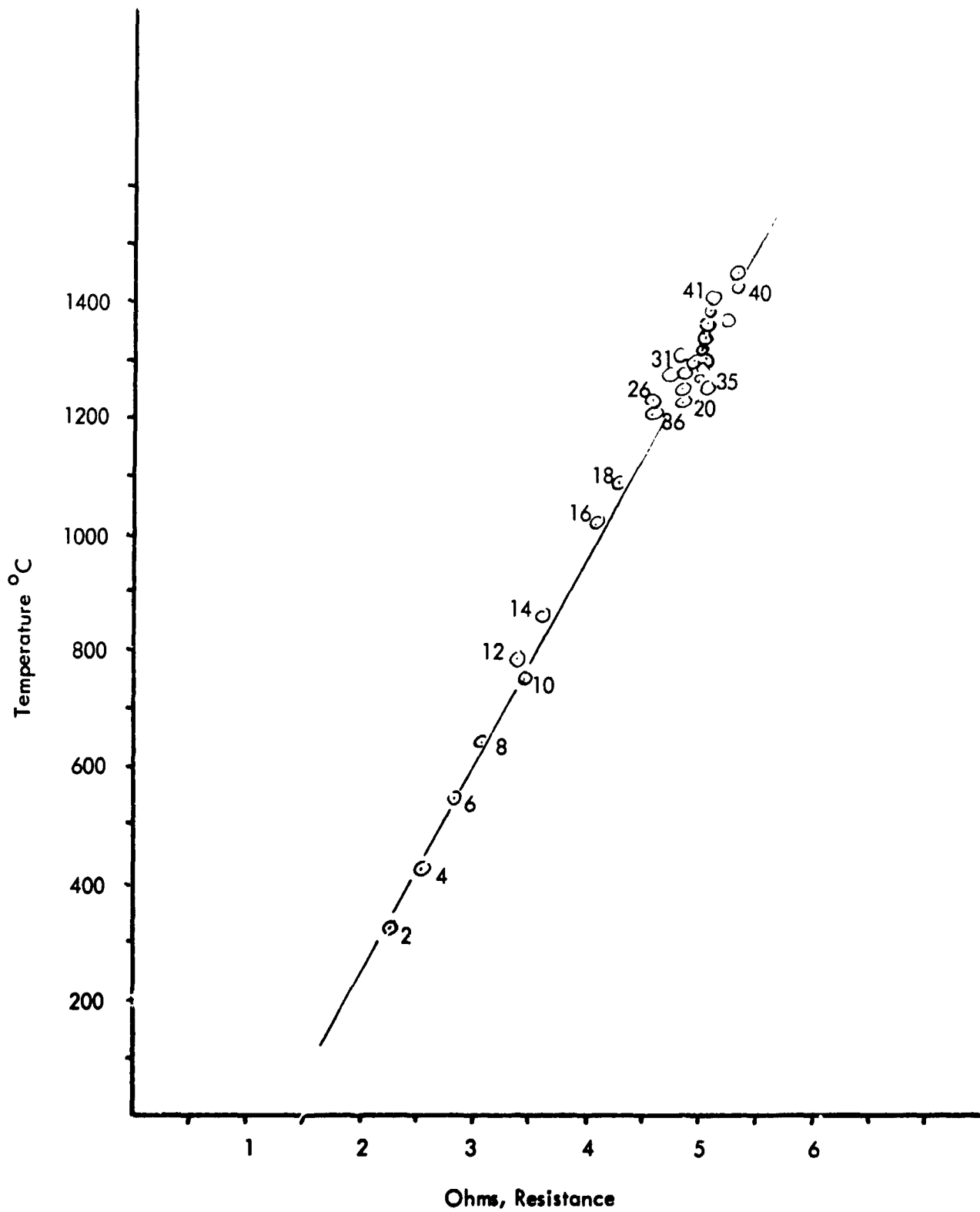


Figure D-22. Resistance Versus Temperature Zone 2 HIP RUN 3

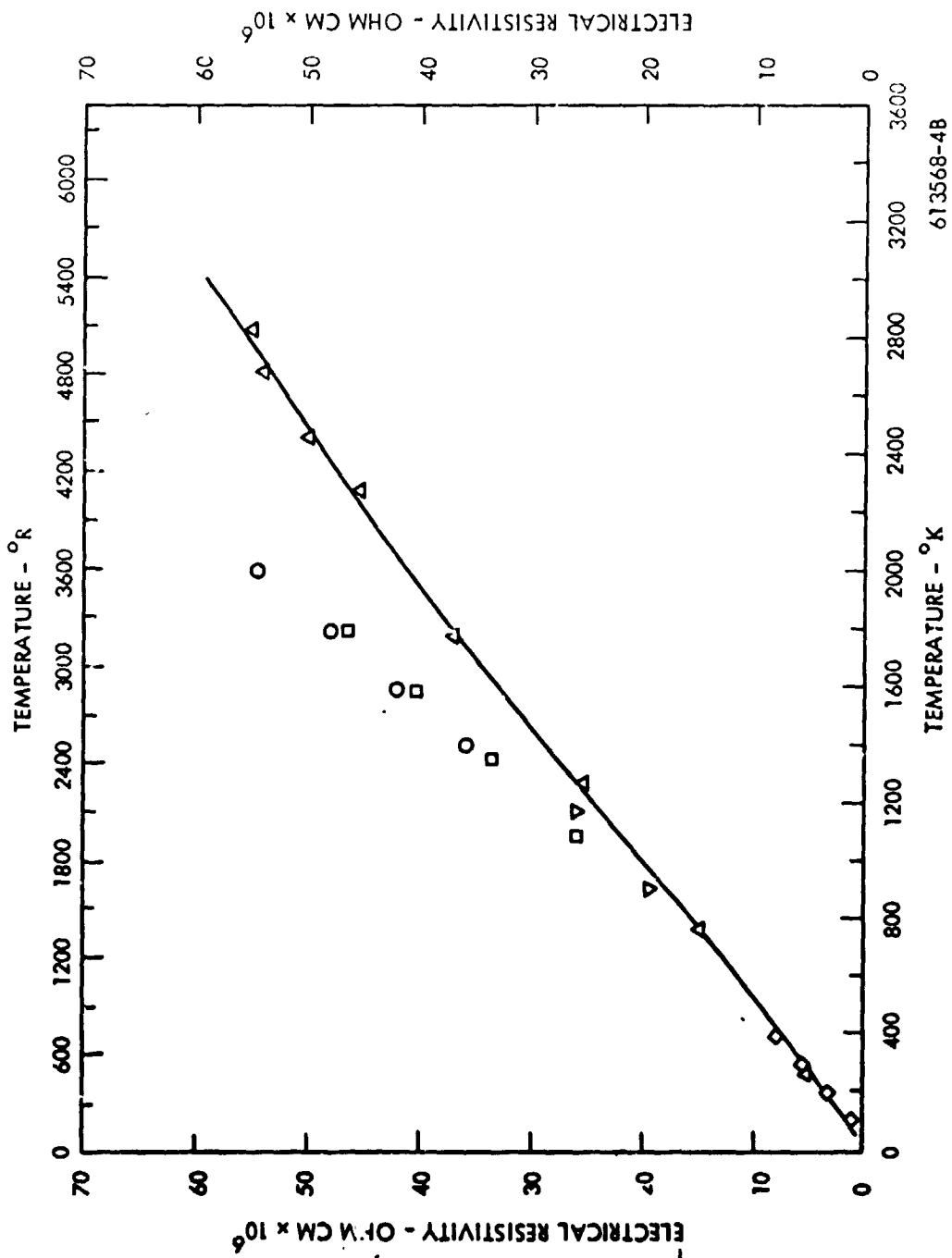


Figure D-23. Electrical Resistance Versus Temperature of Molybdenum

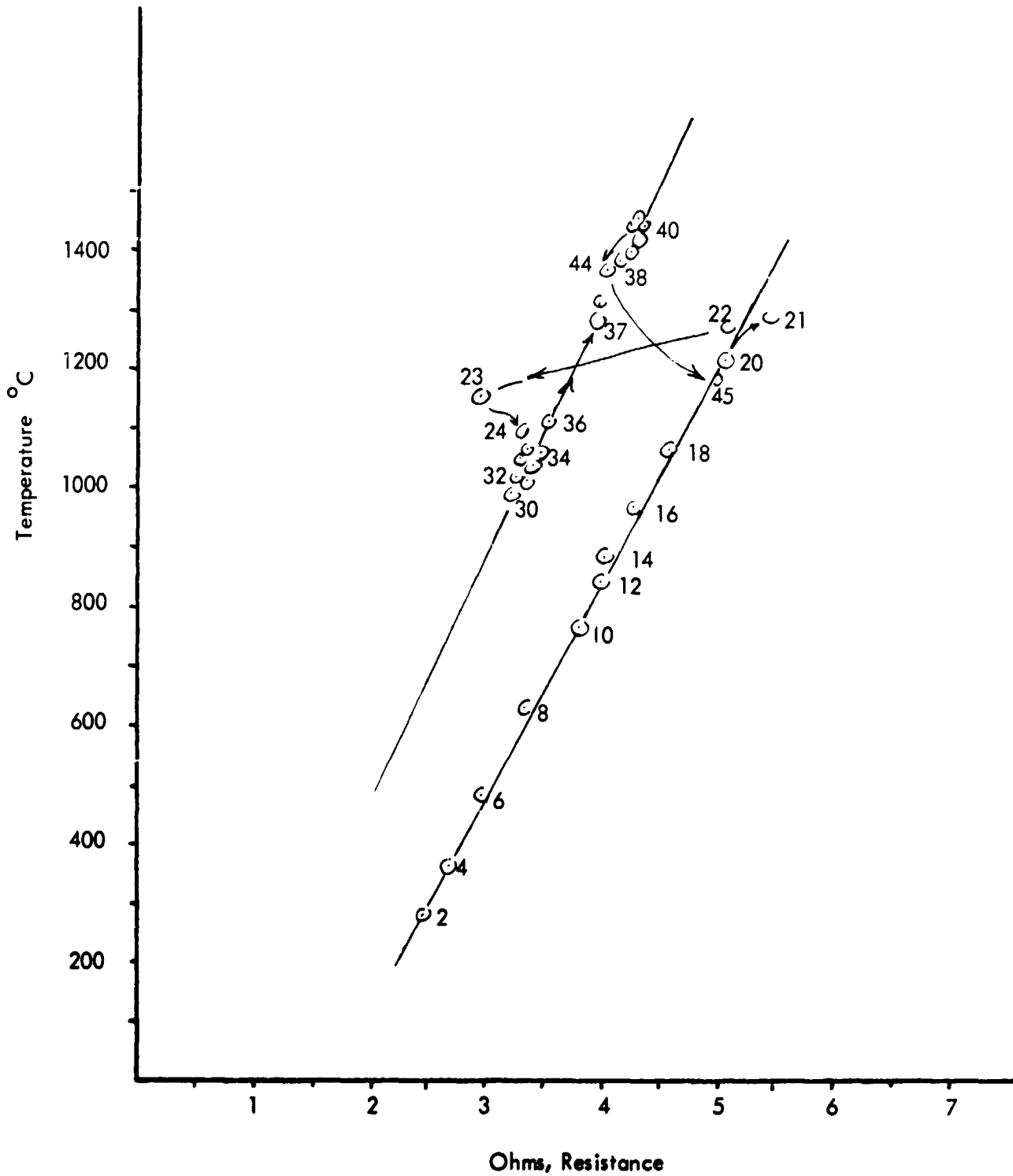


Figure D-24. Resistance Versus Temperature, Zone 3 HIP RUN NO. 3

temperature and essentially produced a different resistance versus temperature curve. On cooling to lower temperatures (the numbered data points are in time sequence) a return to normal resistance (lower curve) was seen on data point No. 45 for zone 3. The top two furnace zones, 1 and 2, displayed the normal linear resistance - temperature relationship throughout the run and no troubles were encountered in maintaining adequate furnace power. Subsequent examination of the furnace following the run indicated that all of the 5 furnace zones had normal resistance both through the winding and from winding to ground. Two power leads were observed to be very close to the grounded furnace shell and the leads were moved and insulated with glass tape in the view that the leads had caused the short at high temperature.

Reason for Resistance Versus Temperature Plots

Several other relationships to furnace temperature, such as amperage, voltage, and power, were evaluated before using the winding resistance. Figure D-25 shows amperes and KW versus temperature and Figure D-26 shows voltage versus temperature for zone 1 on HIP run No. 2. These figures may be compared to the resistance versus temperature plot for the same zone and HIP run, Figure D-22, to see the lack of correlation for the commonly used furnace control factors.

Gas Analysis

The helium gas was monitored by local oxygen and moisture monitoring instruments and also by mass spectrometer analysis of a sample bottle and the results for both are shown in Table D-VI. Analyses were obtained on the helium before and after the HIP-weld run. The results indicated a general high impurity level of nitrogen which was apparently nonreactive to the getter material placed in the autoclave furnace.

Specimen Condition

The molybdenum buckets and packets were clean following the HIP-weld cycle with no evidence of contamination. The tantalum foil in the buckets was bright but generally brittle. Sectioning

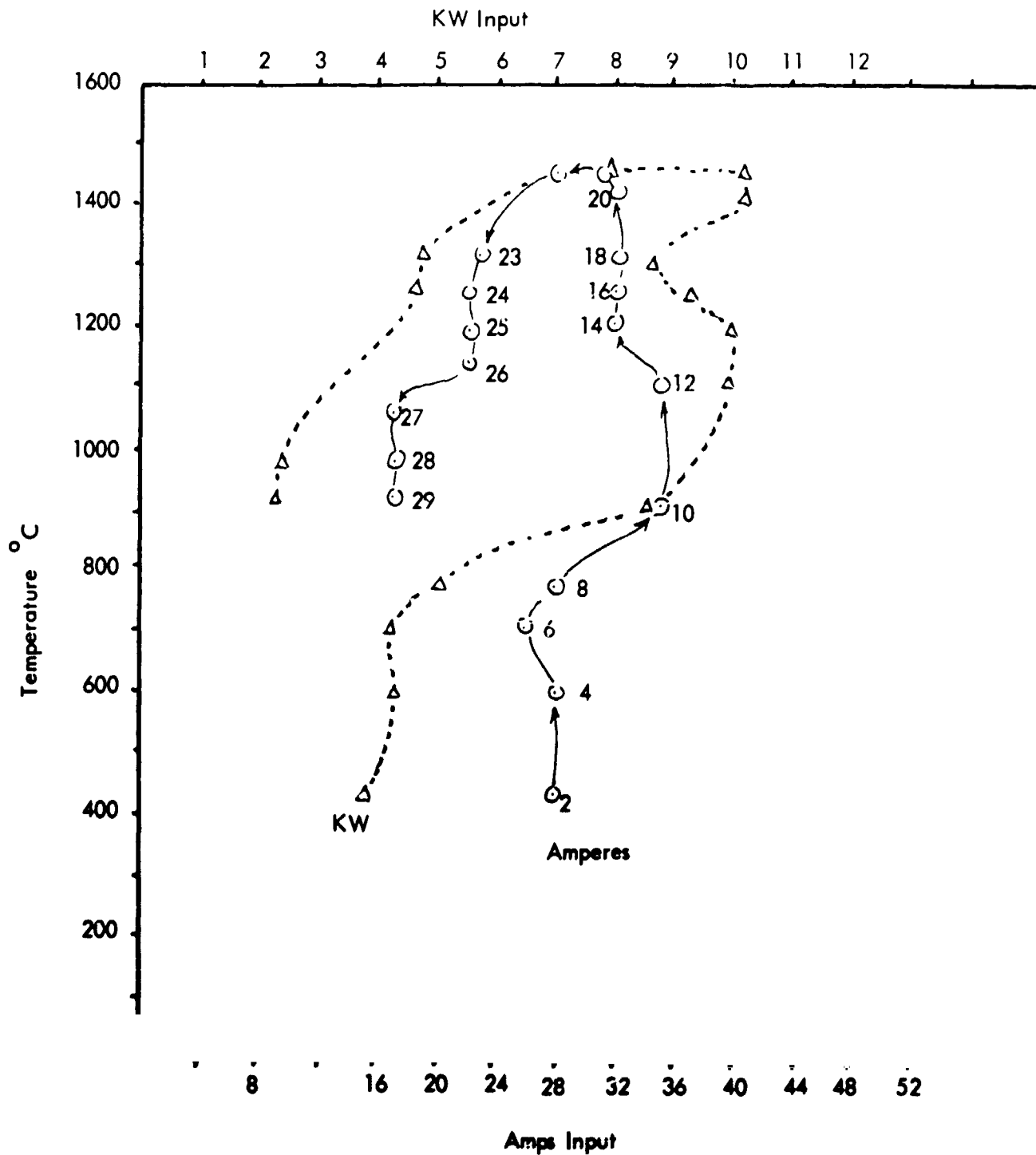


Figure D-25. Poor Relationship of Amps and Watts to Temperature for Zone 1 (Top Zone) HIP RUN NO. 2

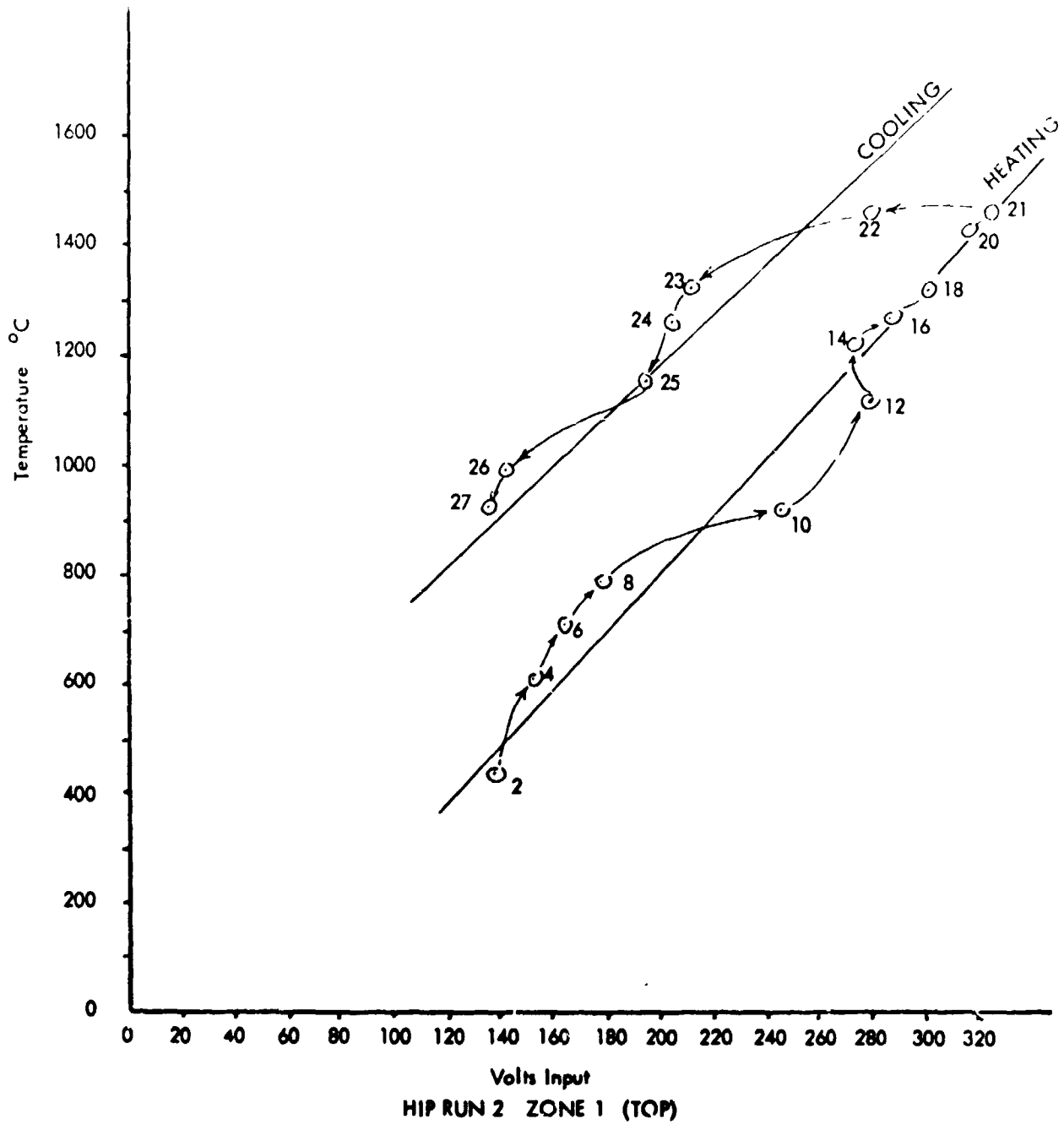


Figure D-26. Relationship of Furnace Voltage to Temperature for Zone 1 (Top Zone) HIP RUN NO. 2

Table D-VI. Mass Spectrographic Analysis of Autoclave Gas for HIP-cycle No. 3

Impurity	Post HIP-cycle	HIP-cycle No. 3 ²	
	No. 1 ¹	Prior to Cycle	Post Cycle
N ₂	900.0 ppm	145.0 ppm	175.0 ppm
CO ₂	100.0	55.3	14.6
H ₂	200.0	29.3	22.5
CO		22.5	66.0
CH ₄		1.6	5.6
O ₂	200.0	0.1	4.2
A		1.2	3.4
C ₂ H ₆		---	1.4
Local Analysis (During HIP-weld Cycles)			
H ₂ O	249.0	10.5	10.0
O ₂	132.0	0.6	0.2

¹ Non-gettered furnace loading

² Gettered furnace loading, packed to remove chimney effect

of several key packets indicated that the pressure and temperature combination obtained was not sufficient to produce complete welding of all but the columbium junctions. The molybdenum packets containing only columbium were segregated and the remaining packets were leak checked and, if necessary, resealed in an outer layer of 0.038 cm thick tantalum foil in preparation for an additional run. Table D-VII presents subjective analysis of the degree of welding in a few selected containment cans. Only cans containing Cb, Cb-1Zr couples were removed from the cycle. The remaining cans were scheduled for a repeat HIP-weld cycle.

cause of the difficulties encountered in HIP-cycle No. 3 in maintaining the temperature of the lower zones, the entire furnace load was shifted upwards 15.2 cm as shown in Figure D-27. Tantalum chips were again used to getter the pressurizing gas as in the previous run. A purging cycle similar to the previous run was used as shown in Figure D-28. Because of the decrease in heating rate as the helium pressure is increased, the furnace was to be heated to 1200°C at $69 \times 10^3 \text{ N/m}^2$ (10 psig) helium instead of 700°C as in the previous run. The heating cycle began normally and the resistance versus temperature curves for the 5 zones were normal, with no sign of the parallel low resistance path observed during the previous run. At 900°C, zones 3 and 4 shifted abruptly to the shorting mode, similarly to the previous run shown in Figure D-24. Helium pressurizing was begun. The decrease in resistance produced a power loss in zones 3 and 4 and the heating rate decreased uncontrollably. At 1100°C, zone 5 also shorted and as in the previous run, all 3 lower zones were deficient in power. Figure D-29 shows the response of the specimen temperature and pressure as a function of time. A gradual decrease in temperature was observed in the lower furnace zones in spite of operation at maximum power levels. Zone 2, which contained molybdenum buckets 3 and 4, was slightly overheated because of an unavoidable delay in estimating the temperature. At approximately midway through the run, after all other attempts to increase the lower zone temperatures had failed, the 50 ampere power input fuses were shorted with copper bars and a maximum of 68 amperes was used which gradually increased the zone temperature. After 20 hours of operating, additional instabilities in power control and transformer overheating made further tests hazardous and the run was terminated.

Table D-VII. Observed Welds in First Autoclave Cycle

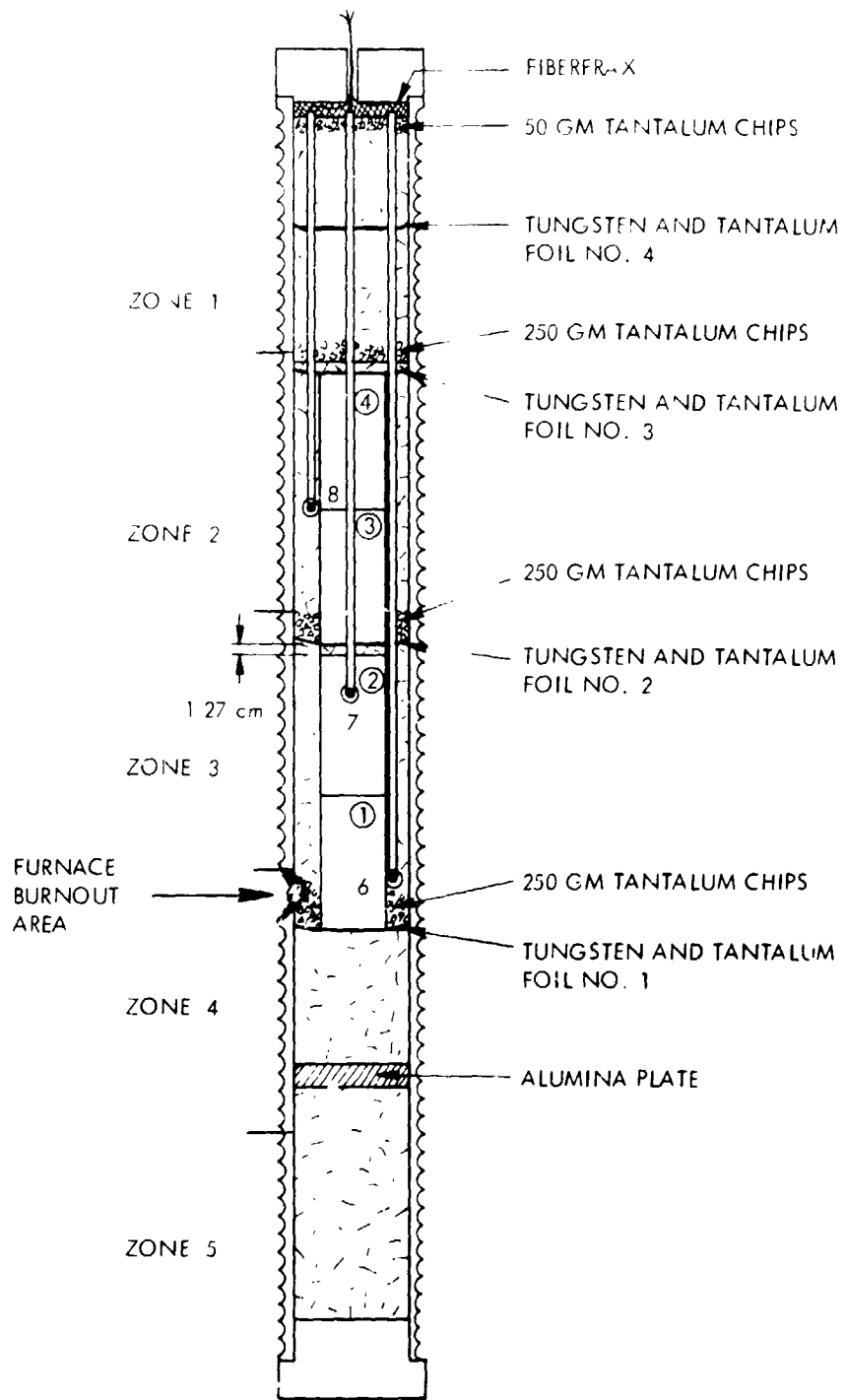
<u>Can Number</u>	<u>Junction</u>	<u>Degree of Welding</u> ¹
1b(B)	Non-leaker ²	
	*W/Cb	100%
	W/Ta Foil	95%
	Cb/Ta Foil	100%
	Mo/Ta Foil	100%
	W/Ta-10W ³	50%
	Mo/Ta-10W ³	100%
	Cb/Ta-10W ³	100%
Ta/Ta-10W ³	100%	
1j (B)	Non-leaker ²	
	W/Ta Foil	100%
	*W/W-25Re	50%
	W/Ta-10W ³	50%
	Ta-10W ³ /W-25Re	100%
	W/Ta-10W ³	100%
	Ta Foil/W-25Re	100%
W-25Re/W-25Re	50%	
1j (A)	Non-leaker ²	
	*W/Re	10%
	W/Ta Foil	100%
	Mo/Ta Foil	100%
	W wire/W	100%
	W wire/Ta	100%
	Ta Foil/Mo	100%
Ta-10W/Ta Foil	100%	
6B	Leaker ²	
	*W/W-25Re	0%
	*W-25Re/Re	0%
	Re/Re	95%
	Re/Ta Foil	95%
Ta Foil/W-25Re	100%	
2i (B)	W/Ta Foil Leaker ²	100%
	W-30.9 Re - 20.1 Mo/Ta	100%
	W-30.9 Re - 20.1 Mo/Mo	100%
	W-30.9 Re - 20.1 Mo/W	0%

*Couple Components

¹Subjective Evaluation from scan of junction at 100X, 400X

²Helium mass spectrograph leak detector

³Ta-10W filler rod in cans D-50



613568-7B

Figure D-27. HIP Welding CYCLE NO. 4 Furnace Layout

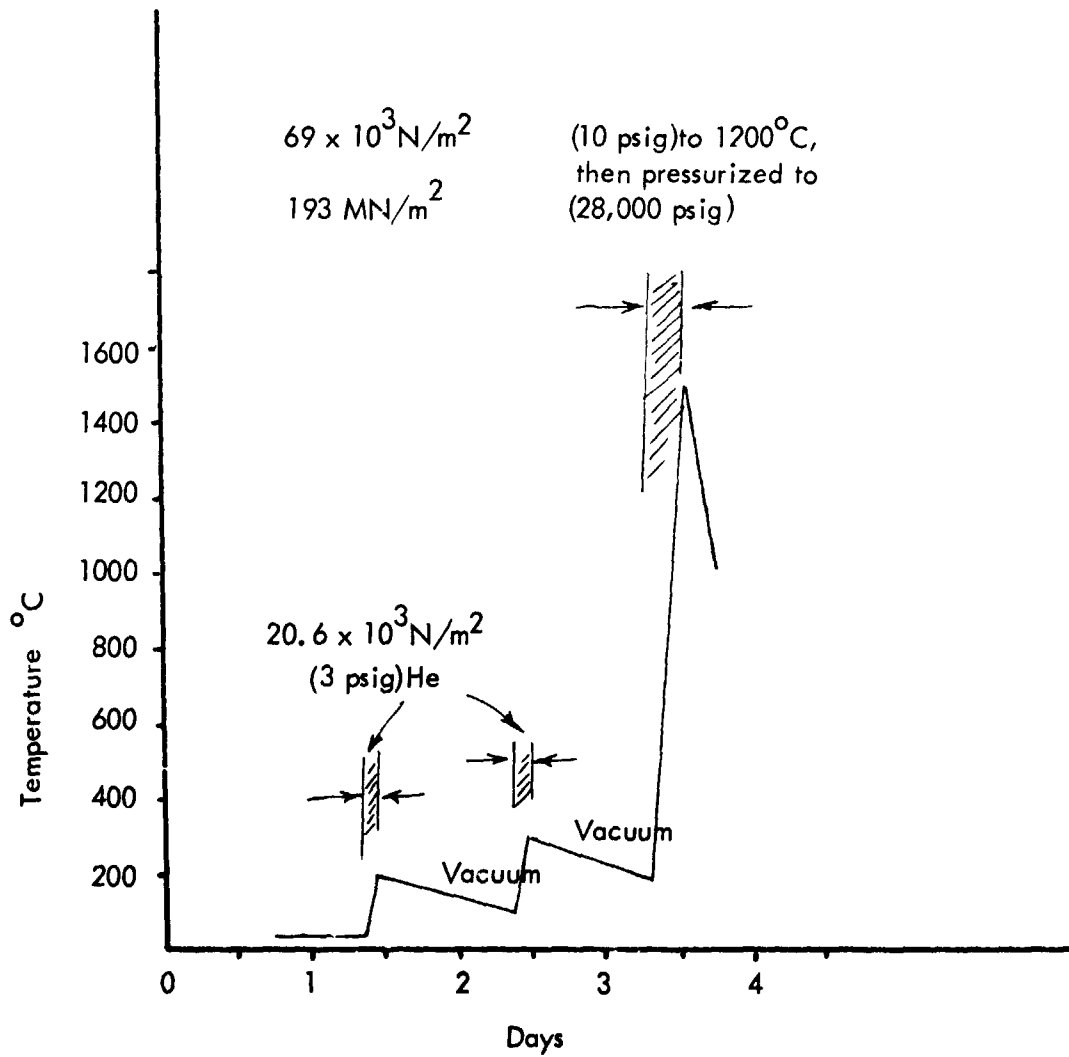
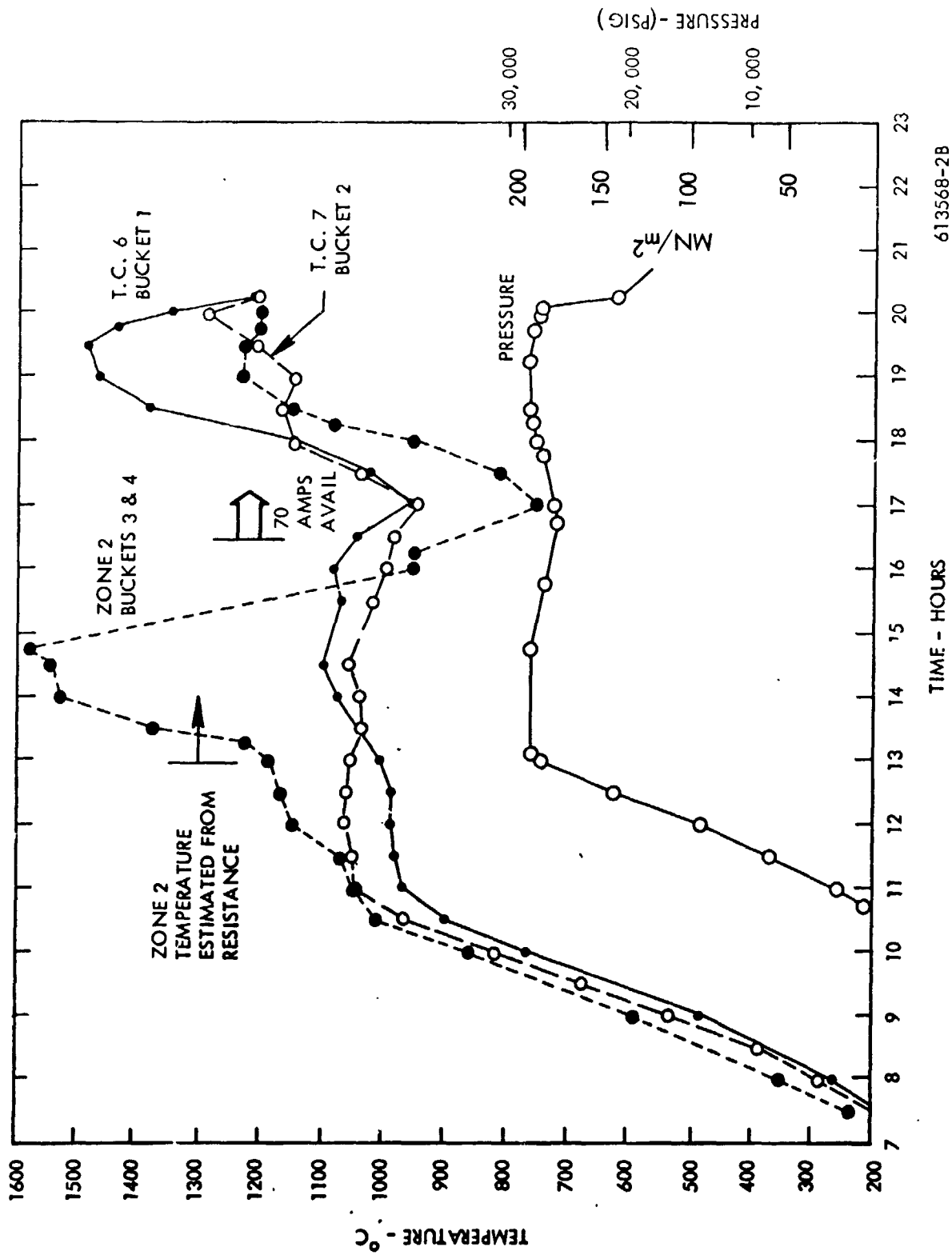


Figure D-28. HIP-Welding CYCLE NO. 4,
Purging and Evacuation Cycle
Prior to Pressure Welding Cycle



613568-2B

TIME - HOURS

Figure D-29. HIP-Welding RUN NO. 4 - Temperature and Pressure Versus Time

Temperature Control

Work thermocouple No. 8 was shorted during the bakeout procedure and the adjacent thermocouple for zone 2 was used to monitor the temperature of molybdenum buckets 3 and 4. At less than six hours into the run, however, the zone 2 thermocouple along with those of all other zones but 5, were lost. (See Figure D-27 for thermocouple locations). The temperature of zone 2 was then estimated using the resistance versus temperature relationship developed in previous non-shortened runs shown in Figure D-22. As shown in Figure D-29, a temperature overshoot occurred in zone 2 before the resistance - temperature estimation was used.

Gas Analysis

Local oxygen and water vapor monitoring equipment were employed to sample the pressurizing helium gas before and after the autoclave run. Mass spectrometer analyses were not available because the sample bottles were still in use from the previous HIP run. The impurity analyses obtained are listed below:

	<u>Oxygen</u>	<u>Water</u>
Prior to Run	0.5 ppm	9 ppm
After Run	0.3 ppm	24 ppm

These values do not differ appreciably from the analyses made during HIP-weld cycle 3.

Furnace Condition

As shown in Figure D-30, a major meltdown occurred in the alumina furnace wall at the juncture between zones 3 and 4. The melting occurred adjacent to the zone thermocouple protection tubes and melted and destroyed all the heater thermocouples above the melt zone. Zone thermocouple no. 5, which is located below the melt zone (see Figure D-27) alone survived the HIP-welding run. The wall melted through and destroyed the zone thermocouples early in the run. The melted zone, which began in the furnace wall adjacent to the bottom of bucket no. 1, did not extend to the bucket, but slumped downward into zone 4 and the



Figure D-30. Illustrating furnace melt-through across zone thermocouples
(in protective molybdenum tube sheaths) between zones
three and four in autoclave HIP-weld furnace.

**REPRODUCIBILITY OF THE
ORIGINAL PAGE IS POOR**

ceramic plate at the bottom of zone 4. The molybdenum bucket in the no. 4 zone did not appear to be overheated, which agreed with work thermocouple no. 6 which indicated a maximum temperature of 1475°C near the end of the run.

The Condition of the Molybdenum Furnace Elements

Following the HIP-weld cycle, the resistance of the five furnace zones was measured as was the resistance to ground. The resistance was normal in both cases indicating the winding was intact and no direct short to ground had occurred. Apparently the molybdenum furnace windings operated normally up to a temperature of 900 to 1000°C, at which point the ceramic coil support became conductive and established a parallel current path. At higher temperatures the significant power produced in the shorted region fused the alumina core and insulation. Upon cooling to lower temperatures, the electrical resistance of the ceramic returned to normal.

Judging from the similar resistance behavior in HIP-welding run no. 3, the shorting mode began during the earlier run and was repeated in HIP-welding run no. 4. Since the melting point of impure alumina is about equal to the expected heater winding temperatures (2100°C), contamination of the alumina coil form or insulation was suspected as markedly lowering the coil melting point.

The high purity commercial alumina which was used for the furnace may have decreased in resistance at the higher operating temperatures to the point where significant electrical shorting and consequent heating occurred. Figure D-31 compares the measured electrical resistance of various aluminas which shows a difference of 10^3 between laboratory grade alumina made from high purity water and 99.996% pure alumina and normal "high purity alumina." Contamination during the furnace operation could further reduce the insulating properties.

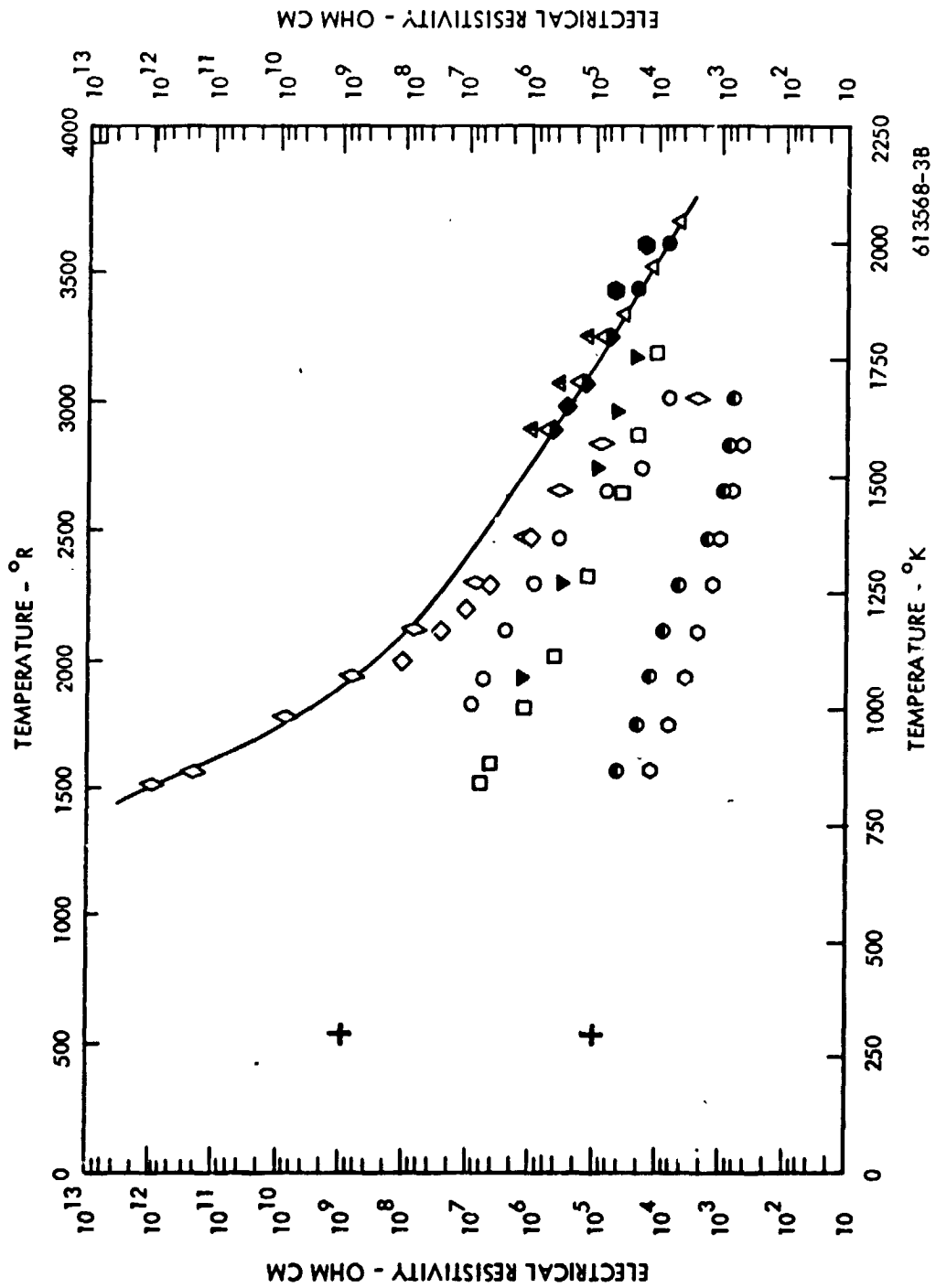


Figure D-31. Electrical Resistivity -- Aluminum Oxide

Future HIP-Welding Capabilities

The top two furnace zones have operated satisfactorily, providing a uniform hot zone of approximately 30.4 cm. In the event that a larger work zone is required, the Westinghouse Research and Development Laboratory is installing a molybdenum resistance heated autoclave furnace with a work zone 16.5 cm in diameter by 50.8 cm long which would be available on a toll basis. A self-supporting molybdenum heater structure will be used on this unit to avoid the electrical breakdown problems with impure alumina. A maximum temperature of 1700°C will be obtainable.

B. Diffusion Couple Condition

A complete photographic record was made of the specimen and furnace condition as the autoclave was unloaded. The molybdenum buckets and specimen packets were clean. The tantalum sheet outer covers used on the packets which leaked from the prior cycle and had been cleaned and resealed for this cycle were clean and apparently well deformed by the welding run. The tantalum enclosed packets were generally brittle and 6 out of 7 indicated leaks following this weld cycle. Figure D-31 shows the post-HIP-weld cycle appearance of bucket number 2, with the T-111 getter machine chips, tantalum foil, etc. removed, and the placement of diffusion couple molybdenum cans in the bucket. A close-up view of three molybdenum cans from bucket number 2 is presented in Figure D-32. Figure D-33 presents a layout view of all of the molybdenum canned diffusion couples after the HIP-weld cycle.

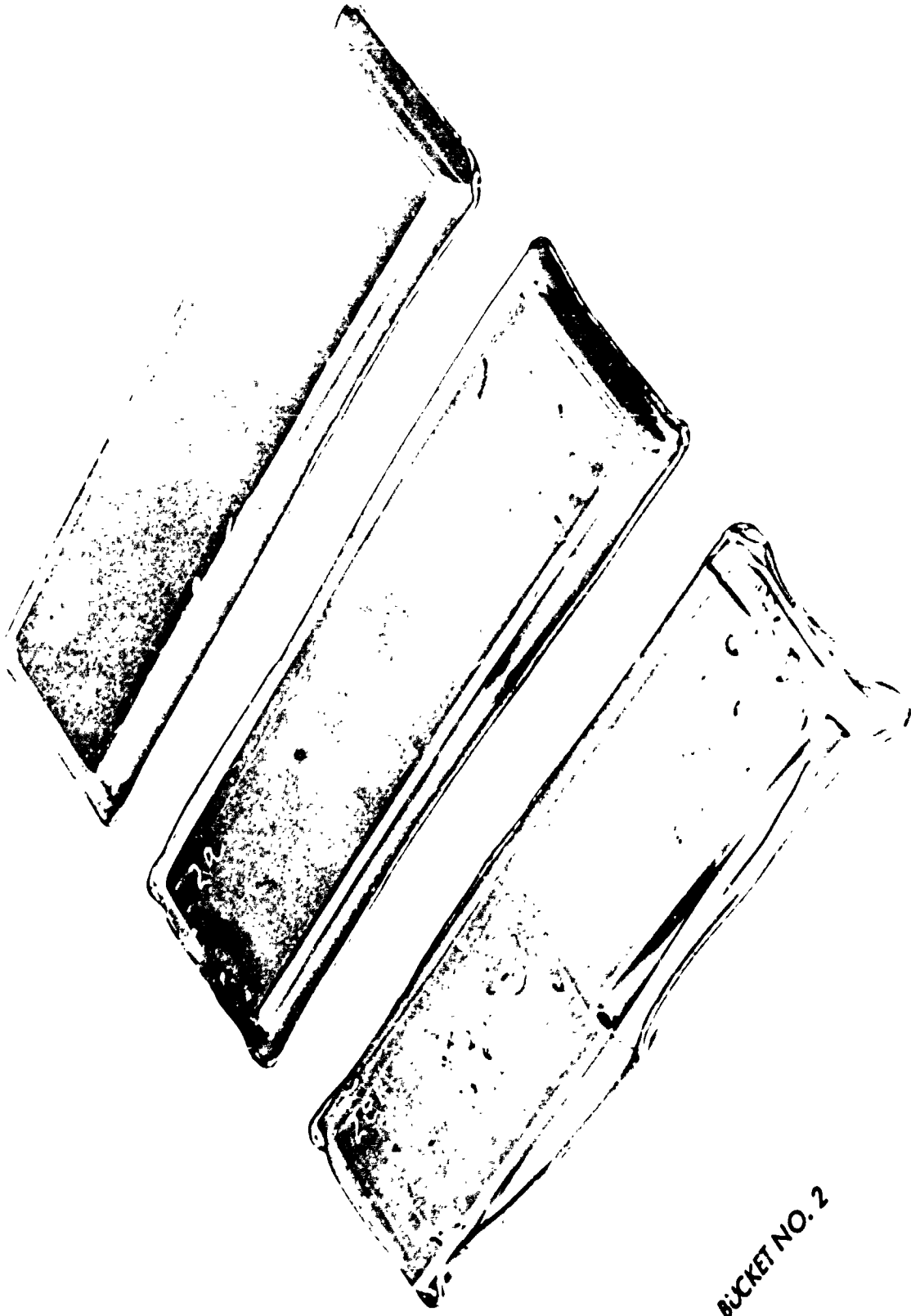
The molybdenum cans in Figure D-34 were all helium mass spectrograph leak checked, and the couple combinations were inspected metallographically for diffusion interface welding. Table D-VIII presents the results of this examination. Several of the more difficult to HIP-weld combinations (i.e., W/W-25 Re, W/ASTAR 811C, W/W-20 Re - 30.9 Mo, etc.) as well as those combinations which did not weld due to can leakage, were scheduled for hot press welding. The remainder were scheduled for diffusion couple preparation for age treatments.



BUCKET NO. 2

Figure D-32. Post HIL-welded Cycle Disassembly of Bucket No. 2

REPRODUCIBILITY OF THE
ORIGINAL PAGE IS POOR



BUCKET NO. 2

D-t

Figure D-33. Close-up View of the Bottoms of Three Couple Cans from Bucket No. 2
(Post Autoclave Cycle)



Figure D-34. Post Hit.-Weld Cycle Couple Cans. Column 1, arc cast tungsten couples; Column 2, CVD tungsten couples; Column 3, powder metallurgical rhenium couples; Column 4, CVD rhenium couples; Column 5, five dummy cans (molybdenum fitted), two tri-layer cans, two chemistry cans.

REPRODUCIBILITY OF THE ORIGINAL PAGE IS POOR

Table D-VIII. HIP-Weld Yield of Diffusion Couples from Autoclave Cycle 4

Can Number	Couple Combination (Primary Side) ¹ X/Y	Post-Cycle He Leak Check of Containment Can ²	% Welded (Subjective Evaluation)	Acceptable for Ageing and Analysis	Can to be Repackaged for Hot-Press Welding of Couple
1a	\widehat{W}_3 /Cb	OK	100%	Yes	---
1b	\widehat{W}_3 /Cb-1Zr	OK	100%	Yes	---
1c	\widehat{W} /Ta-10W	OK	50%	No	Yes
1d	\widehat{W} /Ta	OK	100%	Yes	--
1e	\widehat{W} /T-III	OK	60%	No	Yes
1f	\widehat{W} /Astar811C	OK	50%	No	Yes
1g	\widehat{W} /W-25Re	OK	0%	No	Yes
1h	\widehat{W} /30.9Re20.1Mo	Leak	50%	No	Yes
1i	\widehat{W} /Mo-50Re	Leak	0%	No	Yes
1j	\widehat{W} /Rep	Leak	30%	No	Yes
2a	W_{CVD}^4 /Cb	OK	100%	Yes	--
2b	W_{CVD} /Cb-1Zr	OK	100%	Yes	--
2c	W_{CVD} /Ta	OK	100%	Yes	--
2d	W_{CVD} /Ta-10W	OK	95%	Yes	--
2e	W_{CVD} /T-III	Leak	0%	No	Yes
2f	W_{CVD} /Astar811C	Leak	0%	No	Yes
2g	W_{CVD} /W-25Re	OK	50%	No	Yes

¹ Secondary side of cans contain backup couples

² Couple cans post-autoclave helium leak checked

³ \widehat{W} indicates Arc Cast W

⁴ W_{CVD} indicates CVD formed W

C-2

Table D-VIII (Cont'd.)

Can Number	Couple Combination, (Primary Side) ¹ X/Y	Post-Cycle He Leak Check of Containment Can ²	% Welded (Subjective Evaluation)	Acceptable for Ageing and Analysis	Can to be Repackaged for Hot-Press Welding of Coupling
2h	W _{CVD} /W30. 9Re20. 1Mo	OK	50%	No	Yes
2i	W _{CVD} /Mo-50Re	Leak	5%	No	Yes
2j	W _{CVD} /Re _p	OK	95%	Yes	--
3a	Re _p /Cb	OK	100%	Yes	--
3b	Re _p /Cb-1Zr	OK	100%	Yes	--
3c	Re _p /Ta	OK	100%	Yes	--
3d	Re _p /Ta-10W	OK	100%	Yes	--
3e	Re _p /T-III	OK	90%	Yes	--
3f	Re _p /Astar811C	OK	40%	No	Yes
3g	Re _p /W-25Re	OK	90%	Yes	--
3h	Re _p /W Re _p /W30. 9Re20. 1Mo	OK	100%	Yes	--
3i	Re _p /Mo-50Re	OK	100%	Yes	--
4a	Re _{CVD} /Cb	OK	100%	Yes	--
4b	Re _{CVD} /Cb-1Zr	OK	100%	Yes	--
4c	Re _{CVD} /Ta	OK	100%	Yes	--
4d	Re _{CVD} /Ta-10W	OK	100%	Yes	--
4e	Re _{CVD} /T-III	OK	100%	Yes	--
4f	Re _{CVD} /Astar811C	OK	50%	No	Yes
4g	Re _{CVD} /W-25Re	Leak	50%	No	Yes
4h	Re _{CVD} /W30. 9Re20. 1Mo	OK	100%	Yes	--
4i	Re _{CVD} /Mo-50Re	OK	100%	Yes	--
4j	Re _{CVD} /W	OK	60%	No	Yes

C. Hydrogen and Interstitial Analysis

Approximately 20 to 30 ppm hydrogen had been measured in the helium pressurizing gas before and after the HIP-welding process. This fraction of hydrogen corresponds to a 27 N/m^2 (2×10^{-2} torr) partial pressure of hydrogen at one atmosphere total pressure. At 200 MN/m^2 (2000 atmospheres) total pressure, however, the partial pressure of hydrogen is increased to $5.15 \times 10^3 \text{ N/m}^2$ (38 torr) which can result in significant concentration of hydrogen in hydrogen soluble materials. To prevent hydrogen contamination of tantalum base alloys, in which the hydrogen solubility markedly decreases with increasing temperature, the autoclave pressure may be released at high temperatures of 1200°C and above. Figure D-34 shows the hydrogen solubility isobars for tantalum at 138 MN/m^2 (20,000 psia) total pressure, and 0.31 MN/m^2 (45 psia) total pressure. HIP run number 4 was held to 138 MN/m^2 (20,000 psia) while cooling to prevent thermal contraction stresses from rupturing weld surfaces. From Figure D-34, hydrogen concentrations over one atomic percent, 55 ppm by weight, could be expected in the tantalum base alloys depending on the cooling rate, the diffusion kinetics and the availability of sufficient hydrogen for the several pounds of tantalum. The effect of hydrogen partial pressure on the equilibrium concentration of hydrogen suggests that hydrogen pickup could be nearly eliminated by reducing the autoclave pressure while the specimens were reduced to a low enough temperature, say 900°C , to prevent excessive "zero point" diffusion. The molybdenum cans were found to trap the hydrogen in the specimens (discussed in a later section). Also, an immediate pressure release could have led to a number of fractured couples due to differential thermal contraction strains. Hydrogen was subsequently removed from diffusion couple alloys by vacuum annealing.

Hydrogen, oxygen, and carbon sample chemistries were monitored both before and after autoclave cycles to ascertain the effectiveness of the molybdenum containment cans. Table D-IX taken after the second autoclave cycle, showed hydrogen to be the principle interstitial to be introduced into the samples. Since the source of the hydrogen was not fully resolved (autoclave cycle or post-cycle etch removal of molybdenum can), a selected group of

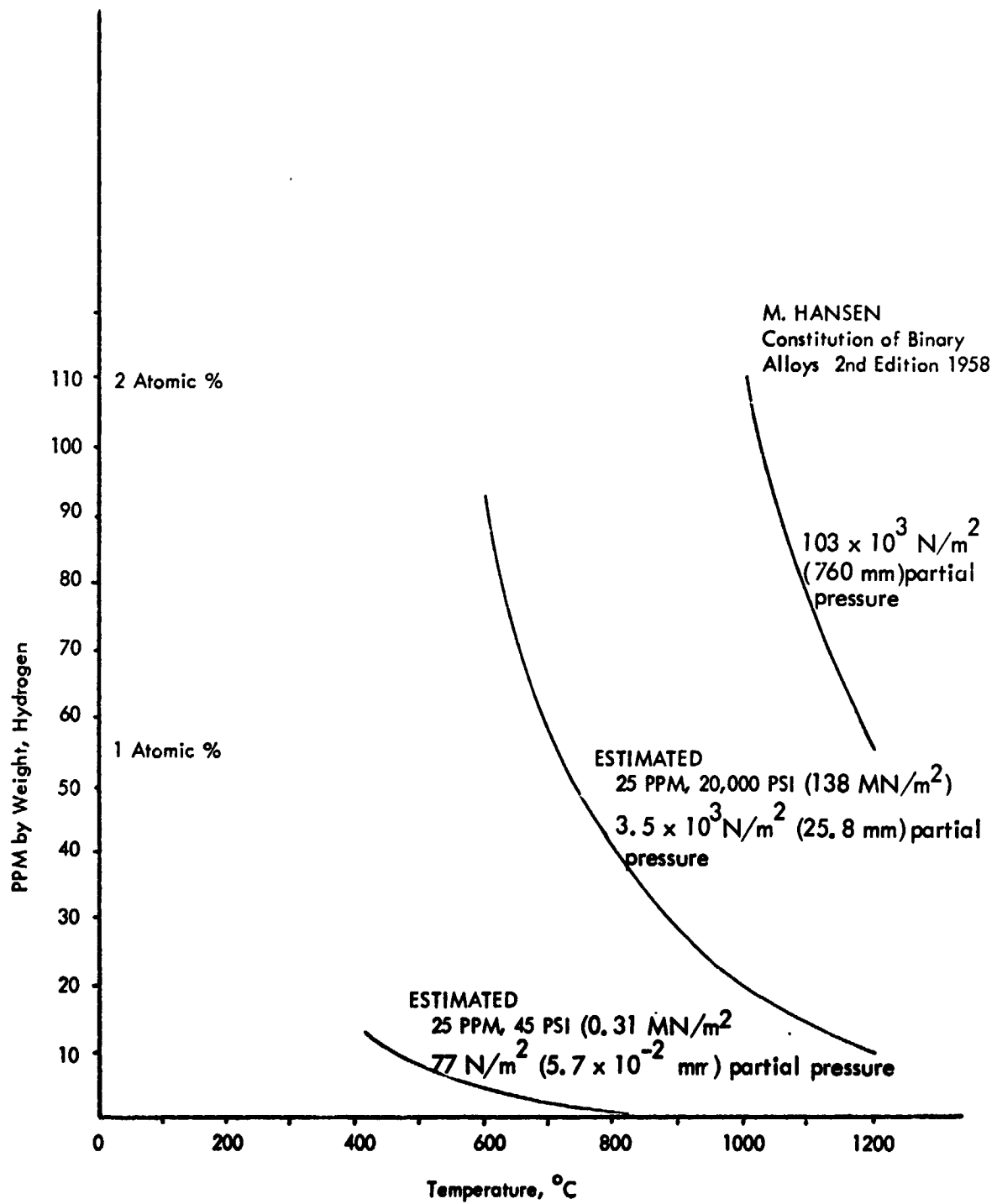


Figure D-35. Hydrogen-Tantalum Solubility (Isobars)

Table D-IX. Comparison of Pre- and Post-HIP Weld Interstitial Chemistries from the Second Autoclave Cycle

Couple Material	Interstitial Element (Concentration in wppm)					
	Oxygen		Carbon		Hydrogen	
	pre	post	pre	post	pre	post
W (powder met.)	< 50	8	< 50	13	10	--
Cb-1Zr	100	106	< 50	45	3	--
Cb	100	---	< 50	27	2	95
Ta-10W	20	33	7	12	2	--
Ta	< 50	34	< 30	12	1.5	33

materials from the third and fourth autoclave cycles were followed for hydrogen and oxygen. Table D-X lists the materials and the interstitial constituency followed.

Table D-XI shows that hydrogen is introduced into the diffusion couple materials by the autoclave process. Post-autoclave annealing at 1200°C for 2 hours in a 10^{-6} torr vacuum was successful in removing the hydrogen, only on the uncanned (molybdenum removed) couple materials.

Since the hydrogen could also be introduced by the nitric acid etch removal of the molybdenum containment can, a treatment of Cb and Ta sheets with molybdenum in nitric acid was made. As shown in Table D-XII, the etch removal of the molybdenum did not introduce hydrogen into the couple materials.

The results of the analyses listed in Table D-XIII for oxygen analysis of the diffusion couple materials before and after the autoclave cycle failed to reveal any definite trend for oxygen contamination. These results are presented in Table D-XIII.

Table D-X. Post-HIP Cycle Chemical Analysis of Selected Diffusion Couple Materials

	<u>Material</u>	<u>Analysis</u>
A.	Group I ¹	
	Mo-50Re	H, O
	Ta	H, O, C
	Cb	H, O
	Ta-8W-2Hf	H, O
	W-30.9Re-20.1Mo	H, O
	Ta-10W	H, O
	W	H, O
	Re	H, O, C
	ASTAR-811C	H, O
B.	Group II ²	
	Mo-50Re	H, O
	Ta	H, O
	Cb	H, O
	Ta-8W-2Hf	H, O
	W-30.9Re-20.1Mo	H, O
	Ta-10W	H, O
	W	H, O
	Re	H, O
	ASTAR-811C	H, O
C.	Group III ³	
	Cb (as received)	H
	Cb (etched)	H
	Cb (etched-vacuum annealed)	H
	Ta (as received)	H
	Ta (etched)	H
	Ta (etched-vacuum annealed)	H

¹Group I: As HIP-welded (autoclave cycled)

²Group II: HIP-welded and vacuum annealed at 1200°C, 2 hours, at 10⁻⁴ N/m² (10⁻⁶ torr)

³Group III: To ascertain degree of hydrogen contamination by acid etch process.

Table D-XI. Hydrogen Analysis Through the Third and Fourth Autoclave HIP-Weld Cycles

Material	Hydrogen Concentration (ppm by weight) ¹			
	Pre-Autoclave ²	Post-Autoclave ³	Post-Anneal	
			Annealed Without Can ⁴	Annealed In Can ⁵
Mo-50Re (L) ⁶	---	0.7	0.3	---
Ta (L)	1.5	37.0	0.2	33.0
ASTAR-811C	---	27.0	0.5	---
Ta-8W-2Hf (L)	5.0	42.0	0.3	---
W-30.9Re-20.1Mo (L)	<1.0	0.4	0.2	---
Ta-10W (L)	1.7	18.0	0.3	---
W	<10.0	0.5	0.5	---
Re	---	2.7	1.1	3.0

¹ Accuracy for

<1 ppm	=	± 0.2
1-2 ppm	=	± 0.3
30-40 ppm	=	± 3.0
100 ppm	=	± 5.0

² Vendor analysis

³ Autoclave at 1440°C for 1 hour, 28,000 psi Helium, approximately 10^5 N/m² (1 atm H₂) (equiv.)

⁴ Annealed at 1200°C for 2 hours at 10^{-4} N/m² (10^{-6} torr)

⁵ 17th Monthly Progress Report, WANL-L-631, November, 1970. (Hydrogen after 2 hours at 900°C, 10^{-4} N/m² (10^{-6} torr) while couples were still in sealed molybdenum cans).

⁶ L denotes post-autoclave leak of containment can (Helium leak check).

Table D-XII. Effect of Acid Etching on Hydrogen Content of Diffusion Couple Materials

Material (.080" thick Sheet)	Hydrogen Concentration (ppm weight) ¹		
	As Received	Post-Etch ²	Post-Anneal ³
Cb	2.4	3.8	1.6
Ta	0.6	0.7	0.8

¹ Accuracy for 1-2 ppm = ± 0.3

² Etched in 50 HNO₃ - 50 H₂O (no HF additive)
Etched with molybdenum sheets clamped to each side.

³ Annealed at 1200°C for 2 hours at 10⁻⁴ N/m² (10⁻⁶ torr)

Table D-XIII. Oxygen Analysis Through the Third and Fourth Autoclave HIP-Weld Cycles

Material	Oxygen Concentration (ppm by weight) ¹			
	Pre-Autoclave ²	Post-Autoclave ³	Post-Anneal	
			Annealed Without Can ⁴	Annealed in Can ⁵
Mo-50Re (L) ⁶	---	<5.0	<5.0	---
Ta (L)	<50.0	34.0	17.0	34.0
ASTAR-811C	---	61.0	27.0	---
Ta-8W-2Hf (L)	<80.0	52.0	39.0	---
W-30.9Re-20.1Mo (L)	4.0	4.0	8.0	---
Ta-10W (L)	<50.0	73.0	92.0	33.0
W	<10.0	<5.0	<5.0	8.0
Re		12.0	15.0	42.0

¹ Accuracy for <5 ppm = ± 2.0
 15-20 ppm = ± 2.0
 100-250 ppm = ± 15

² Vendor analysis

³ Autoclave at 1440°C for 1 hour, 193 MN/m² (28,000 psi) helium

⁴ Annealed at 1200°C for 2 hours at 10⁻⁴ N/m² (10⁻⁶ torr)

⁵ 17th Monthly Progress Report, WANL-L-631, November, 1970. (Oxygen after 2 hours at 900°C, 10⁻⁴ N/m² (10⁻⁶ torr) while couples were still in sealed molybdenum can).

⁶ L denotes post-autoclave leak of containment can (Helium leak check).

V. CONCLUSION - AUTOCLAVE OPERATIONS

Table D-II presents several of the conclusions or recommendations concerning autoclave HIP-welding practice generated during the course of this study. Although hydrogen pickup during the autoclave process was found in this study, it was not deemed a problem since the diffusion couples were destined for 10^{-6} N/m² (10^{-8} torr) vacuum ages. Also, although four autoclave HIP-weld cycles were performed, the molybdenum wound furnace began to degrade on the third cycle and its failure on the fourth cycle prevented 100 percent success in welding the program couples. Those program couples not joined by HIP-welding were scheduled for hot press welding. The autoclave HIP-weld process remains, however, as an excellent low temperature, minimum zero condition interdiffusion zone width method for mass joining of couple materials for diffusion analysis.

APPENDIX D: HIP Welding Operations References

1. D'Annessa, A. T., "The Solid State Bonding of Refractory Metals", Welding Journal Supplement, 1964.

APPENDIX E

HOT PRESS OPERATION

By

F. G. Arcella

APPENDIX E. HOT PRESS OPERATION

I. INTRODUCTION

Diffusion couple materials which were not acceptably joined by the autoclave HIP-weld process were joined by hot press operations. This appendix describes these operations, and their results.

Table E-1 identifies those diffusion couple combinations requiring hot press joining for couple formation. Several of the couple combinations were 50 to 60 percent welded during the autoclave process, but were selected for hot press joining to effect 100 percent welded junctions.

II. HOT PRESS PARAMETER RESOLUTION

Prior to actually hot press cycling the material combinations listed in Table E-1, several parameter determination cycles were performed on representative materials. A hot press die was fabricated from graphite and consisted of a 5.1 cm(2-inch) diameter base with a 3.18 cm(1.25-inch) by 1.59 cm(0.625-inch) rectangular center channel. The female die and the plunger were both 3.81 cm (1.50-inches) high. Hot press operational sequence was as follows:

- Clean all material surfaces (degrease, etch, polish)
- Stack materials as follows:
 - Mo sheet*
 - W
 - Alloy X
 - Mo sheet*
 - Repeat pattern
- The stacked materials were wrapped in Ta foil with a single seam at the top of the package

*Molybdenum sheets facilitated acid etch separation of the hot press welded diffusion couple materials.

Table E-1. Diffusion Couple Material Combinations to Hot Press Weld

<u>No.</u>	<u>Couple ID</u> ¹	<u>Couple Material Combinations</u>
1	1CA	Warc cast/Ta-10W
2	1FA	Warc cast/ASTAR 811C
3	1GA	Warc cast/W-25Re
4	1IA	Warc cast/Mo-50Re
5	1JA	Warc cast/Re
6	1HA	Warc cast/W-30.9 Re-20.1Mo
7	1EA	Warc cast/T-111
8	2EA	W cvd / T-111
9	2FA	W cvd / ASTAR 811C
10	2GA	W cvd / W-25Re
11	2HA	W cvd / W-30.0Re-20.1Mo
12	2IA	W cvd / Mo-50 Re
13	3FA	Re powder /ASTAR 811C
14	4FA	Re cvd / ASTAR 811C
15	4GA	Re cvd / W-25Re
16	4JA	Re cvd / W
17	6A-1 ²	(KVI)Ta/Ta-10W/W ¹
18	6B-1 ²	(KVI)W/W-25Re/Re ¹
19	KVI ²	W/Ta ¹

1 See Appendix F. Diffusion Couple Age/Identification Chart

2 Program plan to hot press

- Insert tantalum foil package into die, die into chamber in hot press
- Evacuate hot press chamber (to 10 N/m^2 (10^{-3} torr)).
- Compress foil seam, sample (i.e., vacuum seal foil container) to 19.3 MN/m^2 (2800 psi)
- Backfill chamber with high purity helium
- Retain constant load while cycling sample to temperature, hold and cool down

The materials stacked in the first hot press parameter determination cycle were as follows:

Layer:	1	Ta
	2	ASTAR 811C
	3	W arc cast
	4	T-111
	5	W-30.9Re-20.1Mo
	6	W arc cast
	7	W-25Re
	8	W-25Re
	9	T-111
	10	Ta

Since low melting eutectics could form at 2300°C , a hot press temperature of 2100°C was selected. A hot press cycle to 2100°C for 20 minutes at 19.3 MN/m^2 (2800 psi) resulted in 100 percent interface welding of the diffusion couple surfaces (metallographic observation).

III. HOT PRESS OPERATIONS

The material combination packages of Table E-1 were each hot press cycle welded (Figure E-1), and post weld inspected metallographically for weld integrity. All samples were found to be 90 to 100 percent welded. Subsequent diffusion couple preparation included trimming of tantalum foil from lateral surfaces with a cutoff wheel and separation of the welded couples by preferential etch removal of the molybdenum spacer sheets.

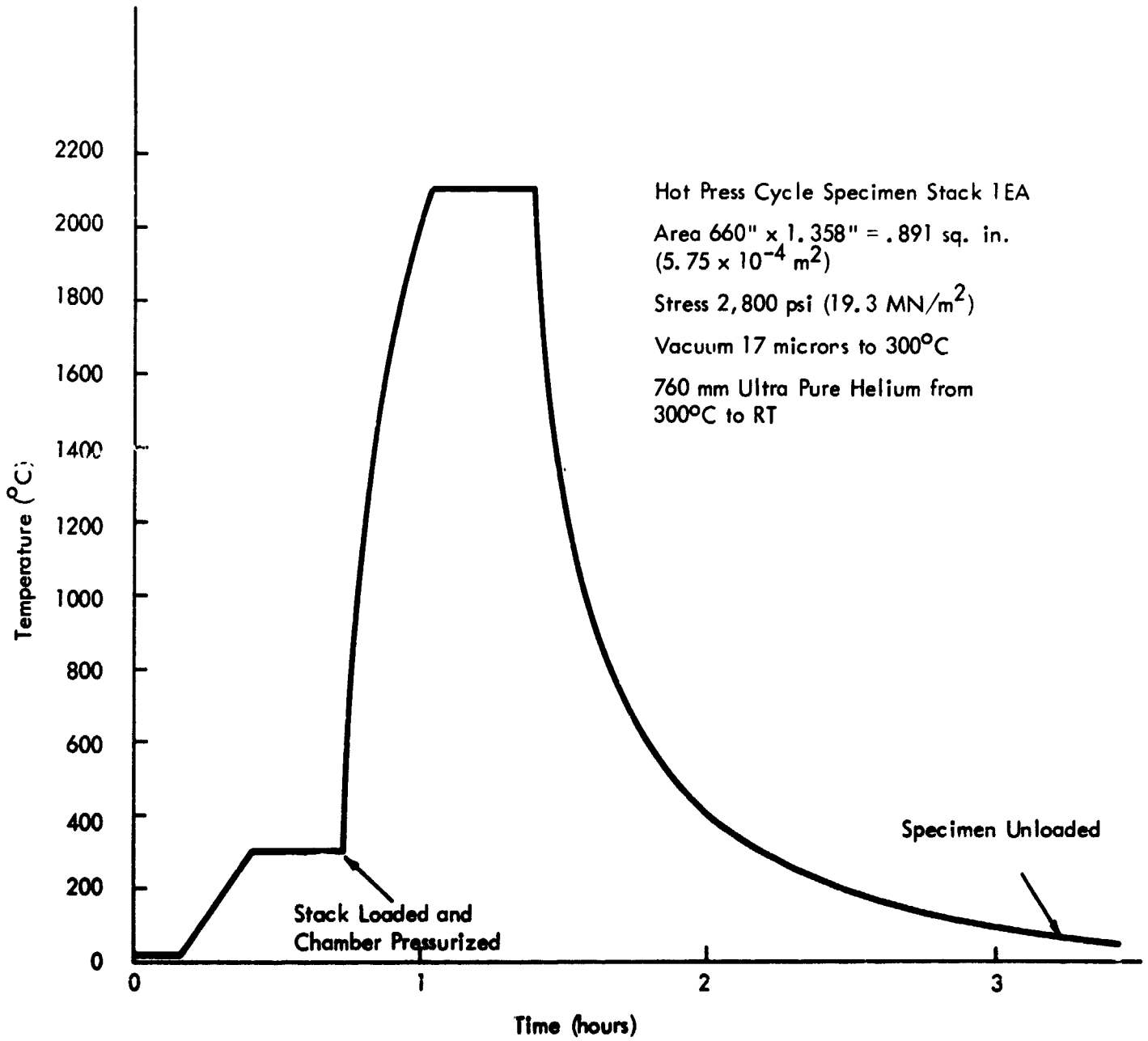


Figure E-1. Typical Hot Press Cycle Temperature-Time History

IV. CONCLUSIONS

All diffusion couple material combinations not welded by the autoclave HIP process were hot press welded by being subjected to 19.3 MN/m^2 (2800 psi) at 2100°C for 20 minutes. Random check of several post-hot press interdiffusion zones showed them to be around 6-10 microns (approximately 0.4 mils), acceptable as a zero condition for interdiffusion ageing.

On a comparative basis, autoclave HIP-welding practices produced better diffusion couples, than hot pressed couples, in that they were less distorted; possessed smaller interdiffusion zones; were less likely to be contaminated by carbon or oxygen; easier to prepare and post-weld section; and, for large numbers of couples could produce welds in one operational cycle.

APPENDIX F
DIFFUSION COUPLE AGE/IDENTIFICATION CHART

APPENDIX F. Diffusion Couple Age/Identification Chart

The following tables describe the diffusion couple age schedule identification system employed in this program. Identification numbers were vibratool scribed (tungsten tip) into the back face of each welded couple after the couples had been removed from their HIP-weld molybdenum cans. Preliminary annealing of some Ta/W couples at 2650°C for 4 hours (accelerated diffusion condition) showed that surface diffusion effects did not remove the scribe marks. Post-age examination of all program couples found all scribe marks to be present and clear.

TABLE F-1. DIFFUSION COUPLE AGE/IDENTIFICATION CHART

Furnace Cycle T (°C) t (hrs)	C	G	D	H	A	E ¹	I	B	F	As Welded	HIP Formed	Hot Press Formed	No. to Analyze	
W ₉₀ /Cb /Co-10W /Ta /Ti-111 /ASTAR /W-250a /W-Ba-Mo /Mo-500a /Ni	2000	2000	1800	1500	1500	1500	1500	1200	1200	1AA-7	X		7	
	1000	1000	1000	100	2000	1000	100	2000	1000	1AA-2	X		6	
		ICA-8	ICA-7	1AA-5 1BA-5 1CA-5 1DA-5 1EA-5 1FA-5 1GA-4 1HA-4 1IA-4 1JA-4	1AA-6 1BA-6 1CA-6 1DA-6 1EA-6 1FA-6 1GA-3 1HA-3 1IA-3 1JA-3	ICA-4 1DA-4 1EA-4 1FA-4 1GA-2 1HA-2 1IA-2 1JA-2	1AA-3 1BA-3 1CA-3 1DA-3 1EA-3 1FA-3 1GA-1 1HA-1 1IA-1 1JA-1	1AA-4 1BA-4	1AA-1 1BA-1 1CA-1 1DA-1 1EA-1 1FA-1	1AA-2 1BA-2 1CA-2 1DA-2 1EA-2 1FA-2	X X X X X X X X X X			6 6 7 7 7 7 6 6 6 7
	W ₉₀ /Cb-17r /Ta /Co-10W /Ti-111 /ASTAR /W-250a /W-Ba-Mo /Mo-500a /Ni			2AA-6 2BA-6 2CA-6 2DA-6 2EA-6 2FA-6 2GA-4 2HA-4 2IA-4 2JA-4	2AA-5 2BA-5 2CA-5 2DA-5 2EA-5 2FA-5 2GA-3 2HA-3 2IA-3 2JA-3	2AA-4 2BA-4 2CA-4 2DA-4 2EA-4 2FA-4 2GA-2 2HA-2 2IA-2 2JA-2	2AA-4 2BA-4 2CA-3 2DA-3 2EA-3 2FA-3 2GA-1 2HA-1 2IA-1 2JA-1	2AA-3 2BA-3	2AA-2 2BA-2 2CA-2 2DA-2 2EA-2 2FA-2	2AA-1 2BA-1 2CA-1 2DA-1 2EA-1 2FA-1	2BA-7 2DA-2 2FA-2 2GA-7 2IA-7	X X X X X X X X X X		6 7 6 6 8 6 8 7 6 6 7
				3AA-6 3BA-6 3CA-6 3DA-6 3EA-6 3FA-6 3GA-4 3HA-4 3IA-5	3AA-5 3BA-5 3CA-5 3DA-5 3EA-5 3FA-5 3GA-3 3HA-3 3IA-4	3AA-4 3BA-4 3CA-4 3DA-4 3EA-4 3FA-4 3GA-2 3HA-2 3IA-3	3AA-4 3BA-4 3CA-3 3DA-3 3EA-3 3FA-3 3GA-1 3HA-1 3IA-2	3AA-3 3BA-3	3AA-2 3BA-2 3CA-2 3DA-2 3EA-2 3FA-2	3AA-1 3BA-1 3CA-1 3DA-1 3EA-1 3FA-1	3AA-7 3CA-7 3EA-7 3GA-7 3HA-7 3IA-8	X X X X X X X X X X		7 6 7 8 7 7 8 7 7 7 8

1 Thermocouple malfunction - 1630°C/1000 hours.

2 No couple.

TABLE F-1. DIFFUSION COUPLE AGE/IDENTIFICATION CHART (Continued)

Furnace Cycle T (°C) t (hr)	C	G	D	H	A	E ¹	I	B	F	As Welded	HIP Formed	Hot Press Formed	Nb to Analyze
Nb Cv/ Cb-12r /Te	2000	2000	1800	1800	1500	1500	1500	1200	1200				6
	1000	100	1000	100	2000	1000	100	2000	1000				7
			4AA-6	4AA-5	4AA-4	4AA-4	4AA-3	4AA-2	4AA-1		X		6
			4BA-6	4BA-5	4BA-4	4BA-4	4BA-3	4BA-2	4BA-1		X		7
			4CA-6	4CA-5	4CA-4	4CA-3	4CA-3	4CA-2	4CA-1		X		6
		4DA-8	4DA-6	4DA-5	4DA-4	4DA-3	4DA-3	4DA-2	4DA-1		X		8
			4EA-6	4EA-5	4EA-4	4EA-3	4EA-3	4EA-2	4EA-1		X		6
			4FA-6	4FA-5	4FA-4	4FA-3	4FA-3	4FA-2	4FA-1		X		8
			4GA-6	4GA-5	4GA-4	4GA-1	4GA-1				X		6
			4HA-6	4HA-5	4HA-4	4HA-2	4HA-1				X		6
		4IA-6	4IA-5	4IA-4	4IA-3	4IA-2	4IA-1			X		7	
		4JA-6	4JA-5	4JA-4	4JA-2	4JA-1				4JA-7	X		7
													57
KVI (Annealed) 2500°C Te/Nb 10 hours													
2500°C 0.9 hours Te/W 2650°C 0.4 hours													
2650°C 3.6 hours Te/W O-cond Rings													
KVI (Alloy) Te-10W													
W-25Nb													

1. Thermocouple malfunction - 1630°C/1000 hours.

TABLE F-1. DIFFUSION COUPLE AGE/IDENTIFICATION CHART (Continued)

Furnace Cycle T (°C) t (hrs)	C		G		D		H		A		E		I		B		F		As Welded	HIP Formed	Hot Press Formed	Nb. to Analyze
	2000	1000	2000	100	1000	1000	1000	100	1500	2000	1500	1000	1500	100	1200	2000	1200	1000				
W arc couples	6		6		10		10		7		10		3		6		6		5			69
WCVD couples	6		6		10		10		7		10		3		6		6		3			67
Rp couples	5		5		9		9		7		9		3		6		6		6			65
RpCVD couples	6		6		10		10		8		10		3		6		6		2			67
KVI Annotated					9		8		8		8								7			40
KVI Alloy	7				4				2										2			15
Nb ¹	30		23		52		47		39		47		12		24		24		25			323

¹ Thermocouple malfunction - 1450°C/1000 hours.

APPENDIX G
DIFFUSION ANALYSIS

By
F. G. Arcella

APPENDIX G. Diffusion Analysis

This appendix reviews some of the fundamentals of solid state diffusion analysis, and extrapolates these principles to engineering considerations applicable to this program of study. Prior to reviewing mathematical treatments, however, there should be a review of laboratory practice, since handling and ageing practice can seriously affect the boundary and analytical conditions necessary for accurate analysis.

I. AGE AND PREPARATION PRACTICE

Accurate diffusion information can only be obtained through careful adherence to practices learned through experience. Laboratory practice and sample handling techniques can seriously affect the value and acceptability of the information generated in a diffusion study. Consideration of the laboratory practices and analytical techniques necessary to analyze the diffusion couples of this program included:

- A diffusion couple characterization. The couples were characterized by phase diagram studies to ascertain if multiple interphases existed, analytical techniques required, temperature limits, etc.
- Couple dimensions. Preprogram selection of couple dimensions was analyzed.
- Pre-ageing condition. Metallographic, microprobe, microhardness, and bond integrity characterization of bonded couples before ageing supplied necessary information for post-age analysis.
- Diffusion ageing anneals. Critical considerations concerning couple cleanliness, couple mounting in the furnace, mount geometries, heat up time (ramp), and quench time to minimize couple contamination and insure accurate calculation of interdiffusion coefficients. (See Appendix K. Error Analysis).
- Post-ageing metallography. Couple preparation in terms of sectioning, mounting, polishing, metallographic inspection including grain size analysis, and couple cleanliness was made to insure accurate microprobe analysis. (See Appendix K. Error Analysis).
- Microprobe analysis. Couples must be clean, properly mounted, and the effectiveness of the microprobe must be properly understood. Microprobe traces were also made to test for grain boundary diffusion.
- Couple efficiency. The couples were related through alloy families and analytical requirements to reduce the total number of couples required, yet still generate accurate information.

These practical considerations, necessary to implement an accurate diffusion study, are discussed in the following text.

The diffusion couples studied in this program can be characterized in several ways. Examination of their binary and ternary phase diagrams^{(1)*} revealed which couples possessed solid solution and/or multiple phase interdiffusion zones. Tables G-I and G-II present these interdiffusion zone characteristics for the tungsten and rhenium couples selected for this program. For two and three elemental components, prediction of the character of the interdiffusion zones is relatively simple. Characterization of the interdiffusion zones for more than four elemental components is more difficult, however the zone characteristics as predicted in Tables G-I and G-II are the most probable. Tungsten couples primarily form solid solution interdiffusion zones and could have been evaluated for diffusion coefficients by the Grube integration⁽²⁾ (common error function solution) if the concentration gradients had been symmetrical about a common interface and the diffusion coefficients had been concentration independent. However, a Boltzmann-Matano^(3,4,5) analysis of the diffusion coefficients was necessary since they were concentration dependent. The Boltzmann-Matano analysis for binary couples could safely be applied to those ternary alloys where concentration of the third (or fourth) element is small.^(6,7) The principal ternary diffusion coefficients will not differ appreciably from those of the binary components in this case of small concentration of the third component. Those couples with an appreciable ternary component concentration could have been analyzed by state-of-the-art ternary analytical techniques^(6,7,8) but such analysis would have required more information than that planned for this program.

The rhenium couples (Table G-II) form three and four phase interdiffusion zones which, as Jost⁽⁵⁾ has pointed out, can be analyzed by the Boltzmann-Matano method. Diffusion coefficients found for these couples by the Boltzmann-Matano method can also be checked by concentration-penetration equations developed by Wagner^(5,10) and Smoluchowski.^(10,11) Again, if the amount of ternary component is small, the major binary components will possess diffusion coefficients similar to those of a binary couple.

These considerations showed that the diffusion couples for this program formed certain types of interdiffusion zones which could be evaluated for interdiffusion coefficients by known formulations and methods.

*References at the end of this Appendix "G".

TABLE G-1. Diffusion Couple Characterization, Tungsten Couples

W	Interdiffusion Zone ¹	Couple Material	Typical Interdiffusion Analysis ²
W	SS ³	Cb	BM
W	SS	Cb-1Zr	BM ⁴
W	SS	Ta	BM
W	SS	Ta-10W	BM ⁴
W	SS	Ta-8W-2Hf	BM ⁴
W	SS	Ta-8W-2Hf-1Re	BM ⁴
W	$\beta \sigma \chi_{\alpha}$	Re	BM, WS
W	SS	W-25Re	BM
W	SS ⁵	W-30.9Re-20.iMo	T
W	SS ⁵	Mo-50Re	T

1. Found from examination of binary and ternary phase diagrams (Ref. 1)
2. Typical method of analyzing for interdiffusion coefficient
 - BM = Boltzmann-Matano analysis (binary) (Ref. 5)
 - W,S = Wagner, Smoluchowski multiphase (Ref. 5, 10, 11)
 - T = Ternary diffusion analysis (Ref. 6, 8, 9)
3. Solid solution or phases
4. Binary Boltzmann-Matano analysis is valid when concentration of the third constituent of ternary is small (Ref. 6, 7)
5. W-Mo-Re phase diagram at 1000, 1500°C (Ref. 1)

TABLE G-II. Diffusion Couple Characterization, Rhenium Couples

Re	Interdiffusion Zone ¹	Couple Material	Typical Interdiffusion Analysis ²
Re	$\beta \times \alpha$	Cb	BM, S
Re	$\beta \times \alpha$	Cb-1Zr	BM ³ , S
Re	$\beta \times \alpha$	Ta	BM, S
Re	$\beta \times \alpha$	Ta-10W	BM ³ , S
Re	$\beta \times \alpha$	Ta-8W-2Hf	BM ³ , S
Re	$\beta \times \alpha$	Ta-8W-1Hf-1Re	BM ³ , S
Re	$\beta \times \sigma \alpha$	W-25Re	BM
Re	$\beta \times \sigma \alpha$	W-30.9Re-20.1Mo	T
Re	$\beta \times \sigma \alpha$	Mo-50Re	T
Re ⁵	$\beta \times \sigma \alpha$	W	BM, WS

1. Found from examination of binary and ternary phase diagrams (Ref. 1)
2. Typical method of analyzing for interdiffusion coefficient
 BM = Boltzmann-Matano analysis (binary) (Ref. 5)
 W,S = Wagner, Smoluchski multiphase (Ref. 5, 10, 11)
 T = Ternary diffusion analysis (Ref. 6, 8, 9)
3. Binary Boltzmann-Matano analysis is valid when concentration of the third constituent of ternary is small (Ref. 6, 7)
4. Mo-W-Re phase diagram (Ref. 1)
5. CVD Re // 0001 planes to W

The proper selection of diffusion couple dimensions is particularly important to analytical techniques as well as to economics. The utilization of generally accepted evaluation formulations (error function or Boltzmann-Matano analysis) requires that the concentration profiles and couple geometries (size) conform to the mathematical boundary conditions imposed in the derivation of these formulations. For instance, if infinite boundary conditions are assumed in deriving the diffusion-concentration profile formulation, then the experimentally determined profile should not approach the boundaries (physical surfaces) of the couples. Considerable error in the value of \tilde{D} (interdiffusion coefficient) can result if the couples are not properly sized. Background studies for this program (Appendix C) showed that for \tilde{D} values predicted for this study, couple widths (in the diffusion direction) should be 0.10 to 0.13 cm (40-50 mils) in order to avoid these errors in determining the true \tilde{D} values. The diffusion couples were thus fabricated from 0.20 cm (80 mil) sheet products.

The pre-ageing conditions of the autoclave welded couples were examined optically for bond integrity, the presence of impurities or oxides at the bond interface, and any other irregularities which could interfere with mass transport. The extent of interdiffusion introduced by the welding process was noted by a series of microprobe traverses and was found to be about 1×10^{-4} cm on the average. Residual strain from the bonding process or from couple preparation was not expected to influence diffusion properties at the elevated temperatures proposed for this study.⁽¹²⁾

Pre-ageing metallographic inspections for grain size, grain boundary precipitates, and x-ray analysis for retention of the preferred orientation of the CVD tungsten and rhenium in the bonded couples were also made. Such information contributed to post-test evaluation.

The ageing treatments of the refractory metal diffusion couples were performed in ion pumped vacuum furnaces at a pressure of 1×10^{-8} torr or less while at temperature. Several diffusion age practices were carefully followed to insure accurate results. Diffusion couples were mounted in free standing support stands in such a fashion that the more volatile constituents of one couple did not vaporize to another couple. If this occurs at high temperatures and during the long time anneals, perturbations to the analytical concentration profiles could result. This potential problem was solved by placing common faces of the couples together in their axial alignment in the stands.

A critical consideration to the ageing cycles is the heatup and cooldown rates of the diffusion couples. For short time anneals, the heatup and cooldown ramps should be as steep as possible since diffusion occurring during these temperature ramps will be at varying diffusivities. Too rapid a heatup ramp could flood the ion pumps (due to outgassing) and cause partial loss of vacuum as well as couple contamination. To accurately determine the time at which the couples were considered to have been at the ageing temperature T , it was necessary to record accurate time-temperature (t-T) curves and to apply a time correction analysis. Check calculations of this correction were made and the correction was found to be minimal. Due to the low mass of the tantalum resistance heaters, quench times were quite rapid and also minimal.

The preparation of diffusion aged couples for analyses must be carefully controlled. The couples were sectioned normal to the couple bond and parallel to the direction of diffusion (Appendix E. Error Analysis). A position well removed from the couple edge was selected for microprobe analysis to avoid surface diffusion effects. Sectioning was performed by EDM machining or on a cooled metallographic wheel to avoid overheating the couple. These cutting techniques avoided distorting or smearing the interdiffusion region. An alignment jig was included in the metallographic mount to insure that the couples were mounted with their bonded plane normal to the polishing plane. Usually cold mounts which avoid the temperatures and pressures of hot mounts are employed for metallographically mounting diffusion couples, but in this study the materials being investigated were unaffected by these conditions. Couples were mounted two per mount and carefully polished to avoid scratching or smearing the interdiffusion zone. The couples were also mounted according to alloy family to facilitate microprobe operation. Initial metallographic inspection for grain size and any indication of reduction of preferentially oriented CVD grains was made. A small grain size at the lower age temperatures usually contributes to grain boundary diffusion at these temperatures.

Microhardness traverses of the interdiffusion zones of several of the mounted couples indicated embrittlement developing in these zones. The correlation of changes in

microhardness with changes in phase structure or composition in the interdiffusion zone has been done by others,⁽¹³⁾ and is not regarded as a precise analytical technique.

Microprobe traces were made on couple surfaces mounted normal to the microprobe source for optimum alignment of the interdiffusion axis. Each couple's elemental constituent was traced for a concentration profile. Traces were made at 45° and 90° angles to the interdiffusion zone. Also, a few microprobe traces were made on selected couples (low temperature age treatments) parallel to and at selected distances from the interdiffusion zone to check for grain boundary diffusion effects. Hartley, et al,⁽¹⁴⁾ in analyzing binary interdiffusion couples have noted that interdiffusion coefficients calculated from microprobe concentration traces in small interdiffusion zones are two to three orders of magnitude greater than values extrapolated from larger interdiffusion gap analyses at higher temperatures. They reasoned that such a small zone has a steep concentration gradient and that a microprobe tends to flatten out and elongate the steep region of the concentration curve. This results in a lower slope, giving a higher calculated diffusion coefficient (Boltzmann-Motano). The effect is believed to be the result of secondary fluorescence, which decreases resolution of the probe trace.^{(15)*} Higher than expected diffusion coefficients at low temperatures can also be due to grain boundary effects or an increasing difference in intrinsic diffusion coefficients. Experience indicates that better diffusion analyses can be made with wide interdiffusion zones, thus dictating emphasis on longer age times at low temperatures.

This study required the complete interdiffusion characterization of two types of tungsten and two types of rhenium:

- (1) Arc Cast W
- (2) Fluoride CVD W // to 100
- (1) Powder Metallurgy Re
- (2) Chloride CVD Re // to 0001

each coupled to the refractory metal alloys presented in Tables G-I and G-II. The couples

*And is also correlated to beam spot diameter (See Appendix K. Error Analysis).

were diffusion aged at 5 temperatures (1200, 1500, 1630, 1800 and 2000°C) for two different time increments (100 and 1000 or 1000 and 2000 hours) at each temperature. The refractory metal couple alloys were grouped by alloy family as:¹

(1) Columbium Family

Cb
Cb-1Zr

(2) Tantalum Family

Ta
Ta-10W
T-111
ASTAR-811C

(3) Rhenium Family

Re (power met product)
(or W (arc cast))
W-25Re
W-30.9Re-20.1Mo
Mo-50Re

¹ Complete couple identification charts and age schedules are in Appendix F. Diffusion Couple Age/Identification Chart.

II. DIFFUSION ANALYSIS

The previous section has discussed the mechanics of conducting the ageing study of the diffusion couples and has mentioned briefly the type of mathematical analyses that the interdiffusion concentration profiles will require. This section will

- Identify the mathematical relations required to solve for the diffusion coefficients of the couples described in the previous section.
- Illustrate the appearance of that diffusion data with respect to various temperature, time, and couple compositional variations.
- Discuss some couple analytical considerations that were mentioned in the previous section.
- Demonstrate the generation of engineering level analysis for the systems of this study.

The mathematics of diffusion are well developed in such texts as Jost⁽⁵⁾ or Crank⁽¹⁶⁾

For the case of a one-directional concentration gradient, the flux J of a solute species diffusing due to that concentration gradient is expressed by Fick's First Law:

$$J = -D \frac{dC}{dX} \quad (G-1)$$

where D is the diffusion coefficient. Most treatments will follow the treatise that diffusion will follow the concentration gradient. Since it is not feasible to measure both J and dC/dX in cases where one metal is diffusing through another, consideration of the change in concentration with time in a volume element with unit cross sectional area and thickness dX results in

$$\frac{dC}{dt} = \frac{d}{dX} \left(D \frac{dC}{dX} \right) \quad (G-2)$$

For D not a function of concentration equation (2) becomes

$$\frac{dC}{dt} = D \frac{d^2 C}{dX^2} \quad (G-3)$$

Upon applying the boundary conditions for a semi-infinite diffusion couple

$$\begin{array}{lll} \text{BC.1} & C = C_o; X < 0; t = 0 & C = C_o; X = -\infty \quad t \neq 0 \\ \text{BC.2} & C = C_f; X > 0; t = 0 & C = C_f; X = +\infty \quad t \neq 0 \end{array}$$

where C is the concentration of substance A at some point in the diffusion zone, the solution to equation (G-3) would be

$$\frac{C - C_f}{C_o - C_f} = 1/2 \left[1 - \text{erf}(\mu) \right] \quad (G-4)$$

where

$$\mu = \frac{X}{2\sqrt{Dt}} \quad (G-5)$$

and

$$\text{erf}(\mu) = \frac{2}{\sqrt{\pi}} \int_0^\mu e^{-t^2} dt \quad (G-6)$$

(where erf is the well tabulated error function)

For symmetrical diffusion concentration profiles about an interface, and D not varying with concentration, a plot of $(C_o - C_f) / (C_o - C_f)$ versus X on probability paper will result in a straight line whose slope will be related to D.

D values for the diffusion couples desired in this study could be determined from this relationship [(equation (G-4))] if they were not a function of concentration. Deviations from linearity on the probability paper plots would readily establish whether the D's for the couples were concentration dependent or not. (Deviations at low temperatures may also be due to grain boundary effects).

Since most metal diffusion couples do not have concentration independent D values, the utility of equation (G-4) is rather small. However, this equation can be employed to generate an approximation to the depth of solute penetration in a diffusion couple. Imagine a couple of W/Ta-10W as depicted in Figure G-1. An approximate D value for 2000°C can be approximated from literature data for refractory metal diffusion at 2000°C.

		Ref.
D(Cb→Mo)	= 10^{-9} cm ² /sec	17
D(Cb&Ta → Ta)	= 10^{-10}	18
D(Cb → Cb)	= 10^{-9}	18
D(Cb - Mo)	= 10^{-10}	14

Using a probable D value of 10^{-10} cm²/sec and a 1000 hour age, the concentration profiles of Figure G-1 result. For this case the range of interdiffusion approaches 0.12 cm (50 mils) (approximately 0.06 cm (25 mils) into each couple). Wyatt and Argent⁽¹⁷⁾ report interdiffusion zones of 20 to 600 microns (i. e., up to 25 mils thick) for Cb-Mo couples aged at 2000 to 1500°C for 25 to 115 hours. Commonly accepted practice in analyzing diffusion profiles is the application of mathematical relations derived with infinite boundary conditions (such as equation (G-4)). Jost⁽⁵⁾ states, however, that solutions for the infinite system may be applied to actual experiments as long as concentration changes have not yet reached the boundaries. Castleman⁽¹⁰⁾ agrees and shows that predictions of the time required for concentration values for finite diffusion couples to approach certain limits as predicted by infinite couple equations can be in error by 40% or more if boundaries are approached. Thus it is extremely important to have proper couple geometries (sizes) for the accurate determination of diffusion coefficients. From the suppositions of Figure (G-1) the proper couple size for 1000 hours at 2000°C for this study was calculated as 0.10 to 0.12 cm (40 to 50 mil) sides on each side of the interface. Actual materials employed were 0.20 cm (80 mil) sheet.

For the situation where the diffusion coefficient is a function of concentration, the solution to equation (G-2) was given by Boltzmann⁽³⁾ by introducing the parameter $y = X/\sqrt{t}$.

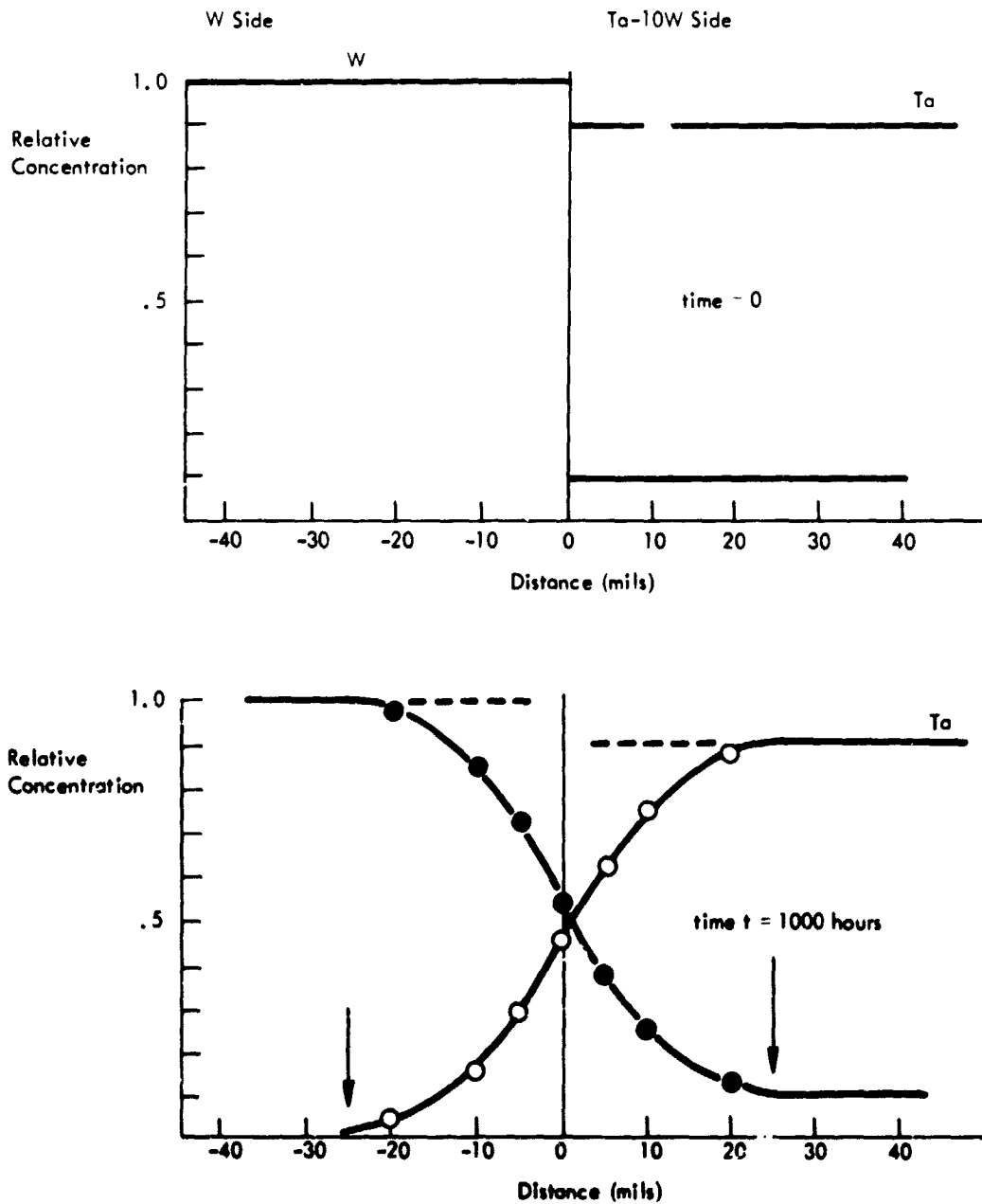


Figure G-1. Illustrating Predicted Interdiffusion for a W/Ta-10W Couple at 2000°C after 1000 Hours (Assume $\tilde{D} = 10^{-10} \text{ cm}^2/\text{sec}$).

Equation (G-2) becomes

$$\frac{d}{dy} \left(\tilde{D} \frac{dC}{dy} \right) = - \frac{y}{2} \left(\frac{dC}{dy} \right) \quad (G-7)$$

Upon integration, equation (G-7) becomes

$$\tilde{D} = -1/2 \left(\frac{dy}{dC} \right) \int_{C_f}^C y dC \quad (G-8)$$

and substituting for y yields the Boltzmann-Matano equation:

$$\tilde{D} = - \frac{1}{2t} \left(\frac{dX}{dC} \right) \int_{C_f}^C X dC \quad (G-9)$$

for the boundary conditions BC.1 and BC.2.

The Matano interface, $X = 0$, is defined by the condition that

$$\int_{C_f}^{C_0} X dC = 0 \quad (G-10)$$

A calculation of \tilde{D} for a time interval of diffusion, t , is shown in Figure G-2, where the diffusion coefficient at C_1 is equal to

$$\tilde{D} = - \frac{1}{2t} \frac{1}{\left(\frac{dC}{dX} \right)_{C_1}} \int_{C_f}^{C_1} X dC \quad (G-11)$$

where the integral in equation (G-11) is equal to area S_2 in Figure G-2.

Hartley⁽¹⁹⁾ has computerized equation (G-9). An error function fit is used to interpolate between and smooth the experimental data (least squares fit), and calculations are performed on the reiterated data. Appendix H demonstrates the curve fitting capability of the program

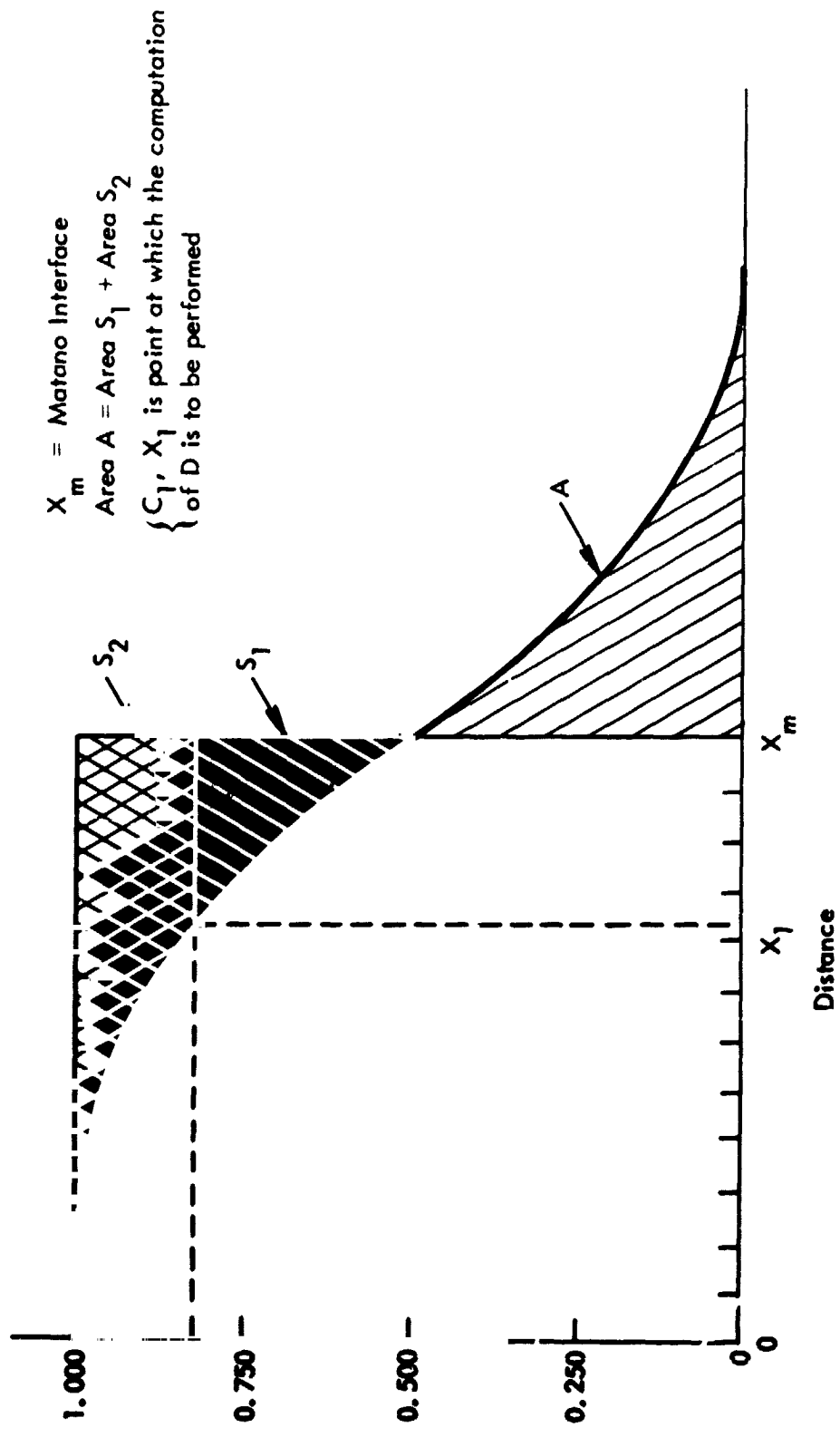


Figure G-2. Schematic Concentration-Penetration Curve for a Semi-Infinite Diffusion Couple, Boltzmann-Matano Analysis

in matching experimental data, and presents the variation in D with composition. The computer time on the CDC-6600 computer for this program is approximately 15 seconds.

Once the interdiffusion coefficients (D) have been resolved at several temperatures, their temperature dependency can be described graphically (through the Arrhenius relation) as

$$\ln \tilde{D} \propto \frac{1}{T} \quad (\text{G-12})$$

This relation results in a graph with a family of straight lines, each line representing one concentration level (ie $\tilde{D}(C_i)$). Each line will also represent a separate activation energy for interdiffusion.

For the formation of two or more phases in the interdiffusion zone, as would be expected with the zirconium couples, two modes of solution are possible. Hartley's Matano analysis computer program⁽¹⁹⁾ will calculate the interdiffusion coefficients through the multiple phase region⁽⁵⁾. This is illustrated in Appendix H. Hartley admits that for small phase widths, the absolute values of the diffusivities calculated are certainly questionable (due to a lack of data points). However, it is possible to calculate reasonably good diffusivities for the other portions (wider phases) of the concentration curve. These diffusivities can be inserted into the equations developed by Wagner^(5, 10) and Smoluchowski^(10, 11) for diffusion in multiphase couples and checked for accuracy.

As an example of multiphase diffusion, consider Figure G-3. Metals A and B, of different structure, are coupled. From the left side of Figure G-3, the diffusion couple interface concentrations remain constant and have the values C_a and C_b as obtained from the equilibrium phase diagram. The interface moves parabolically with the relationship

$$\lambda = b \sqrt{t} \quad (\text{G-13})$$

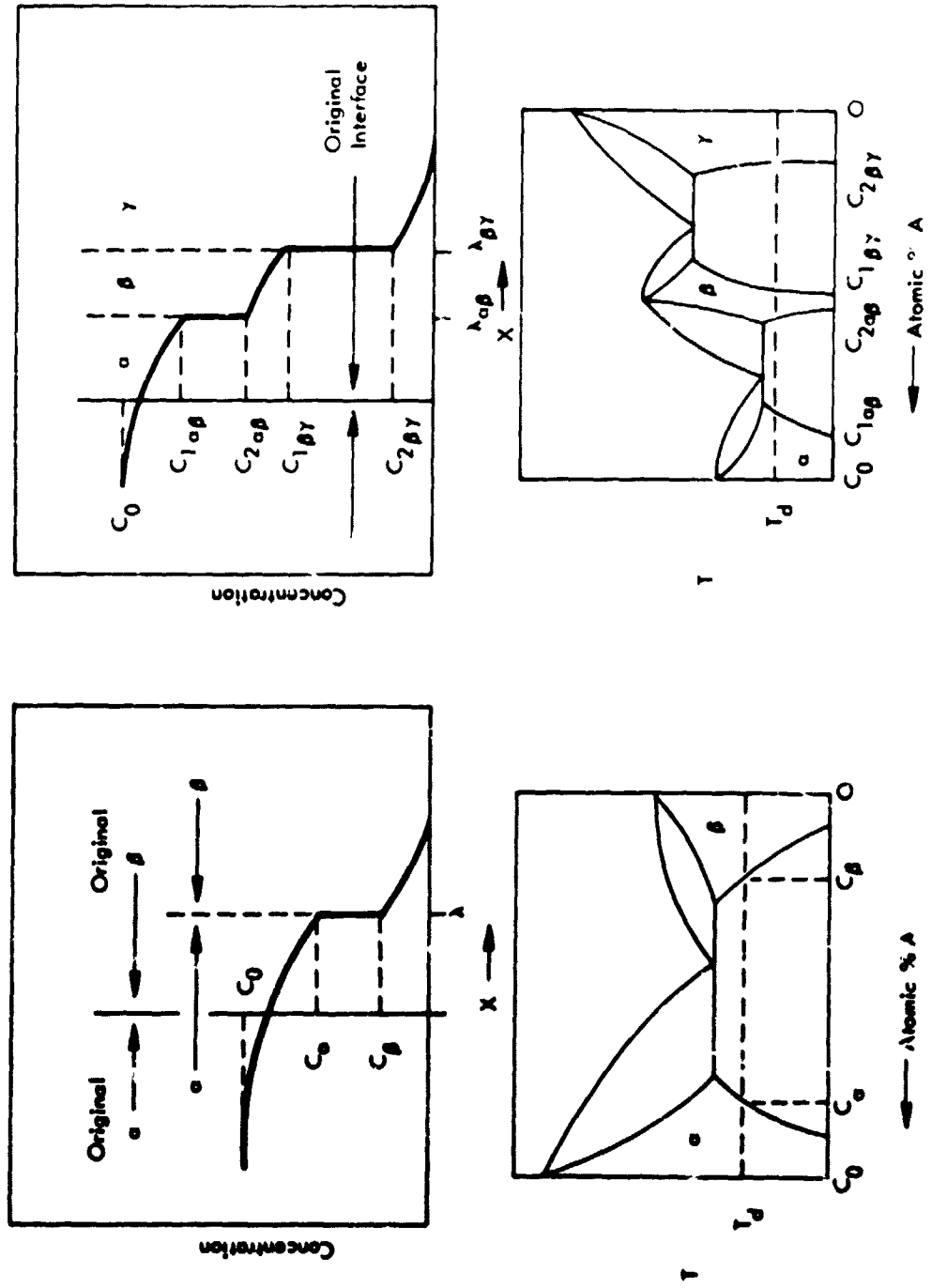


Figure G-3. Illustrating the Interdiffusion of Two (Wagner and Simoluchowski Solution) and Three (Smoluchowski Solution) Phase Diffusion Couples. (Reference 10)

where b is temperature dependent. The solution of the diffusion equation for the situation on the left side of Figure G-3 by Wagner led to the results that

$$\frac{(C_o - C_\alpha) \sqrt{D_\alpha} e^{-b^2/4D_\alpha}}{1 + \operatorname{erf}\left(\frac{b}{2\sqrt{D_\alpha}}\right)} - \frac{C_\beta \sqrt{D_\beta} e^{-b^2/4D_\beta}}{1 - \operatorname{erf}\left(\frac{b}{2\sqrt{D_\beta}}\right)} = \frac{\sqrt{\pi}}{2} b(C_\alpha - C_\beta) \quad (\text{G-14})$$

$$C_\alpha(X,t) = C_o - (C_o - C_\alpha) \left[\frac{1 + \operatorname{erf}\left(\frac{X}{2\sqrt{D_\alpha t}}\right)}{1 + \operatorname{erf}\left(\frac{b}{2\sqrt{D_\alpha}}\right)} \right] \quad (\text{G-15})$$

for $-\infty < X \leq \lambda$

and

$$C_\beta(X,t) = C_\beta \left[\frac{1 - \operatorname{erf}\left(\frac{X}{2\sqrt{D_\beta t}}\right)}{1 - \operatorname{erf}\left(\frac{b}{2\sqrt{D_\beta}}\right)} \right] \quad (\text{G-16})$$

for $\lambda < X < \infty$

where $C_\alpha(x,t)$ is the concentration of A in the α phase at position x and time t and $C_\beta(x,t)$ is the concentration of A in the β phase at position x and time t . The solution of the Fick second law equation for similar boundary conditions for the figure to the right in Figure G-3 has been solved by Smoluchowski.^(10,11) His solution is quite elaborate. The interfaces are still described mathematically by equation (G-3).

The Boltzmann-Matano solution does not require that the true couple interface be known in order to solve for the interdiffusion coefficient \tilde{D} , but is important if intrinsic diffusivities are desired. In a diffusion couple of A and B where A and B interdiffuse at different rates, it is necessary to obtain some parameter other than \tilde{D} in order to obtain the intrinsic diffusivities, D_A and D_B . Kirkendall noted the difference in D_A and D_B in his marker experiment.⁽²⁰⁾ By placing inert markers in the couple interface, Kirkendall and Smigelskas were able to follow the motion of the original interface due to the nonequality of the intrinsic diffusion coefficients. Darken⁽²¹⁾ later showed that the intrinsic diffusivities could be related to the interdiffusion coefficient (\tilde{D}) by the following equations:

$$\tilde{D} = N_A D_B + N_B D_A \quad (G-17)$$

$$V = (D_A - D_B) \frac{\partial N_A}{\partial X} \quad (G-18)$$

where $N_i = C_i/C$, $N_A + N_B = 1$, and V is the velocity of the markers in the diffusion zone with respect to the ends of the couple.

Darken⁽²²⁾ has commented that if we wish to recognize as diffusion only motion relative to markers and thus employ coordinate axes rigidly attached to a marker, then we are led to two intrinsic diffusion coefficients. If, on the other hand, we take the attitude that diffusion and bulk motion are all one and the same process, and that our interest is limited to the relationship between composition, distance and time, then the interdiffusion coefficient will do.

For the purposes of this study, the interdiffusion coefficient will acceptably describe desired interdiffusion characteristics. The interdiffusion coefficient is normally presented as (1) a graph of $\ln \tilde{D}$ vs composition, and (2) as a graph of $\ln \tilde{D}$ vs $1/T$ as a function of couple composition. This results in separate Arrhenius parameters, D_0 -frequency factor, ϕ -activation energy, for each composition.

In a more practical sense, engineering level predictions of interdiffusion zone widths for long age times (extrapolations), and temperature relations to the interdiffusion rate can be resolved without extensive analytical treatments. Perusal of equations G-4, 14, 15, and 16 will reveal that for a constant \tilde{D} , and constant boundary concentrations,

$$\frac{\Delta X}{2\sqrt{\tilde{D}t}} = \text{constant} \quad (\text{G-19})$$

where ΔX is the penetration distance for a certain concentration level, t is the age time at temperature, and \tilde{D} is the interdiffusion coefficient. The proportion constant, for varying times and temperatures, is invariant. A graph (Figure G-4) of total penetration distance ΔX versus \sqrt{t} will thus yield a family of lines (temperature dependence) for each material combination.

If one wishes to know the net interdiffusion zone width (or penetration to a certain concentration level) of a particular couple combination, Figure G-4 can be used. However, Figure G-4 can only be employed for predictions at the temperatures listed. Thus, in order to find ΔX for time t at temperature $T_i \neq T_j$ in Figure G-4, other relationships must be developed.

Appendix C (Interdiffusion Predictive Model) demonstrates the development of a temperature relationship which relates

$$\ln \frac{\Delta X^2}{t} \propto \frac{1}{T} \quad (\text{G-20})$$

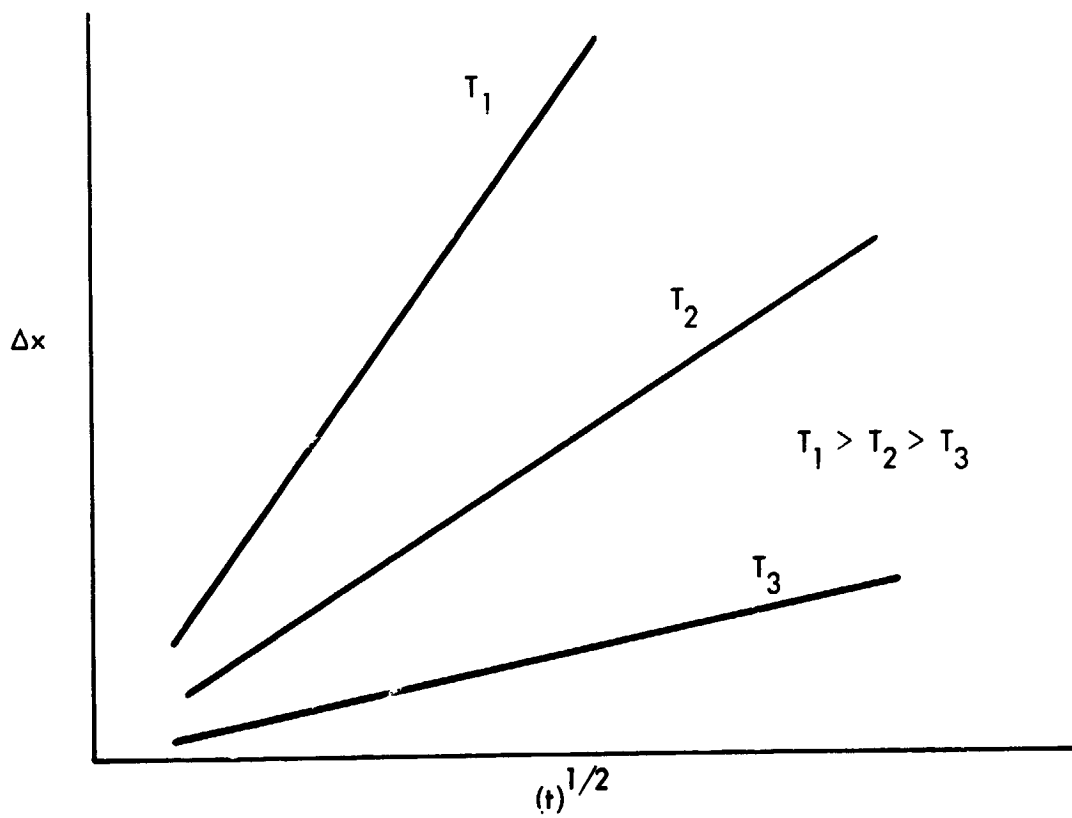


Figure G-4. Predictive extrapolation of interdiffusion zone width (ΔX) as a function of age time (t) for varying temperatures (T).

where

ΔX = interdiffusion zone width

t = age time

T = age temperature ($^{\circ}\text{K}$)

From a typical graph of equation (G-20), (Figure G-5) it is possible to predict the interdiffusion zone width for any age time for any age temperature for the couple material combinations represented in Figure G-5.

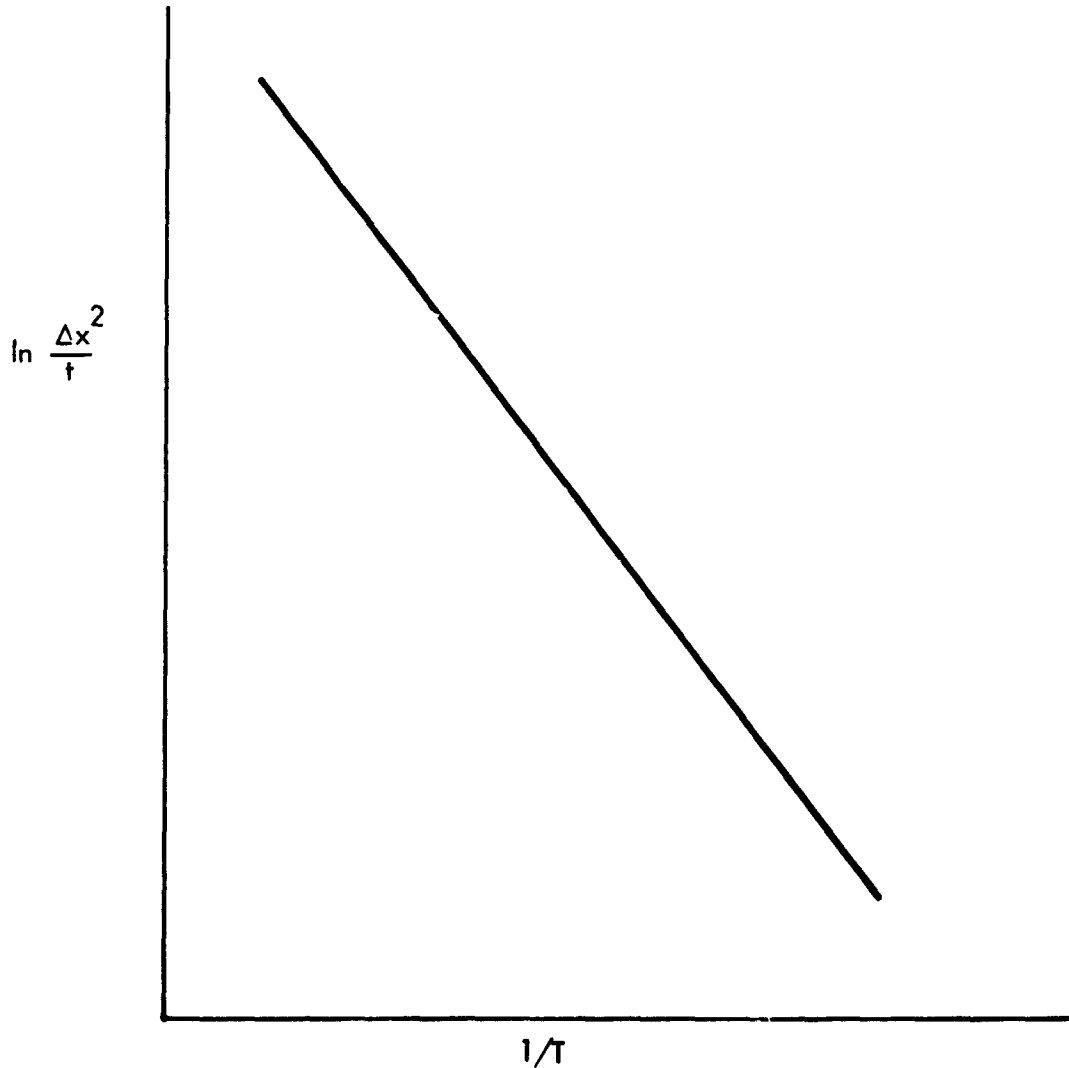


Figure G-5. For one material combination, the interdiffusion zone width can be predicted for any age time for any temperature.

III. SUMMARY

To characterize a material combination with respect to interdiffusion parameters, several relations are necessary:

A. For engineering interests:

1. Relating $\ln \left(\frac{\Delta X}{t} \right)$ vs $1/T$
2. Relating ΔX to \sqrt{t} (at one T)

B. For academic (diffusivity) interests:

1. Relating $\ln \tilde{D}$ vs $1/T$
2. Relating $\ln \tilde{D}$ vs Composition (at one T)

These relations were found, when possible, for the systems of this study.

APPENDIX G. Diffusion Analysis References

1. English, J. J., "Binary and Ternary Phase Diagrams of Columbium, Molybdenum, Tantalum, and Tungsten", DMIC Report 152 (OTS PB 171421), April 28, 1961.
2. Shewman, P. G., Diffusion in Solids, Chapter 1, p. 14, McGraw-Hill Book Co., 1963.
3. Boltzmann, L., Ann. Physik, 53, 960, 1894.
4. Matano, C., Japan. Phys., 8, 109, 1933.
5. Jost, W., Diffusion in Solids, Liquids, and Gases, Chapter 1, Academic Press Inc., New York, 1960.
6. Guy, A. G., Leroy, V. and Lindemer, T. B., "Diffusion Calculations in Three-Component Solid Solutions", Trans. ASM, Vol. 59, p. 517, 1966.
7. Lindemer, T. B., personal communication.
8. Guy, A. G. and DeHoff, R. T., "The Study of Multiphase Diffusion in Three-Component Metallic Systems", AFML-TR-66-37E, December, 1966.
9. Lindemer, T. B. and Guy, A. G., "Analysis of Ternary Diffusion Curves Using a Second Integration of the Fick Law", Trans. of the AIME, Vol. 239, p. 1924, 1967.
10. Castleman, L. S., "An Analytical Approach to the Diffusion Bonding Problem", Nucl. Sci. and Engr., Vol. 4, p. 209, 1958.
11. Smoluchowski, R. and Vasileff, H. D., "Two and Three Phase Intermetallic Diffusion", Unpublished manuscript, Carnegie-Mellon University, 1951.
12. Arcella, F. G., "Determination of the Diffusion Coefficient of Cobalt-60 in Aluminum During Dynamic Straining", M.S. Thesis, Massachusetts Institute of Technology, 1962.
13. Passmore, E. M., Boyd, J. E., and Lemont, B. S., "Investigation of Diffusion Barriers for Refractory Metals", ASD-TDR-62-432, July 1962.
14. Hartley, C. S., Steedly, J. E., Jr., and Parsons, L. D., "Binary Diffusion in Body-Centered Cubic Transition Metals", Chapter 4, Diffusion in Body-Centered Cubic Metals, ASM, 1965.

15. Koffman, D. M., Norelco Rep. XI, 59, 1964. (As cited by Hartley, C.S., et al Ref. 13).
16. Crank, J., The Mathematics of Diffusion, Oxford Clarendon Press, 1956.
17. Wyatt, B. S. and Argent, B. B., "The Interdiffusion of Niobium and Molybdenum", J. Less Common Metals, 11, p. 259, 1966.
18. Lundy, T. S., et al., "A Summary of ORNL Work on Diffusion in Beta Zirconium, Vanadium, Columbium, and Tantalum", Chapter 3, Diffusion in Body-Centered Cubic Metals, ASM, 1965.
19. Hartley, C. S. and Hubbard, K., "A Computer Program for the Matano Analysis of Binary Diffusion Data", ASD-TDR-62-858, 1962.
20. Smigelskas, A. and Kirkendall, E., Trans. AIME, 171, 130, 1947.
21. Darken, L., Trans. AIME, 174, 184, 1948.
22. Darken, L. and Gurry, R., The Physical Chemistry of Metals, Diffusion, McGraw-Hill Book Co., 1953.